THE NUMERICAL SOLUTION OF TRANSIENT SUPERCRITICAL FLOW BY THE METHOD OF CHARACTERISTICS WITH A TECHNIQUE FOR SIMULATING BORE PROPAGATION

A THESIS

Presented to

The Faculty of the Graduate Division

by

Jerome Joseph Zovne

In Partial Fulfillment

of the Requirements for the Degree

Doctor of Philosophy

in the School of Civil Engineering

Georgia Institute of Technology

May 1970

THE NUMERICAL SOLUTION OF TRANSIENT SUPERCRITICAL FLOW

BY THE METHOD OF CHARACTERISTICS WITH A TECHNIQUE

FOR SIMULATING BORE PROPAGATION

Approved:

Chairman

Date approved by Chairman: 27 May, 1970

ACKNOWLEDGMENTS

The author gratefully acknowledges the assistance of his thesis advisor, Dr. Charles S. Martin, who initially suggested this research topic and who provided constant guidance and encouragement. The members of the thesis advisory committee, Drs. P. G. Mayer and D. V. Ho, are thanked for providing the author with much of the academic background required for this study and for their help in the preparation of the final draft.

Special thanks are extended to Dr. W. M. Sangster, Chairman, School of Civil Engineering, for offering financial assistance with an NDEA Title IV Fellowship for three years, a teaching assistantship for two quarters, and a research assistantship for one quarter. Also greatly appreciated is the large amount of computer time made available by the School of Civil Engineering for conducting this investigation.

The author is indebted to the Environmental Resources Center for assistance in publishing and distributing the dissertation as a technical report in its ERC-Series. Permission was granted by the Graduate Division for special pagination and margins so that the dissertation could be published as such a report.

The author's wife, Karen, and daughter, Kari, are acknowledged for their patience and for the inspiration they have given the author during the past four years at Georgia Tech. Also to be thanked are our many friends at St. Luke who have made our stay in Atlanta a most rewarding experience.

TABLE OF CONTENTS

TABLE OF CONTENTS (Concluded)

LIST OF TABLES

LIST OF FIGURES

LIST OF FIGURES (Continued)

LIST OF FIGURES (Concluded)

NOMENCLATURE

A,B,C,D	points of a fixed spatial grid at time level T in Fixed Grid numerical solution
B	width of rectangular channel, ft
C1	positive characteristic curve with slope dx/dt=V+c
C2	negative characteristic curve with slope dx/dt=V-c
c	celerity of a shallow-water wave defined as $(gy)^{\frac{1}{2}}$, ft/sec
c_R	wave celerity at point R
c_S	wave celerity at point S
c_u	wave celerity of a uniform flow
DELT	time increment between specified points on the t-axis for the Characteristics Grid solution
E(x)	error of approximation for integration by rectangular rule
E(t)	error of approximation for integration by rectangular rule
$E_N(t)$	sum of errors (total error) for integration over N intervals
$F(V_P)$	numerator of Newton's Rule for determining V_P
$F'(V_P)$	denominator of Newton's Rule for determining V_P
$\mathbb{F}$	Froude number defined as $V/(gy)^{\frac{1}{2}}$
$\mathbb{F}_1$	Froude number of the initial (upstream) flow of a hydraulic jump
$\mathbb{F}_S$	stability Froude number (Eqn. 42)
$\mathbb{F}_{S1}$	stability Froude number (Eqn. 43)
f	Darcy-Weisbach friction factor
f(x)	function of x which is integrated by rectangular rule

$f'(x)$	first derivative of f(x)
$f(\xi)$	function of x or t evaluated at point ξ
$f'(\xi)$	first derivative of f(x) or f(t) evaluated at point ξ
$f''(\xi)$	second derivative of f(x) or f(t) evaluated at point ξ
$G(y_P, V_P)$	function used in Newton's Method for two unknowns (Eqn. 59)
G_{y_P}	partial derivative of G with respect to y_P
G_{V_P}	partial derivative of G with respect to V_P
g	gravitational constant (32.17 ft/sec^2)
$H(y_P, V_P)$	function used in Newton's Method for two unknowns (Eqn. 60)
H_{y_P}	partial derivative of H with respect to y_P
H_{V_P}	partial derivative of H with respect to V_P
$(H_\ell)_{L\text{-}R}$	energy head loss in a channel reach L-R, ft
k	index indicating iteration level
L	length of channel, ft
N	number of grid points in a numerical solution
n	integer denoting a grid point; n=0,1,2,...,N
P	wetted perimeter defined as B+2y, ft
P	point of intersection of a C1 and a C2 characteristic at which the flow conditions are to be determined (when used as a subscript)
Q	discharge, ft^3/sec
Q(0,0)	initial uniform flow discharge for numerical solution
$Q(0,\Delta T)$	final uniform flow discharge for numerical solution
R	hydraulic radius defined as By/(B+2y), ft
R	point on C1 characteristic at which the flow conditions are known (when used as a subscript)

$R_1, R_2, \ldots, R_N$	points on a C1 characteristic along which the characteristic equations are integrated
$\mathbb{R}$	Reynolds number defined as $4RV/\nu$
$r_1, r_2, \ldots, r_6$	coefficients of a three-point Lagrange interpolating polynomial given by Equations (69)-(74), respectively
S	point on a C2 characteristic in supercritical flow at which the flow conditions are known (when used as a subscript)
S'	point on a C2 characteristic in subcritical flow at which the flow conditions are known (when used as a subscript)
S1,S2,S3	standard flow profiles for steep slopes
S_f	friction slope
S_o	channel bottom slope
S_L	friction slope at point L (left end of section)
S_P	friction slope at point P
S_R	friction slope at point R
S_S	friction slope at point S
T	current (or known) time level of the Fixed Grid solution, sec
$T+\Delta t$	next (or unknown) time level of the Fixed Grid solution
ΔT	duration of the linearly rising or falling upstream hydrograph for the numerical solution, sec
t	time variable in the differential equations
Δt	time increment as determined by Courant condition in the Fixed Grid solution, sec
t_P	time at point P
t_R	time at point R
t_S	time at point S
V	mean velocity of flow, ft/sec

V_A, V_B, V_C, V_D	mean velocities at respective fixed grid points A,B,C,D
V_L	mean velocity at point L (left end)
V_P	mean velocity at point P
$V_{P(k)}$	k^{th} value of V_P in an iterative solution
V_R	mean velocity at point R
V_S	mean velocity at point S
$V_{S'}$	mean velocity at point S'
V(x,0)	initial velocity boundary condition for the solution of the characteristic equations
V(0,t)	upstream velocity boundary condition (hydrograph) for the solution of the characteristic equations
V(L,t)	downstream velocity boundary condition (hydrograph) for the solution of the characteristic equations
V(nΔx,0)	initial velocity boundary conditions specified at N grid points for the numerical solution
V(79,0)	velocity hydrograph at x=79 ft for bore simulation
V_u	mean velocity of a uniform flow
W	weight, lb
x	coordinate direction parallel to channel bottom, ft
x_P	location of point P
x_R	location of point R
x_S	location of point S
x_{Ro}, x_{So}	initial estimates of the locations x_R and x_S
x_0, x_1, x_2, x_3	limits of an integral
Δx	spatial grid spacing for the Fixed Grid solution
y	depth perpendicular to the channel bottom, ft
y_A, y_B, y_C, y_D	depths at respective fixed grid points A,B,C,D
y_L	depth at point L (left end)

y_P	depth at point P
$y_{P(k)}$	k^{th} value of y_P in an iterative solution
y_R	depth at point R
y_S	depth at point S
$y_{S'}$	depth at point S'
$y(x,0)$	initial depth boundary condition for the solution of the characteristic equations
$y(0,t)$	upstream depth boundary condition (hydrograph) for the solution of the characteristic equations
$y(L,t)$	downstream depth boundary condition (hydrograph) for the solution of the characteristic equations
$y(n\Delta x,0)$	initial velocity boundary conditions specified at N grid points for the numerical solution
$y(0,0)$	initial uniform flow depth for the numerical solution
$y(0,\Delta T)$	final uniform flow depth for the numerical solution
$y(79,0)$	measured depth hydrograph at x=79 ft for bore simulation
y_1	initial (upstream) depth of a hydraulic jump
y_2	sequent depth of a hydraulic jump
y_u	depth of a uniform flow
α	angle of inclination of channel
β	momentum correction factor
γ	specific weight, lb/ft^3
$\epsilon, \epsilon_1, \epsilon_2$	error bounds for iterative procedures
θ	grid time-distance ratio, $\Delta t/\Delta x$
λ	coefficient of characteristic equations (Eqn. 9)
ν	kinematic viscosity, ft^2/sec
ξ	a point on the domain over which a function is integrated
ρ	density, $slugs/ft^3$

τ_o	wall shear stress, lb/ft^2
ψ	function used in the Fixed Grid solution (Eqn. 31)
X	function used in the Fixed Grid solution (Eqn. 30)
ψ'	function used in the Fixed Grid solution (Eqn. 51)
X'	function used in the Fixed Grid solution (Eqn. 50)

SUMMARY

This investigation has a twofold purpose; namely, that of proposing and analyzing two finite-difference schemes for the solution of unsteady, supercritical flow problems, and that of proposing a method to simulate bore propagation in supercritical flow. The emphasis is upon the supercritical regime because it has not been studied nearly as extensively as has the subcritical regime. In particular, in the control of flow through artificial channels supercritical flow and bore propagation are important factors. The development of a numerical scheme to allow computation in either sub- or supercritical flow with the presence of a bore discontinuity is therefore a primary objective of this study.

The mathematical basis for the numerical solution is the set of two nonlinear one-dimensional partial-differential equations called the shallow-water wave equations. These equations are written for a rectangular cross section including only the gravity and friction forces. The equations, in characteristic form, are solved in complete form employing two finite-difference schemes programmed on a digital computer. In the Characteristics Grid scheme the characteristics equations are numerically integrated along characteristic curves which results in an uneven distribution of grid points. In the Fixed Grid scheme the integration is also performed along characteristics, however, the flow quantities at a point on a characteristic are determined by interpolation from a specified fixed spatial grid.

The Fixed Grid method is the better method for supercritical flow simulation based upon empirical investigations of stability and accuracy, and upon comparisons with Characteristics Grid solutions. The stability of the Fixed Grid is tested by placing a ± 10 percent perturbation upon a uniform flow in the transient solution. If the disturbance grows the solution is unstable, whereas if the disturbance attenuates the solution is stable. Uniform supercritical flows which are physically unstable ($F > F_S^*$) are found also to be numerically unstable and flows which are physically stable ($F < F_S$) are found to be numerically stable.

Each of the three methods of perturbing the uniform flow are accurate regarding continuity as determined by keeping running totals of the storage of the perturbation. Furthermore, running totals of wave storage compare favorably to the net inflow to or outflow from the wave to give additional support for the Fixed Grid method. Although the Characteristics Grid method is perhaps the more accurate and efficient, the difficulties involved in programming do not warrant its recommendation over the Fixed Grid one. The few solutions which were obtained for the Characteristics Grid were nearly identical to the Fixed Grid solutions.

It is possible to simulate a bore in supercritical flow by employing in conjunction with Fixed Grid method the well-known sequent depth equation for hydraulic jumps. The numerical scheme adequately simulates the propagation of four experimental bores without the necessity of using special finite-difference equations in the vicinity of the bore front.

---

* F_S is a stability Froude number which is approximately 1.6 for turbulent flow in wide rectangular open channels.

The possibility of solving multi-channel problems in sub- and/or super-critical flow is therefore feasible.

CHAPTER I

INTRODUCTION

Definition of the Problem

This investigation is concerned with the numerical simulation of unsteady, supercritical, open-channel flow. A review of the literature concerning rational techniques for analyzing transient open-channel flow reveals that there is a wealth of information available for solving transient problems in the subcritical regime. There is, however, practically none available for the supercritical regime. In many studies reference is made to supercritical flow while computations are carried out exclusively for the subcritical case. The implication is that the techniques applied to subcritical flow are equally applicable to supercritical flow. To the writer's knowledge no actual computations have been carried out to prove it. This study is therefore devoted primarily to the clarification of numerical techniques which can be used to solve transient supercritical flow problems.

As in subcritical flow, a rapidly changing upstream boundary condition in supercritical flow can cause a surge or bore to form in the channel. Some of the numerical solution techniques devised for subcritical flow, however, permit the continuation of the solution although the surge or bore forms. Such a technique is developed in

this study for supercritical flow. Thus, the bore conservation equations can be relaxed and the abrupt discontinuity is replaced with a smooth continuous wave profile. Importantly, for engineering solutions it may not be necessary to consider the conditions in the vicinity of the surge or bore front, since the maximum depth and velocity usually occur some distance behind the front. In the region behind the front the one-dimensional equations are applicable and the solution in this region may give the desired maximum depths and velocities.

Another type of discontinuity occurs in an open-channel when a downstream boundary condition causes a transition from supercritical to subcritical flow. This discontinuity is sometimes called the moving hydraulic jump, but is also referred to as a hydraulic bore. Because of the transition from super- to subcritical flow, it is no longer possible to neglect the bore front. Its location and rate of propagation must be established since different solution techniques must be employed for the two different regimes. Another primary objective of this study therefore is to devise a method to simulate the propagation of an experimental bore.

This study thus has a twofold purpose: that of determining numerical techniques which can be used for the solution of transient, supercritical flow, and that of proposing a method to numerically simulate the propagation of an experimental bore.

Scope and Limitations

The mathematical basis for the numerical simulation carried out in this study is the set of one-dimensional partial differential equations for open-channel flow, which are alternatively called the Saint-Venant equations or the shallow-water wave equations. These two equations, continuity and momentum, appear in the literature in a great variety of forms depending upon the channel geometry used, the form of friction term assumed, and whether extra terms are included for lateral inflow, Coriolis force, or wind force. In this study a simple form of the equations is used. That is, the channel geometry is rectangular; the friction term is expressed in the Chezy form; the channel surface is considered hydraulically smooth; there is no lateral inflow and external forces other than gravity are neglected.

The normal procedure for obtaining a numerical solution is to apply a finite-difference scheme to the partial differential equations, resulting in a set of algebraic equations which can be programmed on a digital computer. A similar procedure is followed here except that the shallow-water wave equations are converted to characteristic form before the finite-difference scheme is applied. This technique is employed because the characteristic form exhibits very clearly the wave propagation properties of the original equations. Experience has shown that it has been perhaps the most successful method of solution when applied to subcritical flow problems.

The basic equations as well as the two finite-difference schemes used in this study are those originally proposed by Streeter and Wylie

[1967].* Their schemes were used because they are quite simple and yet mathematically sound. The first difference scheme is a fixed grid scheme in which the differences are taken between points in the domain which have a predetermined fixed spacing. This scheme also includes an interpolation technique which allows the solution to proceed along the actual characteristic lines. The second scheme is called a characteristics grid method because the grid points are computed as the solution progresses, resulting in an uneven spatial and temporal distribution of points. These two schemes are used to solve identical supercritical problems in order to satisfy the first objective of this investigation. A set of problems are formulated to cover a reasonable range of the fundamental parameter involved, the Froude number. The problems are solved by each of the two schemes for identical boundary conditions and the solutions are subsequently compared for speed and accuracy. The Fixed Grid solution is then studied further for its properties regarding stability and continuity.

The Fixed Grid method is used exclusively to carry out the second objective of the study, that is, to numerically simulate the propagation of a positive bore in a rectangular channel. The experiment consists of establishing a stationary hydraulic jump in the flume. This jump is then forced to propagate upstream against the flow under the influence of a rising gate downstream. The entire problem is then duplicated numerically in which an internal boundary condition is incorporated for

---

*All literature citations will appear between square brackets and the references are listed in the Bibliography.

the purpose of following the propagation of the bore.

Historical Sketch and Literature Review

The origin of the one-dimensional equations for unsteady, open-channel flow can be traced back to the nineteenth century; its original derivation is attributed to de Saint-Venant [Favre, 1935]. Because of the nonlinear nature of the equations they were rarely treated in their complete form until the computer made it possible to do so by the early 1950's. The theory of characteristics was also developed before the turn of the century and provided the basis for graphical techniques for solving partial differential equations of open-channel flow such as proposed by Massau [1889], Escoffier [1950], and Lin [1952]. The graphical technique has been traditionally called the method of characteristics although in recent times the term has been extended by many to include numerical solutions which use the characteristic equations as a basis. All future references to the method of characteristics in this report imply the numerical rather than the graphical application of the characteristic theory.

The first attempt to solve the shallow-water wave equations in their complete form by numerical methods using the computer is discussed in Stoker [1953, 1957] and Isaacson, Stoker, and Troesch [1954, 1956]. In these reports the method of characteristics is developed to predict the movement of floods in the Ohio River and at the junction of the Ohio and Mississippi Rivers. Stoker's text [1957] contains a detailed discussion of the method of characteristics as applied to open-channel flow problems and is perhaps the best basic reference available.

These early works were followed by a great number of reports in which the method of characteristics was applied to a variety of unsteady, open-channel flow problems such as flood propagation, overland flow and tidal oscillations in estuaries. A summary of these numerical methods applied to open-channel flow can be found in a dissertation by Miller [1970], which contains a bibliography with more than 600 entries. As stated earlier, only a few reports mention unsteady, supercritical flow and even fewer actually include any calculations. Stoker [1957] mentions only the change in boundary conditions required for conversion from subcritical to supercritical flow. Iwagaki [1955] describes supercritical experiments conducted in a twenty-four meter long flume. The data, however, are not complete enough to duplicate his runs numerically. Liggett [1959] discusses the possibility of supercritical flow occurring during the runoff process on steep slopes and gives a qualitative indication of how to solve for this case based upon the theory developed in the text. Again, no actual calculations are presented and the theory is strictly applicable only to an idealized runoff model and is devised to avoid having to use the method of characteristics. Garrison, Granju, and Price [1969] describe a computer program which has been used to solve a variety of unsteady problems in TVA reservoirs and rivers. Two of the listed limitations of the program were that neither supercritical flows nor bores could be computed, indicating that there are cases where the ability of a program to handle these types of flow would be useful. The author found only one reference in which a numerical scheme is actually proposed to allow computation in either of the two regimes of open-channel flow [Streeter and Wylie, 1967]. This technique is called the method of

specified time intervals. No mention is made of any actual calculations performed in the supercritical regime, however. As stated earlier, this scheme as well as another one proposed by Streeter and Wylie are used in this study.

The occurrence of surges and bores in open-channels has always been a topic of major concern to hydraulic engineers. One account of the rather disastrous effects of bores which occur as a result of dam failure dates back to 1889 [The Johnstown Disaster, 1889]. There is some confusion in the literature as to the appropriate use of the terms surge and bore. Surge is the more general term which is applied to any rapidly-varied unsteady open-channel flow while the bore usually refers to the steep-fronted surge which advances up a river due to tidal effect [Henderson, 1966; Chow, 1959; Schönfeld, 1955]. Elsewhere the term bore is associated with any surge which has an abrupt breaking front, regardless of its origin [Stoker, 1957; Martin and DeFazio, 1969]. Since this thesis treats a type of surge with a breaking front without associating it with any specific physical origin, the term bore is used here. This corresponds to the A.S.C.E. definition of a bore [Nomenclature for Hydraulics, 1962], which is stated as follows:

> A wave of water having a nearly vertical front, such as a tidal wave, advancing upstream as a result of high tides in certain estuaries; a similar wave advancing downstream as a "cloudburst," or sudden release of a large volume of water from a reservoir. The bore is analogous to the hydraulic jump in that it represents the limiting condition of the surface curve wherein it tends to become perpendicular to the bed of the stream....

Theoretical and experimental studies of surges and bores date back to the early Nineteenth century as described in a classical book by Favre

[1935], in which the various existing theories for computing surges are reviewed and compared to experimental results obtained in a 74 meter wooden flume. All of the experiments were conducted in the subcritical regime as was the case in subsequent studies by Benjamin and Lighthill [1954]; Schönfeld [1955]; Dronkers [1964]; Vasiliev, Gladyshev, Pritvits, and Sudobicher [1965]; and Martin and DeFazio [1969]. In particular, Dronkers presents a finite-difference method in which artificial terms are added to the differential equations and the discontinuity is smoothed by extending it over a small interval Δx, in order to calculate the progress of the bore. He indicated that this procedure was still in the developmental stage, however, and results were not presented. The study by Martin and DeFazio is of particular interest because it is one of few attempts to numerically simulate the propagation of a surge in subcritical flow. They simulated surges with some success using the shallow-water wave equations which are strictly applicable only to flows of a gradually-varied nature. In that investigation, special flow equations were not used in the vicinity of the rapidly-varied surge front. A similar approach is taken in this study in that no special finite-difference equations are used in the vicinity of the bore front. The jump from sub- to supercritical flow at the bore front, however, poses several additional numerical difficulties which are not encountered when the flow is restricted to either the subcritical or the supercritical regime. First, the numerical solution must establish the initial location of the stationary hydraulic jump. Second, two variations of the finite-difference scheme must be programmed. One of these must operate in the subcritical regime where surface disturbances can propagate either

upstream or downstream, while the other must operate in the supercritical regime where surface disturbances can propagate only downstream. Third, and most importantly, an internal boundary condition must be devised to track the location of the propagating bore since this position represents the boundary between the two flow regimes. The primary difference between the surge simulation carried out by Martin and DeFazio and the bore simulation carried out in this investigation is the requirement of this additional internal boundary condition.

A problem which must be recognized whenever working with supercritical flow is that the flow may become unstable above a certain limiting, or stability, Froude number. The outward manifestation of instability is the development of roll waves. A number of theories have been proposed to predict the stability Froude number: [Jeffreys, 1925; Thomas, 1940; Keulegan and Patterson, 1940; Vedernikov, 1946; Dressler, 1949; Craya, 1952; Iwasa, 1954; Binnie, 1959; Mayer, 1959], of which Iwasa's theory deserves special comment. His criterion is derived directly from the momentum equation for unsteady, open-channel flow and has been tested by Koloseus and Davidian [1966] in an extensive series of flume experiments which were designed to determine the friction laws for unstable flow. They concluded that the stability Froude number is approximately 1.6 for turbulent flow in a channel with a large aspect ratio (i.e. $B/y > 10$). This theory has a very important connotation regarding the interpretation of results in this thesis.

CHAPTER II

THE SHALLOW-WATER WAVE EQUATIONS AND CHARACTERISTIC THEORY

The shallow-water wave equations are the one-dimensional equations of momentum and continuity for gradually-varied unsteady open-channel flow. They are derived by applying the laws of conservation of momentum and mass to an elemental control volume such as that shown in Figure 1. The momentum equation is obtained by equating the three external forces (Fig. 1) to the rate of change of linear momentum through the control volume. The three forces are identified as the component of weight force in the x-direction, the net hydrostatic force and the total wall shear (friction) force. The continuity equation is obtained by equating the rate of volume storage within the control volume to the net volume flow out of the control volume since the fluid is incompressible. The resulting shallow-water wave equations as derived by Streeter and Wylie [1967] are,

Momentum:

$$\frac{\partial V}{\partial t} + \frac{V}{y}\frac{\partial y}{\partial t} + 2V\frac{\partial V}{\partial x} + \left(\frac{V^2}{y} + g\right)\frac{\partial y}{\partial x} = g\,(S_o - S_f) \qquad (1)$$

Continuity:

$$\frac{1}{y}\frac{\partial y}{\partial t} + \frac{V}{y}\frac{\partial y}{\partial x} + \frac{\partial V}{\partial x} = 0 \qquad (2)$$

in which the channel cross section is assumed to be rectangular of width B. The symbols used in the equations are defined as follows:

- x the coordinate direction parallel to the channel slope
- y denotes either the coordinate direction perpendicular to x or the depth of flow in the channel
- t the time
- V the mean velocity of flow in the channel
- S_o the channel slope; equals $\sin\alpha$
- S_f the friction slope
- τ_o the wall shear stress
- g the gravitational constant
- ρ the density
- R the hydraulic radius; equals $By/(B+2y)$
- P the wetted perimeter; equals $B+2y$

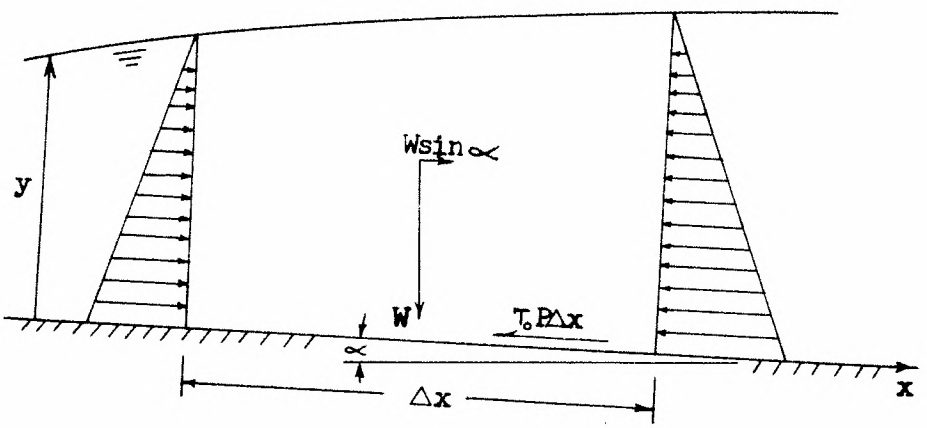

Figure 1. Elemental Control Volume for the Derivation of the Equations

A most important requirement in the derivation of the momentum equation is that the flow must be "gradually-varied unsteady." This restriction insures that hydrostatic conditions prevail in the channel. The equations therefore do not apply in rapidly-varied flow regions where vertical accelerations are large enough to disturb the hydrostatic condition significantly.

The term S_f in Equation (1) is called the friction slope in open-channel flow. From steady state momentum analysis the following relationship between the wall shear stress, τ_o, and S_f is obtained,

$$\tau_o = \gamma R S_f \tag{3}$$

The friction slope is evaluated here using the Darcy-Weisbach relation for open-channel flow,

$$S_f = \frac{f}{4R} \frac{V^2}{2g} \tag{4}$$

in which f is the friction factor. The parameter f can be related logarithmically to the Reynolds number, $\mathfrak{R} = 4RV/\nu$, for hydraulically smooth channels. The relationship used in this study for turbulent flow was found experimentally by Tracy and Lester [1961] and by the writer (using the same channel) to be,

$$\frac{1}{f^{\frac{1}{2}}} = 2.03 \log_{10} \mathfrak{R} f^{\frac{1}{2}} - 1.30 \tag{5}$$

It is tacitly assumed that the friction slope for gradually-varied unsteady flow is the same as that for steady flow inasmuch as the effect

of unsteadiness upon the friction slope is generally unknown.

Together Equations (1) and (2) form a system of hyperbolic partial differential equations which have wave propagation properties that are best analyzed using the theory of characteristics. The equations are initially cast into two pairs of ordinary differential equations called the characteristic equations. This can be done in a simple manner suggested by Streeter and Wylie [1967], as follows. Equation (2) is multiplied by V and then subtracted from (1) yielding the simplified momentum equation,

$$\frac{\partial V}{\partial t} + V \frac{\partial V}{\partial x} + g \frac{\partial y}{\partial x} - g (S_o - S_f) = 0 \qquad (6)$$

Equation (2) is then multiplied by λy and added to Equation (6), giving,

$$\left[\frac{\partial V}{\partial t} + (V + \lambda y) \frac{\partial V}{\partial x}\right] + \lambda \left[\frac{\partial y}{\partial t} + \left(\frac{g}{\lambda} + V\right) \frac{\partial y}{\partial x}\right] - g (S_o - S_f) = 0 \qquad (7)$$

The quantities within the brackets are made total differentials of V and y respectively by specifying the following condition

$$\frac{dx}{dt} = V + \lambda y = \frac{g}{\lambda} + V \qquad (8)$$

Solving for λ in Equation (8) yields the result,

$$\lambda = \pm \left(\frac{g}{y}\right)^{\frac{1}{2}} \qquad (9)$$

which allows Equation (7) to be rewritten as,

$$\frac{dV}{dt} \pm \left(\frac{g}{y}\right)^{\frac{1}{2}} \frac{dy}{dt} + g\,(S_f - S_o) = 0 \qquad (10)$$

in which, from Equation (8),

$$\frac{dx}{dt} = V \pm (gy)^{\frac{1}{2}} \qquad (11)$$

The two ordinary differential Equations (10), called the characteristic equations, when integrated along their respective characteristic curves in the x,t-plane given by Equation (11), describe the surface gravity wave propagation properties along the curves. The important quantity $(gy)^{\frac{1}{2}}$ is known as the celerity, c, of a shallow-water wave which is the velocity of propagation of the wave. Thus Equations (1) and (2) are actually wave propagation equations and are appropriately named the shallow-water wave equations.

The characteristic Equations (10) have a well-known interpretation as regards unsteady open-channel flow in the subcritical regime. Stoker [1957] discusses quite thoroughly the theory of characteristics as applied to this regime. The interpretation for supercritical flow is not nearly as well known and there are some important differences that modify the techniques used to numerically integrate the equations. The primary differences are in the required boundary conditions and the effect of the occurrence of discontinuities. The following discussion of these differences is patterned somewhat after Stoker's treatment of the theory for subcritical flow.

There are four boundary conditions required for the solution of Equations (10). Two are the initial or starting conditions in which the

flow must be completely specified at time zero. These two conditions, y(x,0) and V(x,0), are required for solution in either regime. The other two boundary conditions, however, are depth or velocity hydrographs which are specified at different locations depending upon the regime of flow. In subcritical flow one of the hydrograph boundary conditions, y(0,t) or V(0,t) or a relationship between them, must be specified upstream. The other boundary condition, y(L,t) or V(L,t) or a relationship between them, is specified at a downstream location. In supercritical flow both the hydrograph conditions y(0,t) and V(0,t) must be specified upstream, since a shallow-water wave cannot propagate upstream. The two families of characteristic curves (Eqn. 11) therefore fill the x,t-plane differently for the two regimes (Fig. 2). That is, if the flow is subcritical ($\mathbb{F} < 1$), the C2 family ($dx/dt = V-c$) is generally negatively sloped (Fig. 2a); whereas if it is supercritical ($\mathbb{F} > 1$), the C2 family is positively sloped (Fig. 2b).*

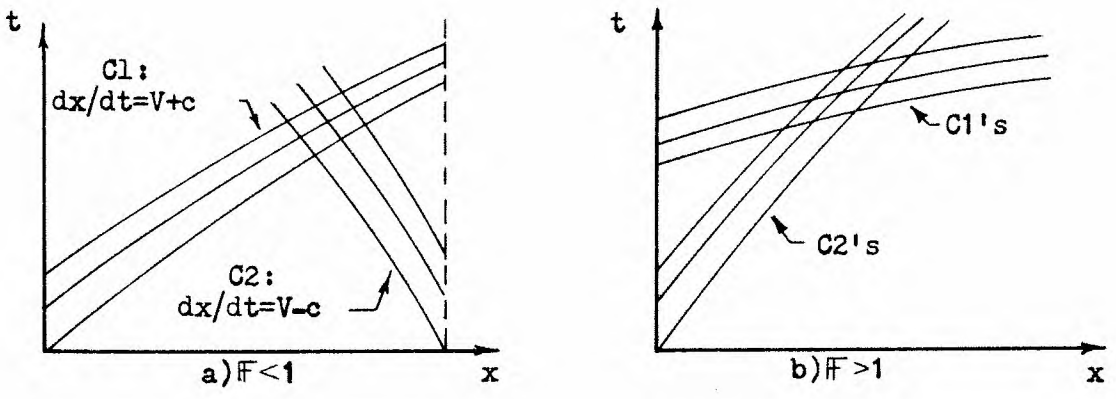

Figure 2. Families of Characteristic Curves for Subcritical and Supercritical Flow

*It is assumed throughout this study that V is never negative or zero. Also the Froude number is defined for the rectangular channel as $\mathbb{F} = V/c$, where $c = (gy)^{\frac{1}{2}}$.

Furthermore, the notions of range of influence and domain of determinacy are interpreted differently for the two regimes (Figs. 3 and 4). That is, the range of influence of a point Q in subcritical flow (Fig. 3) includes points both upstream and downstream of Q between the bounding characteristics while an equivalent point in supercritical flow (Fig. 4) influences only points downstream of Q. Similarly, a point R in subcritical flow is influenced by points on the domain of dependence lying both upstream and downstream of R while the equivalent point R in supercritical flow is influenced only by points lying upstream of R.

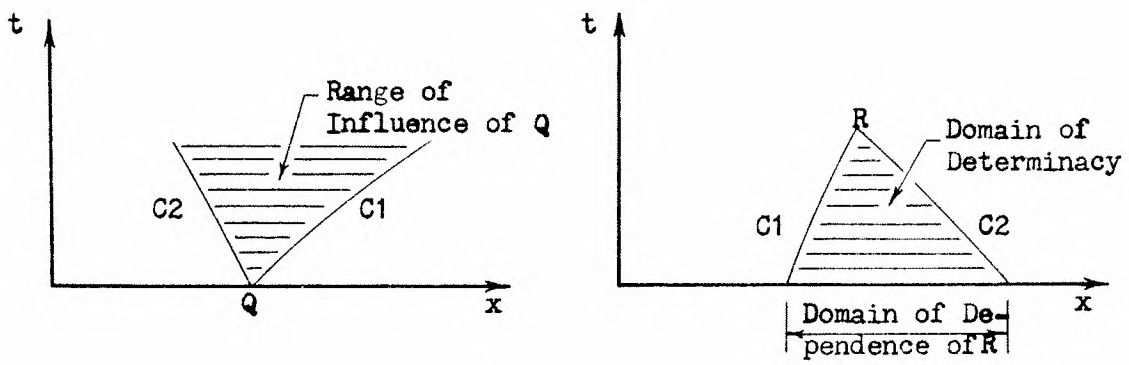

Figure 3. Range of Influence and Domain of Dependence for Subcritical Flow

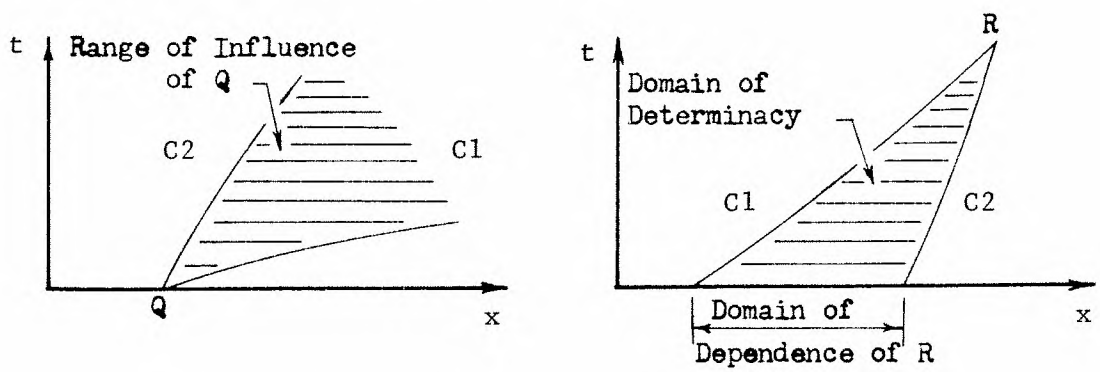

Figure 4. Range of Influence and Domain of Dependence for Supercritical Flow

In view of the foregoing discussion of the properties of characteristic curves the four boundary conditions can be interpreted as defining the domains of dependence on the x,t-plane. In subcritical flow, the bounding C1 characteristic between the initial and the upstream conditions and the bounding C2 characteristic between the initial and the downstream conditions divide the plane into four different zones (Fig. 5). In zone 1 the values of y and V are influenced only by the initial boundary conditions. In zone 2 they are influenced by both the initial and the downstream conditions. In zone 3 they are influenced by both the initial and upstream conditions. Finally in zone 4 they are influenced by all four boundary conditions.

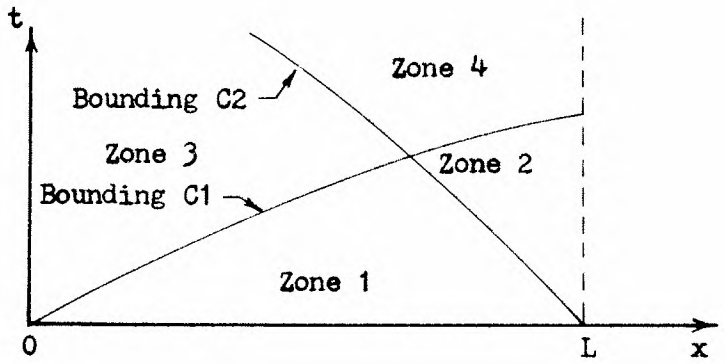

Figure 5. Zones of Influence for Boundary Conditions in Subcritical Flow

In supercritical flow only three zones are delimited because both of the hydrograph boundary conditions are specified upstream (Fig. 6). Thus in zone 1, as in subcritical flow, the solution is influenced only by the initial conditions. In zone 2 it is influenced only by the two

upstream conditions. In zone 3 it is influenced by all four boundary conditions. Since zones 1 and 2 are independent of each other, it is readily apparent that in supercritical flow the solutions can be obtained in either of these zones independently. The same remark cannot be made for subcritical flow because none of the zones 2, 3, or 4 is completely independent of the initial boundary conditions as is zone 2 in the supercritical regime. If the methods of numerical solution for supercritical flow are to be drawn from the experience in subcritical flow, the foregoing fundamental differences should be taken into account.

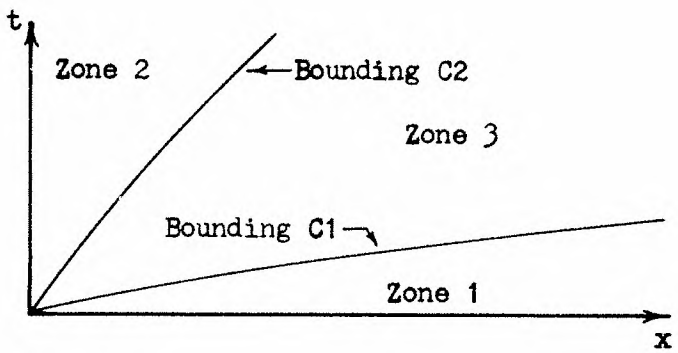

Figure 6. Zones of Influence for Boundary Conditions in Supercritical Flow

According to the theory of characteristics, a solution breaks down when characteristics of the same family intersect. In certain cases for supercritical flow, however, the boundary conditions are such that intersection is inevitable and the result is the formation of a shock discontinuity better known in hydraulics as bore or surge formation. Whether a numerical solution actually breaks down or not is dependent

upon the regime of flow, the severity of the boundary conditions, and the particular finite-difference method used. Again there are qualitative differences between the two regimes which can modify the basic approach to solution. For instance, the occurrence of discontinuities, or shock conditions, is considerably more predictable in supercritical flow because y and V are completely specified on the upstream t-axis (i.e. $y(0,t)$ and $V(0,t)$, allowing the computation of the slope of the characteristic along this axis. Take for example the slope of the C1 characteristics, $dt/dx = 1/V+c$; if the quantity $V+c$ increases with time along the t-axis, the characteristic slopes correspondingly decrease resulting eventually in the convergence and crossing of curves (Fig. 7) to form a shock discontinuity. The term rising hydrograph is used to describe the type of boundary condition which results in an increasing $V+c$.

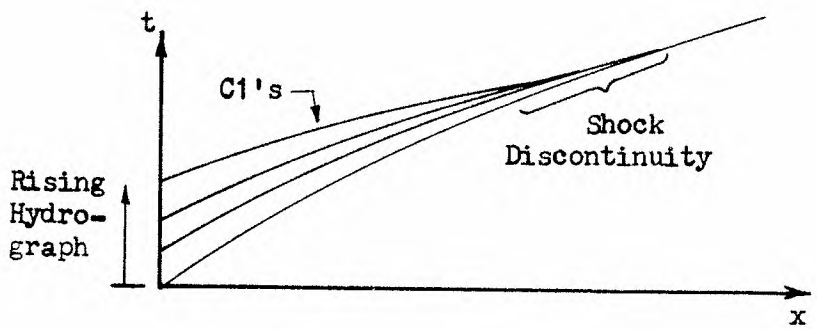

Figure 7. Shock Discontinuity Resulting from a Rising Hydrograph

Since only one condition, $y(0,t)$ or $V(0,t)$, is specified either upstream or downstream in subcritical flow, the slopes of the characteristic cannot be calculated in advance as they can in supercritical flow. In fact, the

shocks which occur in subcritical flow are usually the result of the interaction of all four boundary conditions and are therefore quite difficult to predict in any case.

In supercritical flow a shock discontinuity cannot occur as a result of a downstream control condition unless the control forces a change in regime. If this happens, the result is the occurrence of a bore, or a moving hydraulic jump. Generally, this is a predictable event since it is relatively easy to determine in advance whether or not the sequent depth will be exceeded downstream. Again, this predictability can modify and perhaps simplify the numerical approach for supercritical flow as compared to subcritical flow.

CHAPTER III

FINITE-DIFFERENCE SCHEMES

Since most classical mathematical methods are only useful for linear differential equations, there have not been many closed-form solutions to the basically nonlinear shallow-water wave equations. As shown by Lamb [1932] and Baltzer and Shen [1961] the classical solutions that are available are based upon linearizing assumptions as well as a frequent neglecting of friction. A great variety of finite-difference schemes have been employed to solve these equations either in their original form or in the characteristic form. An excellent summary of these methods is given by Liggett and Woolhiser [1967], in which the great majority of the work is directed toward the subcritical regime. In this study, the complete equations are solved approximately by numerical methods in which the digital computer is employed to carry out the myriad calculations required. The present investigation is primarily concerned with the numerical solution of the characteristic form of Equations (1) and (2) in the supercritical regime. Two finite-difference methods of solution which have been used for subcritical flow are introduced here along with the modifications required for application to supercritical flow. In addition to the presentation of the two methods of solution, there is a discussion of certain related aspects of stability.

Finite-Difference Approximation

The finite-difference approximation used here was described originally by Lister in Ralston and Wilf [1960] for the solution of the compressible gas dynamics equations which are mathematically analogous to the shallow-water wave equations [Stoker, 1957]. Two finite-difference approximations are described by Lister. The first one, which is used here, is a linear approximation while the second is based upon the trapezoidal rule formula, which is a second-order approximation. The linear approximation was applied to Equations (10) and (11) by Streeter and Wylie [1967], while the second-order approximation was applied to another form of the shallow-water wave equations by Liggett and Woolhiser [1967]. The linear approximation is used here because it offers the primary advantage of simplicity. The linear equations that result from this approximation can be solved algebraically to obtain the unknowns directly. The second-order approximation yields a set of nonlinear equations which must be solved iteratively, usually requiring considerably more programming effort and machine time.

Lister furthermore describes two different methods of solution using either the linear or the second-order finite-difference approximation; namely, the method of specified time intervals and the grid of characteristics. Streeter and Wylie [1967] used both methods in conjunction with the linear approximation while Liggett and Woolhiser [1967] used only the grid of characteristics in conjunction with the second-order approximation. In this study the two methods of solution are applied to the equations which result from the linear approximation.

The finite-difference scheme is based upon the following integration rule,

$$\int_{x_o}^{x_1} f(x)\, dx = f(x_o)(x_1 - x_o) + E(x) \qquad (12)$$

in which $E(x)$ is the error of the approximation. This rule is applied to the total derivatives in the two Equations (10) which are directed along the C1 and C2 characteristics given by Equations (11). Allowing P to be the intersection of C1 and C2 characteristics passing through points R and S, as shown in Figure 8,

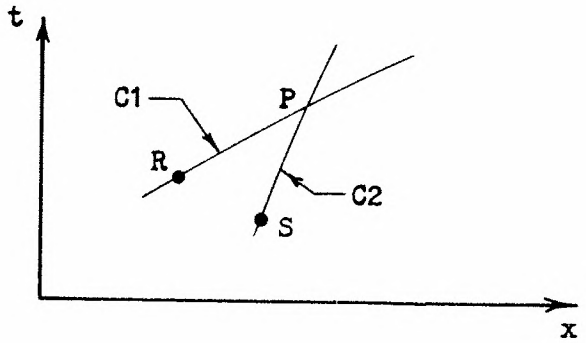

Figure 8. Illustration of the Intersection of Characteristics at the Unknown Point P, which is Determined from Known Points R and S Using the Difference Equations

and assuming that x_R, x_S, t_R, t_S, V_R, V_S, y_R, and y_S are known and that x_p, t_p, y_p, and V_P are to be found, the linear approximation (12) to the set of Equations (10) and (11) is obtained as follows:

$$\int_{t_R}^{t_P} \left[\frac{dV}{dt} + \lambda \frac{dy}{dt} + g\,(S_f - S_o)\right] dt = V_P - V_R + \lambda\,(y_P - y_R) \qquad (13)$$

$$+ g\,(S_f - S_o)_R\,(t_P - t_R) \approx 0$$

$$\int_{t_R}^{t_P} \left[\frac{dx}{dt} - (V + c)\right] dt = x_P - x_R - (V + c)_R\,(t_P - t_R) \approx 0 \qquad (14)$$

$$\int_{t_S}^{t_P} \left[\frac{dV}{dt} - \lambda \frac{dy}{dt} + g\,(S_f - S_o)\right] dt = V_P - V_S - \lambda\,(y_P - y_S) \qquad (15)$$

$$+ g\,(S_f - S_o)_S\,(t_P - t_S) \approx 0$$

$$\int_{t_S}^{t_P} \left[\frac{dx}{dt} - (V - c)\right] dt = x_P - x_S - (V - c)_S\,(t_P - t_S) \approx 0 \qquad (16)$$

where y_R is the value of y at point R, etc. Equations (13-16) are the finite difference equivalent of Equations (10-11). They are a linear system of four equations in four unknowns and can be solved simultaneously. Each of these equations can be shown to be approximately equal to zero because of the smallness of the error term E(x) associated with the numerical integration rule (12). For Equation (12) the error term* can be

---

*This error term is derived in Conte [1965]. The integration rule (12) is called the rectangular rule approximation and is a Newton-Cotes open type formula. It is the least accurate and simplest of the Newton-Cotes formulas. The open-type formulas are useful when the functional value of the upper limit of the integrand is unknown as is the case here. This formula (12) is often used to provide initial values to the more accurate second-order integration rules (e.g., trapezoidal rule, which is a closed type Newton-Cotes formula) which require iterative techniques for solution since the upper limit is unknown. An interesting study might be to use the Newton-Cotes open-type formula of second-order accuracy,

$$\int_{x_o}^{x_3} f(x)\,dx = \frac{3\,\Delta x}{2}\,(f(x_1) + f(x_2)) + \frac{f''(\xi)\,\Delta x^3}{4} \qquad (17)$$

(continued)

shown to be

$$E(x) = \frac{(x_1 - x_o)^2}{2} f'(\xi) \qquad x_o < \xi < x_1 \tag{18}$$

For Equations (13) and (14) the error is,

$$E(t) = \frac{(t_P - t_R)^2}{2} f'(\xi) \qquad t_R < \xi < t_P \tag{19}$$

For Equations (15) and (16) it is,

$$E(t) = \frac{(t_P - t_S)^2}{2} f'(\xi) \qquad t_S < \xi < t_P \tag{20}$$

If Equation (12) is used to integrate along the C1 characteristic over N equal Δt time intervals (Fig. 9) such as R_1-R_2, R_2-R_3, etc., the expression for the total error of the individual error terms is,

$$E_N(t) = \frac{(t_P - t_{R_1})\,\Delta t}{2} f'(\xi) \qquad t_{R_1} < \xi < t_P \tag{21}$$

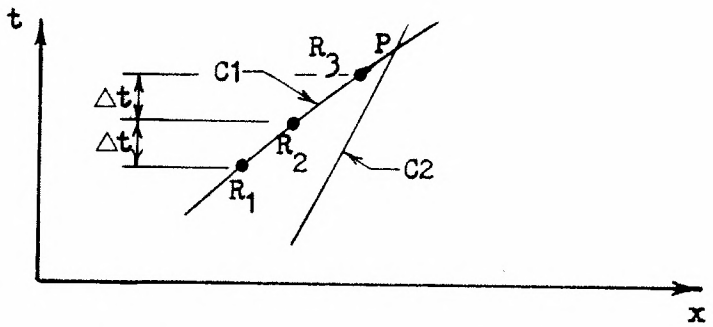

Figure 9. Integration Along a C1 Characteristic

---

which would give second-order accuracy yet still allow simple simultaneous solution of Equations (10-11).

Therefore, as the number of intervals, N, is increased, the error term will approach zero linearly. The error term for the trapezoidal rule can be shown to converge quadratically so that it takes approximately $N^{\frac{1}{2}}$ as many intervals to get the same accuracy as the first-order approximation. These deficiencies in the first-order approximation may, however, be offset by the physical requirement that the flow be gradually-varied unsteady. On the other hand, in rapidly-varied flow regions where the shallow-water wave equations do not apply, the first-order finite-difference approximation is likely also inaccurate.

Characteristics Grid Method of Solution

In this method the solution is carried out along the actual characteristic curves in the x,t-plane.

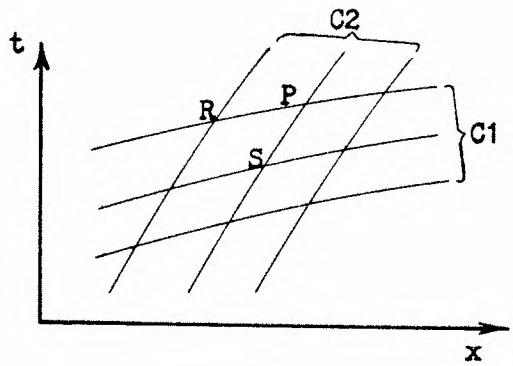

Figure 10. Solution by the Characteristics Grid Method

In Figure 10, the solution at R and S is known from initial conditions or from previous computation. The point P is determined by simultaneous solution of the Equations (13-16) as follows:

$$t_P = \frac{x_S - x_R + t_R (V_R + c_R) - t_S (V_S - c_S)}{V_R + c_R - V_S + c_S} \tag{22}$$

$$x_P = x_R + (V_R + c_R)(t_P - t_R) \tag{23}$$

$$y_P = \frac{V_R - V_S + c_R + c_S - g (S_R - S_o)(t_P - t_R) + g (S_S - S_o)(t_P - t_S)}{(g/y_R)^{\frac{1}{2}} + (g/y_S)^{\frac{1}{2}}} \tag{24}$$

$$V_P = V_R - (g/y_R)^{\frac{1}{2}} (y_P - y_R) - g (S_R - S_o)(t_P - t_R) \tag{25}$$

in which S_R is the friction slope evaluated at point R and S_S is the friction slope evaluated at point S.

The computation proceeds from known values to unknown values in a predetermined orderly fashion until the x,t-plane is filled with an uneven distribution of grid points. The computation is very rapid and efficient because each point satisfies exactly the Courant condition* for stability. Unfortunately, the results are not as useful in the unevenly distributed form. The values of y and V must be interpolated to get useful information such as the variation of y, or V, with time at a given location or the variation of y, or V, along the channel at a given time.

Another difficulty with this method lies in the specification of boundary conditions when working with supercritical flow. The difficulty is in choosing the proper spacing of known points on the x- and t-axis and an orderly scheme for progressing from the known points to the unknown

---

*The necessary condition for stability, $dt \leqq dx/V+c$.

points so that the solution adequately covers the x,t-plane. The situation is illustrated in Figure 11,

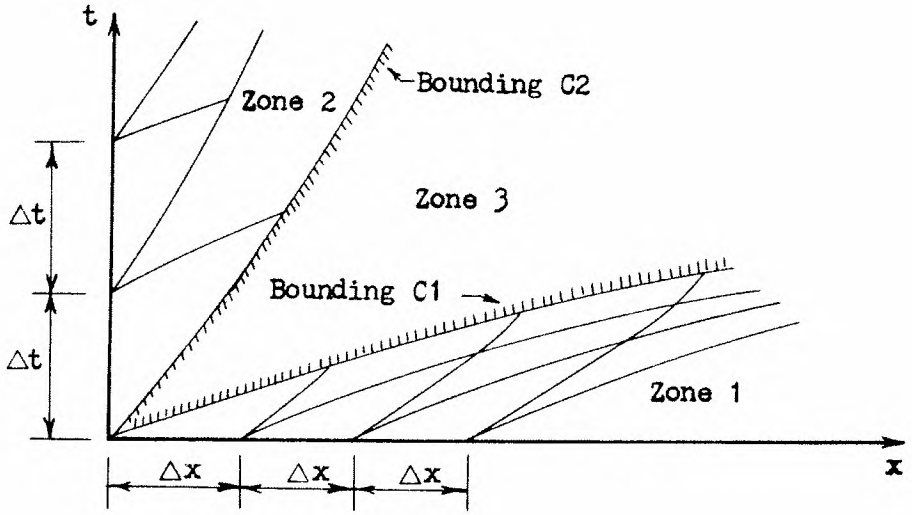

Figure 11. Effect of Boundary Conditions for the Characteristics Grid Method

in which the boundary values are specified at an evenly distributed set of points on the x- and t-axis. Since the solution progresses along the characteristics starting from the given boundary points, the resulting grid pattern may be "loose" or "tight" depending upon the size of Δx and Δt. If Δx and Δt are too large, the resulting numerical solution progresses rapidly but may be inaccurate because of the loose spacing. If they are too small, the numerical solution may take too much computer time to be economical. Since the characteristics are curved, it is difficult to predict in advance how "loose" or "tight" the grid pattern will be for a particular problem. A final difficulty with this method is that, as discussed previously, the solutions in zones 1 and 2 are independent

of each other. The boundary spacing Δx for zone 1 may therefore be incompatible with the boundary spacing Δt for zone 2 to obtain a solution for zone 3. In order to advance the solution into zone 3, the numerical solution must therefore include a method to determine a proper relationship between Δx and Δt. The characteristics grid method of solution thus presents some very serious programming difficulties in that neither the sizes of Δx and Δt nor the proper relationship between them can be determined a priori.

The modification of using average friction slopes instead of S_R and S_S was tested for this method. This modification is described in Appendix A.

Fixed Grid Method of Solution*

In this method the values of V and y are presumed to be known on a predetermined fixed spatial grid at time T (Fig. 12), such as represented by A,B,C,...., etc. The values are known either from the initial conditions or as a result of a previous stage of computations. The values of y and V are to be found on the grid points of the line $T+\Delta t$. Thus the values x_p and t_p are known for the typical point P on $T+\Delta t$, as shown in Figure 12, while the values y_p and V_p are to be found. The C1 and C2 characteristics through P intersect the T line at unknown points R and S which can be found by applying a linear interpolation from the known values at points A and C as follows.

---

*Called the method of specified time intervals by Lister [Ralston and Wilf, 1960] and by Streeter and Wylie [1967].

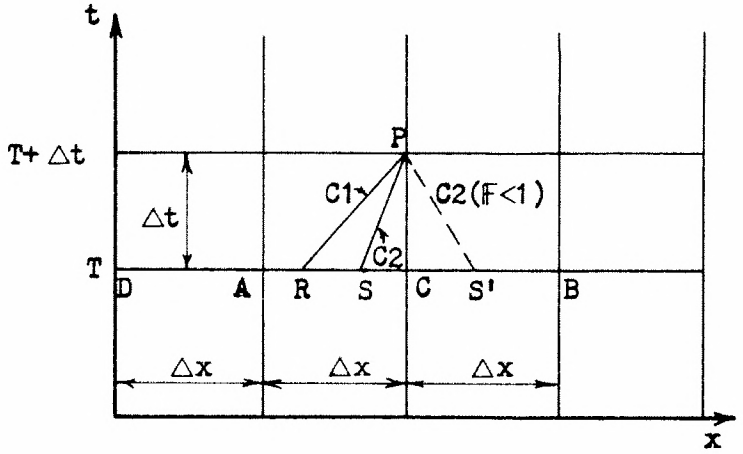

Figure 12. Solution by the Fixed Grid Method

The C1 characteristic (Eqn. 14) gives the x-coordinate of R as,

$$x_R = x_P - (V_R + c_R)\ \Delta t \tag{26}$$

A linear interpolation along the x-axis gives the values of y_R and V_R as

$$\frac{y_C - y_R}{y_C - y_A} = \frac{x_C - x_R}{x_C - x_A} \tag{27}$$

and

$$\frac{V_C - V_R}{V_C - V_A} = \frac{x_C - x_R}{x_C - x_A} \tag{28}$$

Equations (26-28) can be solved for y_R, V_R, and x_R. The correct root of the resulting quadratic equation in y_R is given by

$$y_R = \tfrac{1}{2}\chi^2 - \psi - \chi \left|\left(\frac{\chi^2}{4} - \psi\right)^{\frac{1}{2}}\right| \tag{29}$$

where

$$\chi = g^{\frac{1}{2}} \left[\frac{\theta \, (y_C - y_A)}{1 + \theta \, (V_C - V_A)} \right] \tag{30}$$

$$\psi = \frac{\theta \, V_C \, (y_C - y_A)}{1 + \theta \, (V_C - V_A)} \tag{31}$$

and

$$\theta = \frac{\Delta t}{\Delta x} \tag{32}$$

Then

$$V_R = \frac{V_C - (V_C - V_A)\theta(gy_R)^{\frac{1}{2}}}{1 + \theta \, (V_C - V_A)} \tag{33}$$

and x_R can be found directly from Equation (26). The values x_S, y_S, and V_S are found in a similar manner using the difference Equation (16) of the C2 characteristic. Thus,

$$x_S = x_P - (V_S - c_S) \, \Delta t \tag{34}$$

$$\frac{y_C - y_S}{y_C - y_A} = \frac{x_C - x_S}{x_C - x_A} \tag{35}$$

$$\frac{V_C - V_S}{V_C - V_A} = \frac{x_C - x_S}{x_C - x_A} \tag{36}$$

These three equations are solved simultaneously for y_S to yield the root of the quadratic equation,

$$y_S = \frac{\chi^2}{2} - \psi + \chi \left| \left(\frac{\chi^2}{4} - \psi \right)^{\frac{1}{2}} \right| \tag{37}$$

Then

$$V_S = \frac{V_C + (V_C - V_A)\theta(gy_S)^{\frac{1}{2}}}{1 + \theta \, (V_C - V_A)} \tag{38}$$

and x_S is found from Equation (34). It has been assumed that the slopes of the characteristics are straight lines given by (V_R+c_R) and (V_S-c_S).

The values of y_P and v_P can now be found by solving simultaneously the difference Equations (13) and (15) as follows:

$$y_P = \frac{V_R - V_S + g\,(S_S - S_R)\,\Delta t + c_R + c_S}{(g/y_R)^{\frac{1}{2}} + (g/y_S)^{\frac{1}{2}}} \tag{39}$$

and

$$V_P = V_R - (g/y_R)^{\frac{1}{2}}\,(y_P - y_R) - g\,(S_R - S_o)\,\Delta t \tag{40}$$

The computation proceeds as follows:

1) The Δx and the number of spatial grid points are established.

2) The initial conditions are specified for each grid point, that is, $y(n\Delta x,0)$ and $V(n\Delta x,0)$, $n=0,1,2,3,\ldots N$, in which N is the number of grid points.

3) The solution is then advanced to all but the first grid point of the next level $(T+\Delta t)$ using Equations (26-40). The Δt is determined by the Courant condition

$$\Delta t = \frac{\Delta x}{V+c} \tag{41}$$

This criterion, which is usually necessary for stability, is computed for each grid point of the known level T. The minimum value of the Δt for level T is used in Equations (26-40) so that every grid point on the unknown level will lie within the region of determinacy of level T.

4) When the solution is advanced to $T+\Delta t$, the values of y and V for the first grid point $(n=0)$ are determined from the specified upstream boundary condition functions $y(0,t)$ and $V(0,t)$.

This basic method can be modified to obtain greater accuracy in the solution. Two modifications were tested in this study to determine whether or not they offered any advantages over the basic method. The first was the substitution of a three-point interpolation for the two-

point interpolation given by Equations (27), (28), (35), and (36). In this modification the additional point D (Fig. 12) was used to get a quadratic instead of a linear interpolation of the values y_R, V_R, y_S, and V_S. The equations are derived in Appendix B.

The second modification was the substitution of the average friction slope between points P and R and points P and S for the friction slopes S_R and S_S used in Equations (39) and (40). The resulting equations are presented in Appendix C.

A technique was devised whereby a solution by the Fixed Grid method could be checked to determine whether or not continuity was being satisfied. The technique involves an accounting procedure in which running totals of storage and net inflow are kept for each Δx reach for each Δt time increment of the numerical solution. In the computer programs for the Fixed Grid method listed in Appendix D the values of storage and net inflow are computed for each Δx reach after the computation of all values of y_P and V_P for the time level $T+\Delta t$ (Fig. 12). The volume storage for each reach and for a single Δt increment is computed from the average of the endpoint depths as shown in Figure 13. Similarly, the net volume inflow for the reach during the time period Δt is computed from the average values of discharge passing through the end sections of the Δx reach as shown. These values are then accumulated for each reach for the duration of the run. The values of storage and net inflow are only linear approximations and may therefore be in error if the water surface has a large curvature between grid points. Since the shallow-water wave equations are also limited to flows having small curvatures, the linear approximation should be adequate for the continuity computation.

The check then involves the comparison of the accumulated storage and net inflow for each Δx reach. If these values are not equal for a reach, continuity is not being satisfied in the transient solution.

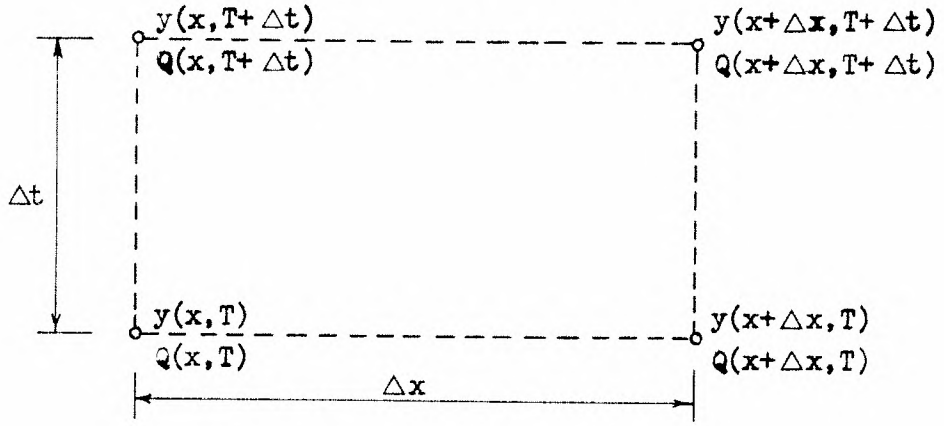

$$\text{Volume Storage} = B\Delta x \left[\frac{y(x,T+\Delta t) + y(x+\Delta x,T+\Delta t)}{2} - \frac{y(x,T) + y(x+\Delta x,T)}{2}\right]$$

$$\text{Net Volume Inflow} = \Delta t\left[\frac{Q(x,T) + Q(x,T+\Delta t)}{2} - \frac{Q(x+\Delta x,T) + Q(x+\Delta x,T+\Delta t)}{2}\right]$$

Figure 13. Storage and Net Inflow Computations for a Single Reach and a Single Time Increment

Stability Considerations

Precise and rigorous stability criteria for various difference schemes applied to nonlinear hyperbolic differential equations are not available. Thorough discussions of stability of this type of equation are contained in Richtmyer and Morton [1967], and in Godunov and Ryabenki [1964], in which the derived stability criteria are based upon linearizing

assumptions and are therefore deficient from a practical point of view. It is, however, unwise to promote a particular difference scheme without giving thought to the accuracy and stability of the scheme, as pointed out by Liggett and Woolhiser [1967]. They found that the Courant condition is a necessary but not sufficient condition for stability. In some of the schemes they investigated the Courant condition was satisfied but the difference scheme was unstable. They also found that the second-order difference scheme (trapezoidal rule) applied to the characteristics equations using the Characteristics Grid method was generally the most stable method when tested empirically for stability.

Another important aspect of stability is the effect that the friction germ, gS_f, has in damping both physical and numerical solutions. Perkins [1968] discusses the role of this term when considering the stability of a numerical solution. He points out the work of others who have shown that the friction assumption can either act to improve or to reduce the stability of a difference scheme. He furthermore derives from a linearized equation a stability criterion which includes the damping term. The use of this criterion helped to stabilize a flood-routing scheme developed by the Flood Control Branch of the Tennessee Valley Authority.

In this study numerical (empirical) stability experiments were conducted on the solutions by the Fixed Grid method. The results of these investigations are discussed in the following. The experiments essentially consisted of: 1) perturbing a steady state solution and observing the growth or attenuation of this disturbance with time, and 2) observing whether or not continuity is satisfied over a long period of time in a transient solution.

CHAPTER IV

TESTING OF NUMERICAL SCHEMES

The two methods of solution, the Fixed Grid and the Characteristics Grid, were programmed in Fortran V for solution on the Univac 1108 computer. A number of hypothetical unsteady, supercritical flow problems were posed for solution in order to determine the efficiency, stability, accuracy, and range of applicability of each of the methods. The results for many of these runs were graphed by the Calcomp plotter and are presented in the following. The Calcomp reads and plots digitized data from a magnetic tape recording which is created by the Univac 1108 during the solution of a problem. The characteristics of a solution can be conveniently determined by means of the graphs. Hence, the necessity of analyzing many pages of printed output is virtually eliminated.

Fixed Grid Method

Of the two schemes the Fixed Grid method was tested more extensively in this study. There were two fundamentally different series of computer runs programmed for this method. The first, Series AS, was devised empirically to test the stability of the method. In this series the two initial boundary conditions, $y(n\Delta x,0)$ and $V(n\Delta x,0)$, were specified in the following manner. A uniform flow depth was first calculated by trial-and-error from a given discharge and slope. The uniform flow velocity was then calculated using the relation $V=Q/A$. Finally, at each grid point $n\Delta x$, the initial depth was set equal to the calculated uniform

flow depth while the initial velocity was set equal to the uniform flow velocity. The two upstream hydrograph boundary conditions, $y(0,t)$ and $V(0,t)$, were not variable with time but rather were held constant at the initial uniform flow values, $y(0,0)$ and $V(0,0)$, for the duration of the run. At a specified time and location such as at point C in Figure 12, the depth was suddenly increased or decreased by 10 percent to create a single perturbation in the flow profile which propagates downstream. If this disturbance, which propagates only downstream, attenuated with time, the solution was considered stable; whereas if it amplified with time it was considered unstable.

The second series of runs, Series AL, was devised to analyze the effects of varying the input parameters under specified unsteady upstream boundary conditions. For this series a uniform flow was specified for all $y(n\Delta x,0)$ and $V(n\Delta x,0)$ in the same manner as described for Series AS. The two upstream hydrograph boundary conditions, however, were variable with time. That is, $y(0,t)$ and $Q(0,t)$ were each varied linearly from the initial uniform flow values, $y(0,0)$ and $Q(0,0)$, to precomputed final uniform flow values, $y(0,\Delta T)$ and $Q(0,\Delta T)$, in which ΔT is the specified duration of the hydrographs. In each run the initial and final uniform flows were specified in such a manner that $y(0,t)$ and $Q(0,t)$ were either both rising or both falling for the duration, ΔT. This results in the propagation of either a single positive wave or a single negative wave downstream. By observing the effect of varying such input parameters as Δx, L, and ΔT upon this single wave the accuracy, efficiency, and applicability of the Fixed Grid method can be demonstrated.

In both series of runs, AS and AL, the four solution variations of the Fixed Grid method discussed earlier were tested; namely, 1) the two-point interpolation, 2) the two-point interpolation with averaged friction slopes, 3) the three-point interpolation, and 4) the three-point interpolation with averaged friction slopes. Computer program listings for Series AS and Series AL are given in Appendix D.

Results of the Stability Runs (Series AS)

In all, 46 stability runs were performed using six different input uniform flows. For 26 of the 46 runs, selected depth or velocity hydrographs and depth profiles were plotted directly by the Calcomp plotter. A sample of the graphs plotted for a stability run is shown in Figure 14. The title and legend in Figure 14a indicates the type of solution and identifies each of the nine graphs shown. In Figure 14a three depth hydrographs at locations x=80, 1000, and 2000 ft, respectively, are plotted. In each of these graphs every point computed at the particular location for the duration of the run (480 sec) is plotted so that none of the peaks in the hydrograph is inadvertently excluded. The peak in each hydrograph of Figure 14 is the result of the single, +10 percent depth perturbation of the uniform flow at x=80 ft and just prior to the solution at time level T=13.09 sec. That is, in Figure 12, if C is the 80 ft grid point and $T+\Delta t=13.09$ sec, the depth at C is perturbed by +10 percent just prior to the solution for point P. Hence, the depth at point P should be less than the full +10 percent change because of the required interpolations of depth for points R and S. The actual solution is therefore perturbed by somewhat less than 10 percent. For instance in Figure 14a, the hydrograph at x=80 ft indicates that the

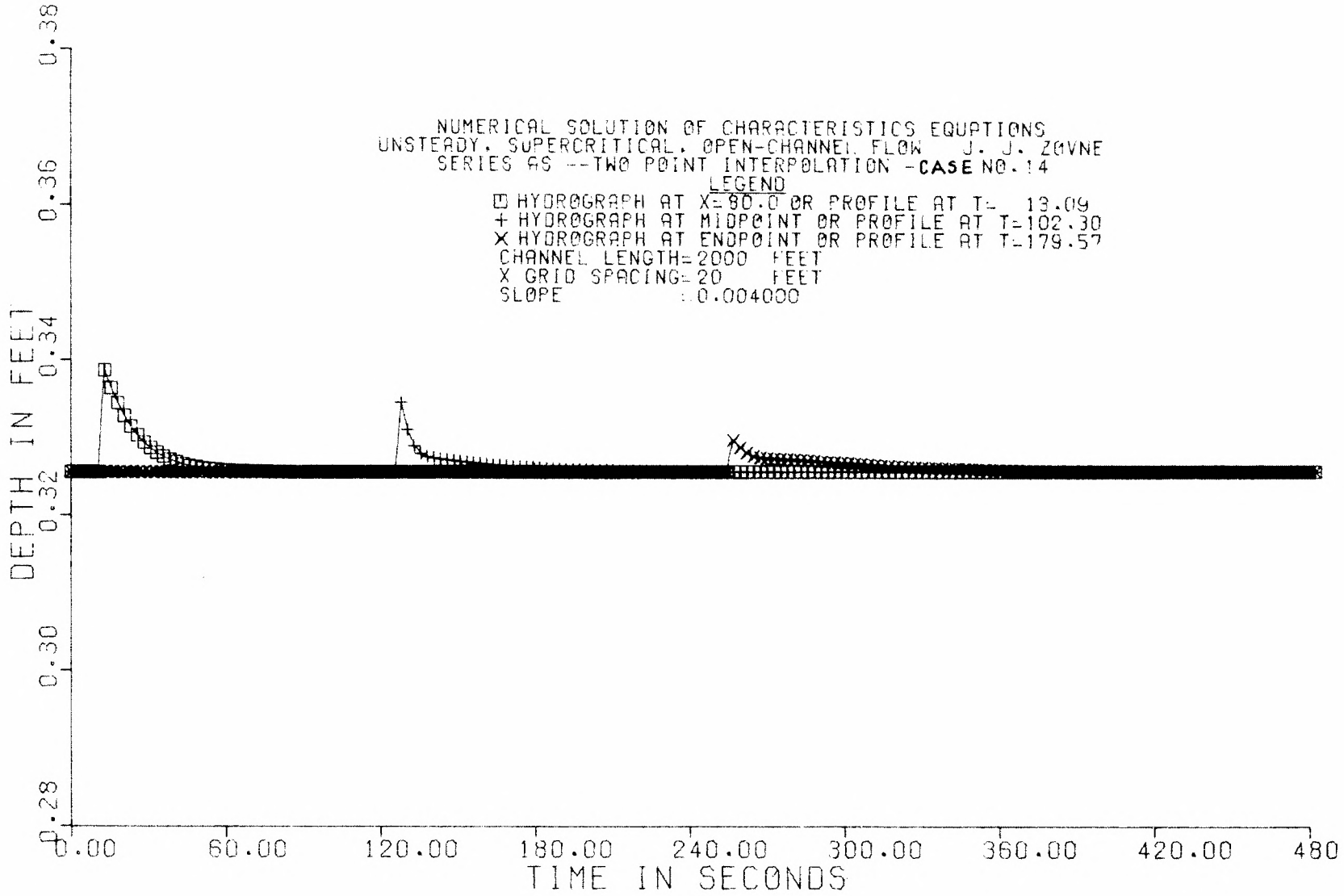

Figure 14a. Typical Calcomp Plotter Output for Case AS14 (Depth Hydrographs)

Figure 14b. Typical Calcomp Plotter Output for Case AS14 (Velocity Hydrographs)

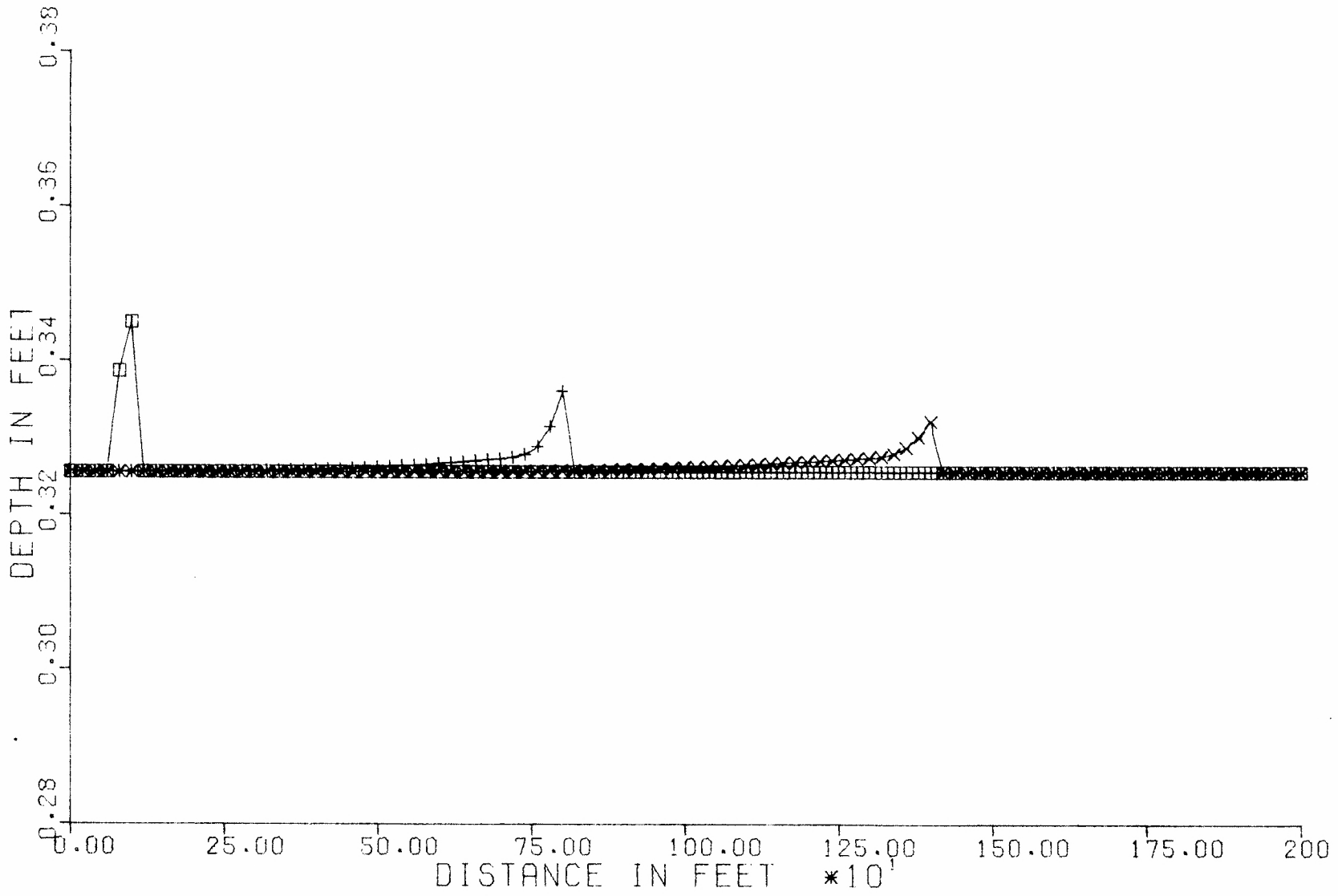

Figure 14c. Typical Calcomp Plotter Output for Case AS14 (Depth Profiles)

uniform flow is perturbed by only plus four percent. The size of the perturbation, however, is not the main issue, but rather the growth or attenuation of it as it propagates downstream. Since the solution shown in Figure 14a clearly attenuates with distance it is adjudged to be stable.

The reason for specifying the initial flow as a uniform flow may be demonstrated with reference to Figure 14a. First, the attenuation of the perturbation is immediately observable because each of the hydrograph peaks is referenced to the same uniform depth. Second, a stable solution such as that shown returns to the original uniform flow once the disturbance has passed. The convergence of the solution back to the uniform flow is an important aspect of numerical stability. If the initial flow were not uniform, this convergence would not be so readily observable.

Figure 14b reveals a perplexing aspect of the numerical solution. The velocity hydrograph at x=80 ft has a minus four percent disturbance as expected from continuity requirements of the plus four percent depth disturbance. Downstream, however, the velocity disturbance reverses to the positive side in an apparent violation of continuity. It will be shown later that this reversal is in fact a requirement for continuity.

The depth profiles are shown in Figure 14c for the entire channel (L=2000 ft) at three different times. The first profile at time T=13.09 sec shows the channel profile immediately after the +10 percent perturbation. It should be noted that two points are shown in the peak of this profile because both the 80 ft and 100 ft grid points would be affected by the disturbance at point C (Fig. 12). The profiles at later times show once again that the solution is stable and that the sharp peak is dispersing as it propagates downstream.

The case number in the title of Figure 14a (Case No. 14) refers to the input uniform flow conditions. As mentioned previously, six different uniform flows were used in the stability tests. The parameters of these cases are listed in Table 1. The Series AS computer runs for the uniform flow cases listed in Table 1 are presented in Table 2. The sets of runs in Table 2a are those for which Calcomp graphs were usually obtained to visualize and evaluate the stability of the runs for the different variations of the solution method. In Table 2b are the sets in which the solutions were checked for continuity. Since the continuity checks could not be obtained simultaneously with Calcomp graphs because of computer output limitations, the results of such runs were obtained separately.

Perturbation Propagation Tests. Sets I-VIII in Table 2a were run primarily to test whether or not the different variations in the solution method had any effect upon the stability of Cases AS9 - AS12. In Figure 15, the depth hydrographs at x=80, 1000, and 2000 ft are plotted for each of the solution variations of Case AS9 in Sets I-VIII. The amplitude of the disturbance is decreasing with time regardless of the solution type and there are only relatively minor differences between the five different solutions for this run. This case therefore exhibits stable behavior as did Case AS14 of Set XIII in Figure 14a. At least for these runs no advantage appears to be gained by programming the more accurate but time consuming solution methods. The propagation rate of the positive disturbance in Figure 15 can be calculated to be approximately 4.4 ft/sec while the propagation rate of the negative disturbance is approximately 4.2 ft/sec. Although the rates of propagation of these disturbances should

Table 1. List of Uniform Flows Used in Fixed Grid Stability Tests (Series AS)

Case No.	Uniform Depth y_u	Uniform Velocity V_u	Slope	Froude No. $F=\frac{V_u}{(gy_u)^{\frac{1}{2}}}$	Kinematic Viscosity ν	Reynolds No. $R=\frac{4R_uV_u}{\nu}$	Friction Factor f	Channel* Width B
	ft	ft/sec			$(ft^2/sec)x10^5$	$x10^{-5}$		ft
9	0.0911	2.605	0.0060	1.522	0.897	1.006	0.0197	3.487
10	0.3614	5.958	0.0060	1.748	0.897	7.953	0.0130	3.487
11	0.0889	3.869	0.0125	2.288	0.897	1.460	0.0182	3.487
12	0.1964	6.322	0.0125	2.515	0.897	4.976	0.0142	3.487
13	0.0785	1.828	0.0040	1.150	1.104	0.497	0.0231	3.487
14	0.3256	4.404	0.0040	1.361	1.104	4.378	0.0146	3.487

*Corresponds to the width of flume used in the bore propagation experiments.

Table 2. Series AS Computer Run List

a) Perturbation Propagation Tests

Set*	Type**	Case Nos.	Δx ft	L ft	Approximate computer time per run, Min	Comments
I	+2	9,10,11,12	20	2000	1.5	Cases 9,10 stable; 11,12 unstable.
II	-2	9,10,11,12	20	2000	-	Cases 9,10 stable; 11,12 unstable.
III	-4	9,10,11	20	2000	Case 10;1.9 Case 11;15+	Cases 9,10 stable; 11 unstable, no plot (Max. time).
VI	+1	9,10,11,12	20	2000	1.1	Cases 9,10 stable; 11,12 unstable.
VII	-3	10,11	20	2000	Case 10;1.2 Case 11;15+	Case 10 stable; Case 11 unstable.
VIII	-1	9,10,11,12	20	2000	1.1	Cases 10,11 stable; 11,12 unstable.
IX	-2	9	30	5280	3.5	Case 9 continues stable -1 mile.
X	+1-3%	9,10,11,12	20	2000	1.1	Small dist. does not make 11,12 stable.
XI	+1	9,10	2	200	1.0	Attenuates wave very quickly.
XII	+1	9,10,11,12	20	2000	1.0	Diff. pert. method used; no change.
XIII	+1	13,14	20	2000	1.2	Low F runs, very stable.

*The sets are sequenced in chronological order. Sets IV and V (+3 and +4 solutions) were not run.

**Type number refers to the variation of solution method used and the sign indicates either a + or -10 per cent perturbation. The solution types are numbered as follows: 1) two-point interpolation; 2) two-point interpolation with average friction slope; 3) three-point interpolation; 4) three-point interpolation with average friction slope.

b) Sets Specifically Run with Continuity Check

					Method of Perturbing flow	Comments
III	+1	9,10,11,12	20	2000	y_p (Q const.);after interpolation.	Continuity satisfied.
IV	+1	9,10,11,12	20	2000	y_p (V_p const.);after interpolation.	Continuity satisfied.
V	+1	9,10,11,12	20	2000	y_p (V_p const.);before interpolation.	Continuity satisfied.

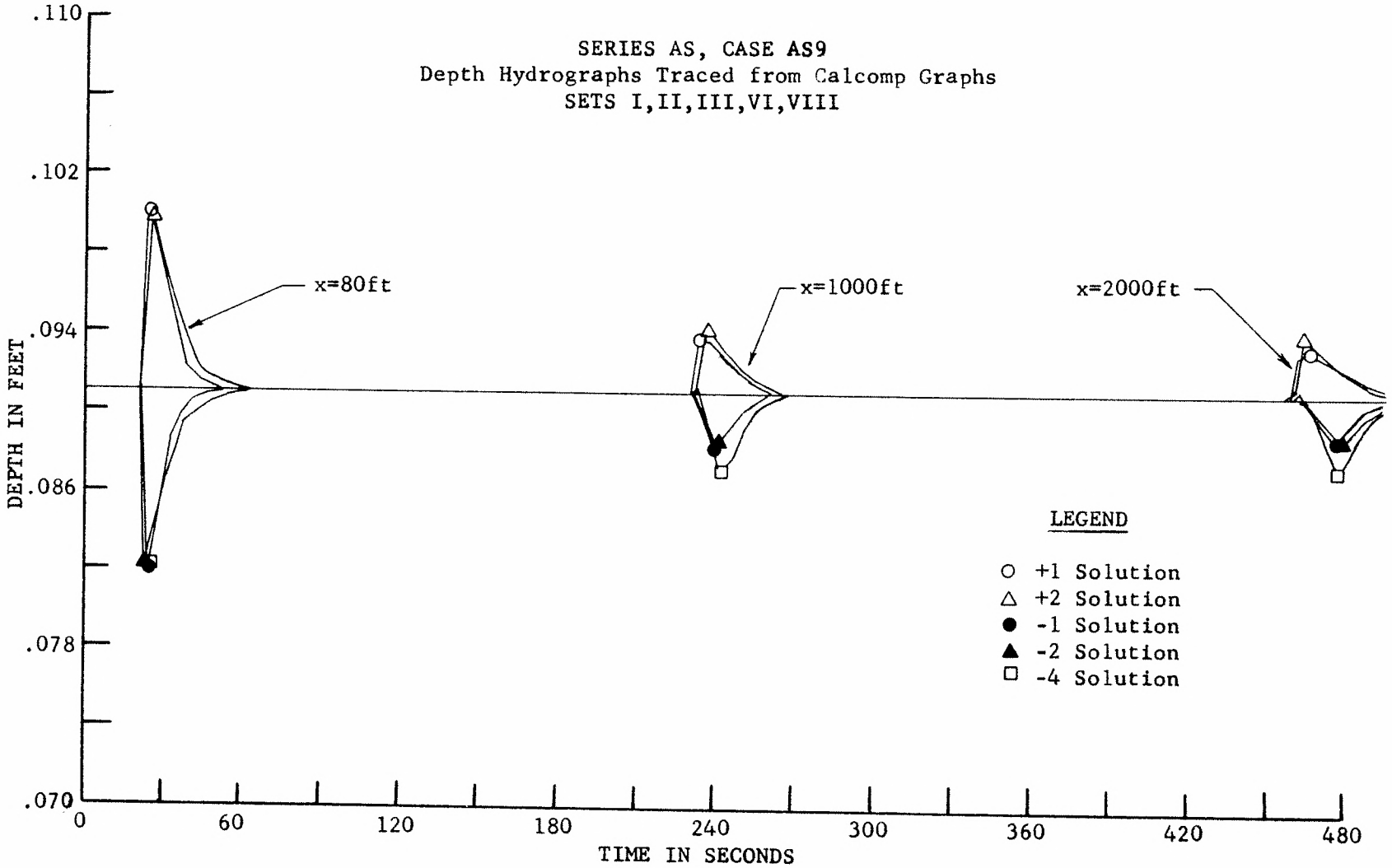

Figure 15. Comparison of Depth Hydrographs for Case AS9

be changing with distance because the amplitudes are attenuating with distance, they should be nearly equivalent to the propagation rate of an infinitesimal wave of the uniform flow. For this case the propagation rate of the uniform flow ($dx/dt=V_u+c_u$) is 4.3 ft/sec, which checks very well with the aforementioned values. This affords additional support for the conclusion that the simpler ±1 and ±2 solutions are sufficiently accurate.

Essentially the same results were obtained for Case AS10, as shown in Figure 16. This case does not appear to be as definitively stable because of the appearance of small disturbances ahead of the imposed disturbance. Since the amplitudes of all disturbances are attenuating, however, this case should perhaps be classed as being nominally stable.

A considerably different behavior resulted with Cases AS11 and AS12, which are shown in Figures 17 and 18. These cases are definitely unstable because of the rapid growth of the amplitudes as the disturbance propagates downstream and because of the rapid growth of additional perturbations with high amplitudes ahead of the main imposed disturbance. Six different solution types were used for Case AS11, including the more accurate minus three and minus four types. These later two solution types served only to increase the severity of the instability. In fact, the amplitudes increased so rapidly that negative depths were encountered shortly after the disturbance reached 1000 ft. When negative depths occur during the solution, the computer program automatically terminates before any of the data are plotted, hence, no Calcomp graphs were obtained for these solution types. Instead, the hydrographs for the x=1000 ft hydrographs were plotted in Figure 17 from printed output which was obtained

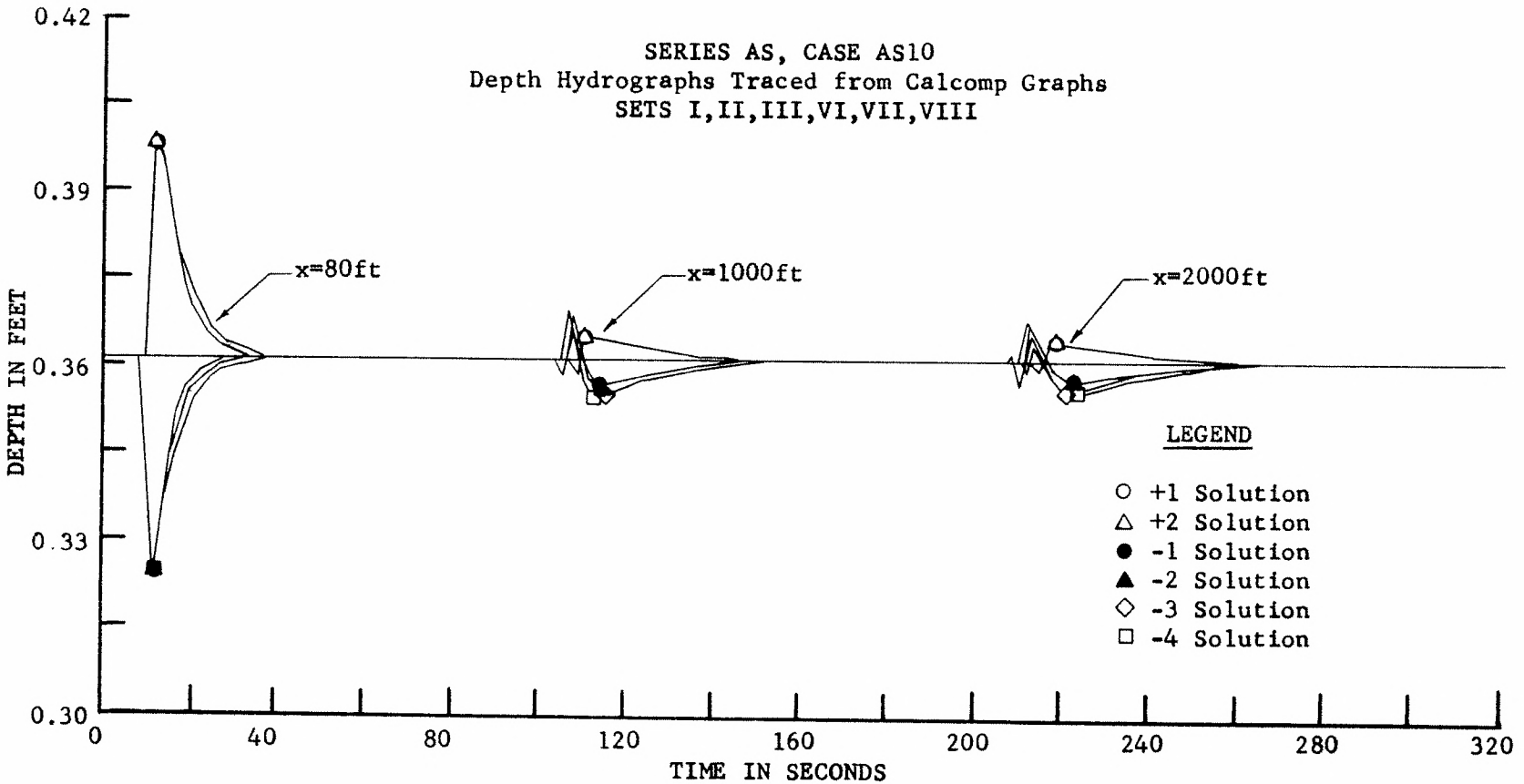

Figure 16. Comparison of Depth Hydrographs for Case AS10

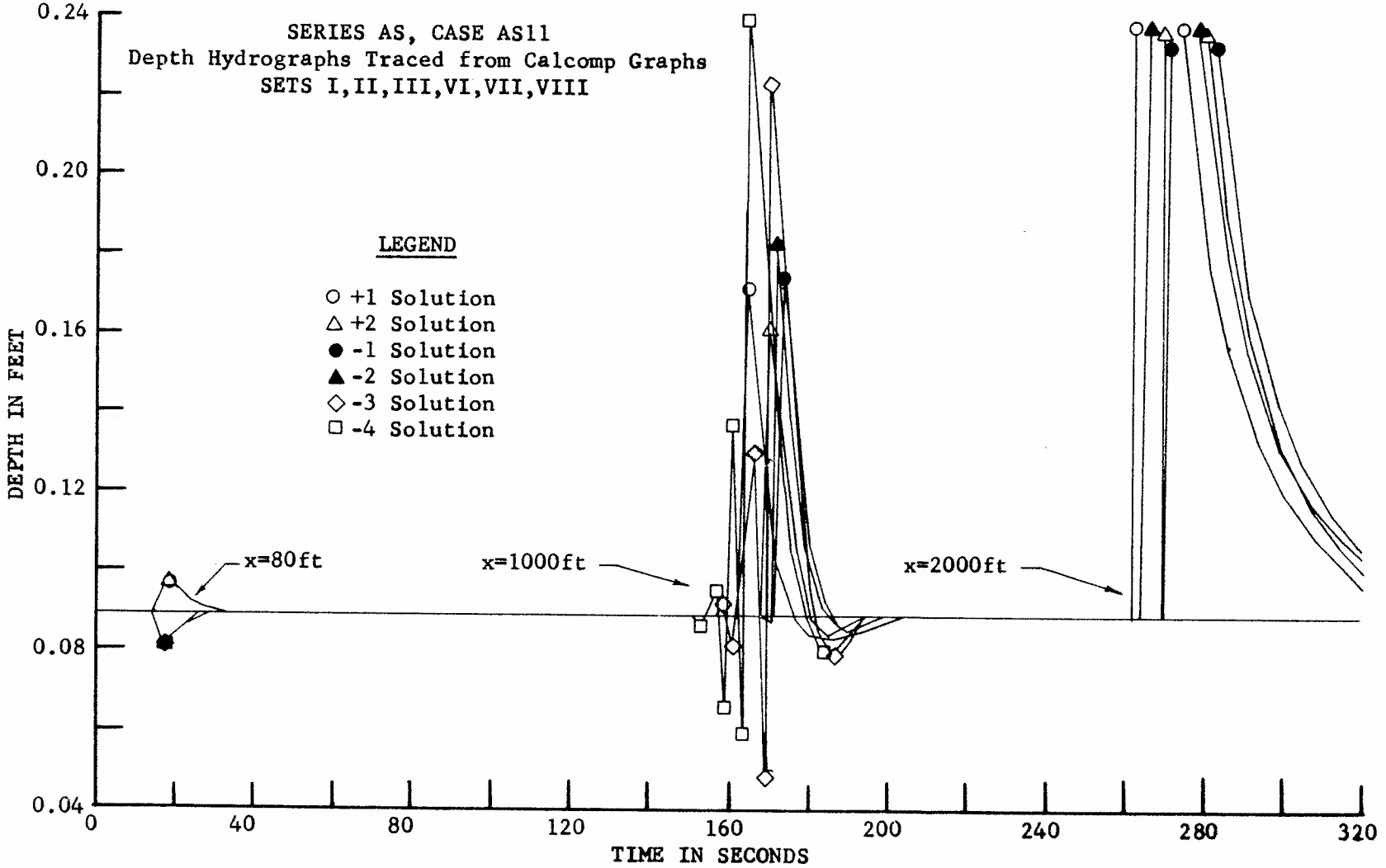

Figure 17. Comparison of Depth Hydrographs for Case AS11

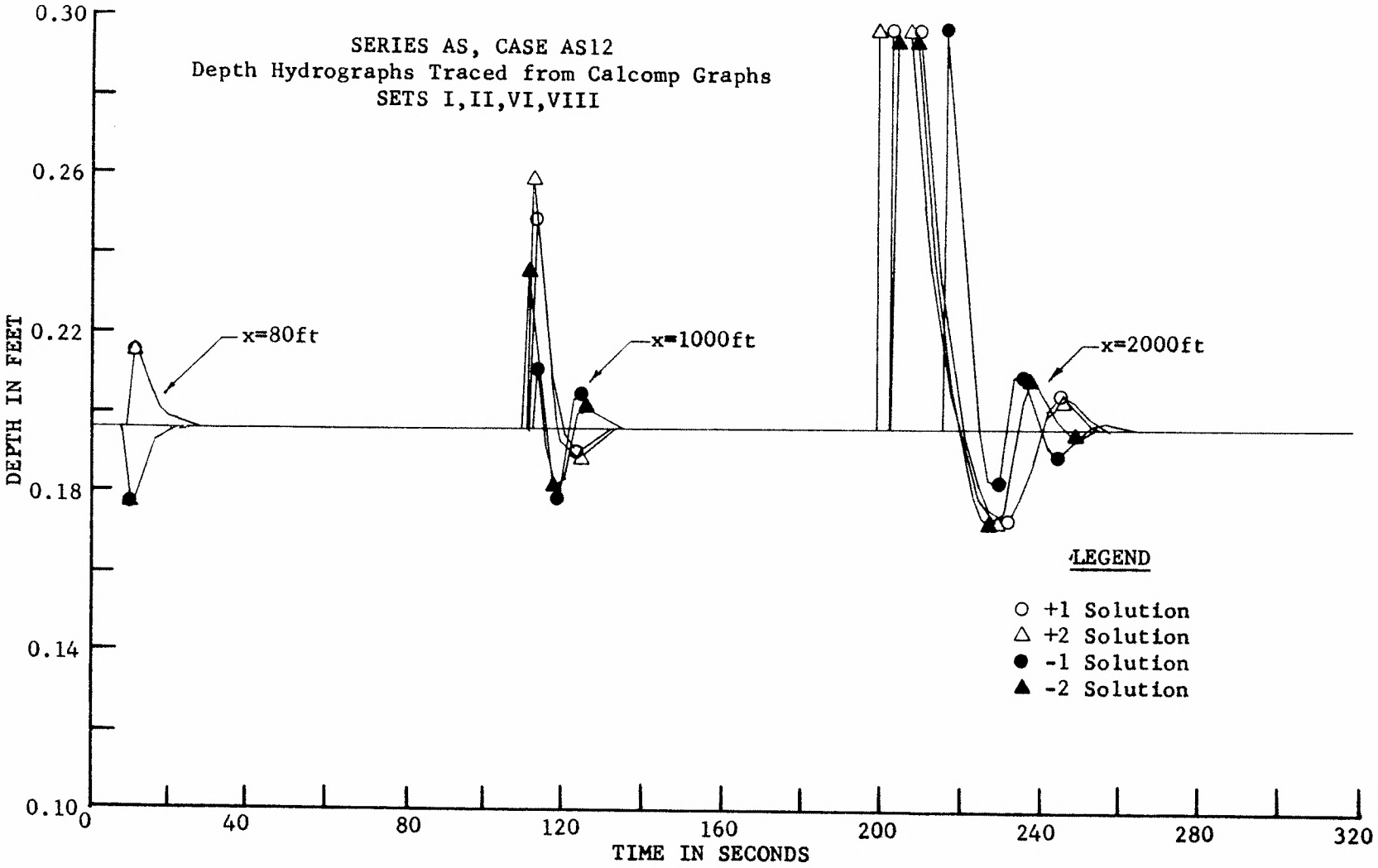

Figure 18. Comparison of Depth Hydrographs for Case AS12

for the minus three and minus four solutions up to the point of termination. Although the peaks of the x=2000 ft hydrographs could not be shown in Figure 17, the original Calcomp graphs reveal that the peaks occurred at approximately 0.45 ft. The more accurate solution types were not even attempted for Case AS12 after the problems encountered for Case AS11. Only the four simpler solution types (±1 and ±2) were run for this case. Although the results for Case AS13 are not exhibited here, it had the very same stable characteristics as Cases AS9 and AS14.

The entertaining question here is why Cases AS9, AS10, AS13, and AS14 were stable while cases AS11 and AS12 were unstable. As mentioned previously, the Courant condition for stability, $\Delta t \leq \Delta x/V+c$, was satisfied at each grid point for each Δt increment, which normally insures numerical stability. On the other hand, Perkins [1968] indicated that the Courant condition is insufficient to insure stability for an explicit scheme used by the Tennessee Valley Authority. He therefore proposed a modified Courant stability criterion that included a linearized friction term. The use of this criterion subsequently stabilized the TVA method. It is clear, however, that no generalized stability criteria for the complete nonlinear shallow-water wave equations with the friction term included are available, although, as mentioned earlier, Richtmyer and Morton [1967], and others, have proposed stability criteria for similar equations based upon linearizing assumptions. The preponderance of experience in using the Courant condition in conjunction with the method of characteristics [see Liggett and Woolhiser, 1967] shows that this stability criterion is generally sufficient to insure numerical stability. It was therefore assumed here, a priori, that the Courant

condition is sufficient to insure the stability of the Fixed Grid method of solution under discussion.

The instabilities encountered in Cases AS11 and AS12 are theorized here to be of a physical rather than a numerical origin. It is widely known in steady open-channel hydraulics that an imbalance between the gravitational and frictional forces results in an instability and the growth of roll waves for turbulent flow at high Reynolds numbers. As mentioned earlier, many investigators of this phenomenon have developed criteria for the prediction of the occurrence of roll waves. Iwasa [1954] derived a criterion by considering the momentum and continuity equations in a form similar to that used in this study.* The stability Froude number, F_S, given by Iwasa** for a uniform flow in a smooth, rectangular channel assuming $\beta=1+0.781f$ is

$$F \begin{bmatrix} \text{unstable} \\ \text{stable} \end{bmatrix} \gtrless F_S = \frac{1}{\left[\left\{\frac{1.303f^{\frac{1}{2}}+0.5}{\left(\frac{2}{B/y_u}\right)+1} - 0.781f\right\}^2 - 0.781f(1+0.781f)\right]^{\frac{1}{2}}} \qquad (42)$$

Koloseus and Davidian [1966] found experimentally from observations of 23 flows that the correlation between this stability criterion and the presence of roll waves was surprisingly good. They also concluded that

---

*With the exception that Iwasa retained the β velocity distribution factor and the $\cos\alpha$ term in the momentum equations.

**Iwasa derived the general form of this equation considering the time growth or decay of an infinitesimal wave using the Chezy representation of shear stress, τ_o. Koloseus and Davidian then derived Equation (42) using Iwasa's general equation and the logarithmic law of resistance (Eqn. 5).

unstable flows having $\mathbb{F}$ greater than $\mathbb{F}_S$ exhibited increased channel resistance over that for uniform flow and they gave experimental evidence that f is a function of both $\mathbb{F}$ and $\mathbb{R}$ for unstable flows in smooth channels.

The stability Froude numbers for Cases AS9-AS14 calculated from Equation (42) are given in Table 3.

Table 3. Stability Froude Numbers for Cases AS9-AS14

Case No.	B/y_u	f	$\mathbb{F}$	$\mathbb{F}_S$ Eqn.(42)	$\mathbb{F}_{S1}$ Eqn.(43)	Relative Degree of Instability
9	38.3	0.0197	1.52	1.61	1.54	0.99
10	9.65	0.0130	1.75	1.93	1.86	0.94
11	39.2	0.0182	2.29	1.61	1.55	1.48
12	17.7	0.0142	2.51	1.77	1.70	1.48
13	14.1	0.0231	1.15	1.56	1.50	0.77
14	10.7	0.0146	1.36	1.88	1.81	0.75

The $\mathbb{F}_{S1}$ stability Froude numbers in this table were computed from

$$\mathbb{F}_{S1} = \frac{1 + 2y_u/B}{1.303f^{\frac{1}{2}} + 0.5} \tag{43}$$

which was obtained by setting $\beta=1$ in Equation (42).

Equation (43) is Iwasa's stability criterion for the momentum equation used in this study. The stability Froude numbers give an approximate indication of whether or not the flows of Cases AS9-AS14 are physically stable. In the right-hand column in Table 3 the relative degree of instability for each case is listed. If the relative degree of instability

is less than unity, the flow is categorized as being stable, and if it is greater than unity, the flow is categorized as being unstable. According to this criterion, the flows of Cases AS9, AS10, AS13, and AS14 are physically stable and the flows of Cases AS11 and AS12 are physically unstable. It will be recalled that Cases AS9, AS10, AS13, and AS14 were also numerically stable, while Cases AS11 and AS12 were numerically unstable. Since the flows which are physically stable were also numerically stable and since the flows which are physically unstable were also numerically unstable, the instabilities observed in Figures 17 and 18 are thought to occur for physical rather than for numerical reasons.

In the numerical solution an artificial surface disturbance was imposed upon the uniform flow, whereas in a real flow surface disturbances are an inherent characteristic of turbulent supercritical flow. If a real flow is unstable, these surface disturbances will grow and eventually form roll waves. Since a supercritical flow with roll waves is two-dimensional, the shallow-water wave equations do not apply to this case. Hence, the artificially imposed disturbance in the numerical solution is not anticipated to develop into an actual roll wave. The amplitudes and wavelengths shown in Figures 17 and 18 are therefore not real and serve only to reveal the instability of the solution. Similarly, the amplitudes and wavelengths of the disturbances in the stable flows of Figures 14, 15, and 16 are unreal because the vertical accelerations associated with the abrupt disturbance of the surface are neglected in the numerical solution. The primary function of these stability tests was not to simulate a real flow, but rather to severely test the numerical stability of the Fixed Grid method of solution. Without the supporting information of the

stability Froude numbers for supercritical flow, the results in Figures 14-18 would have been interpreted differently. That is, the method of solution would have been declared unstable and an investigation might have been performed to modify the Courant condition to obtain stability. If one would desire to investigate the development of roll waves numerically, a two-dimensional representation of the momentum equation would probably be required.

Continuity Tests. The continuity tests were run to clarify the reasons for the velocity reversals observed in all of the runs listed in Table 2a. In each of the three sets of continuity tests listed in Table 2b a different method of perturbing the flow is indicated. In Set III the uniform flow was perturbed at x=80 ft immediately after the interpolation for all grid points at T=23.16 sec. For this set y was perturbed by +10 percent while V was computed from the perturbed y and the uniform flow discharge Q_u. This method of perturbing the flow was used in Sets I-XI of Table 2a (with the exception that in several cases y was perturbed by -10 percent). When the flow is perturbed in this manner, the effect is to add channel storage which represents the volume of water contained in the perturbation. This is more clearly seen in Figure 19 which shows schematically the perturbation storage for Case AS9. The volume contained in the perturbation (B=3.49 ft) can be computed to be 0.635 ft^3. Since the discharge is invariant from x=60 to x=100 ft, there is no net inflow or outflow for the perturbation. Thus, the uniform flow discharge is initially unaffected. As the perturbation propagates downstream, the volume of storage within the attenuating perturbation should remain constant while, in order to satisfy continuity, the net inflow to

or outflow from the perturbation for each Δt increment should remain zero. At T=100.4 sec the perturbation volume stored for Case AS9 was 0.690 ft^3, while the net inflow was negligible (0.00002 ft^3). The nine percent increase in perturbation volume over that put into the channel is perhaps attributable to the linear approximation of the water surface curvature.

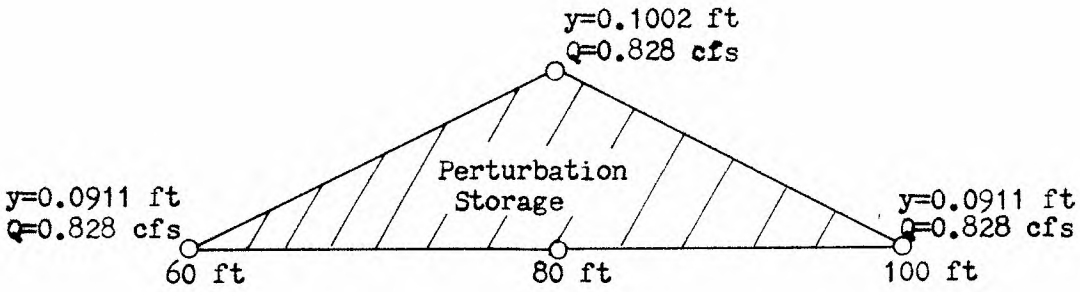

Figure 19. Perturbation Storage for Case AS9

The printed results show that most of this increase occurs in the first two Δt increments after T=23.16 sec. Thereafter the increase is less rapid. The results for Case AS10 were similar. The initial perturbation volume for this case was 2.520 ft^3 and the accumulated volume after 101.9 sec was 2.782 ft^3 corresponding to a net increase of 10 percent. The accumulated net inflow (or outflow) for this case was negligible at T=101.9 sec. The results of Cases AS9 and AS10 give at least some evidence that continuity is being satisfied in the numerical solution.

An explanation can now be forwarded with regard to the velocity reversals. When the +10 percent perturbation is placed upon the flow, the volume of the perturbation augments the uniform flow discharge. That is, if the perturbation attenuates downstream, the discharge within

the perturbation must always be greater than that for the uniform flow in order to account properly for the volume storage of the perturbation. In Table 4 the characteristics of the perturbation for two different time levels of Case AS9 are listed. For the time level T=32.31 sec the perturbation has propagated to station x=140 ft and the maximum depth of the perturbation has attenuated to 0.0952 ft. The discharges at the grid points within the perturbation are greater than the uniform flow discharge to reflect the additional volume flowing with the perturbation. The net volume outflow from the reach 60-100 ft, however, exactly balances the net inflow of the reach 100-140 ft during the Δt increment.* Hence, there is no net accumulated inflow (or outflow) for the 60-140 ft reach. This indicates that the volume of the perturbation is remaining constant, or similarly, that there is no net discharge into or out of the perturbation which would cause it to grow or attenuate. The attenuation of the perturbation for Case AS9 is therefore a result of the conservation of momentum rather than the conservation of mass. Only one of the velocities at T=32.31 sec is less than the uniform flow velocity and this velocity corresponds with the peak depth of the perturbation so that the discharge at this point (80 ft) is still larger than the uniform flow discharge. For the time level T=100.4 sec all velocities are greater than the uniform flow velocity. By this time the perturbation has attenuated enough so that all of the velocities must be greater than the uniform flow velocity in order to yield discharges greater than uniform flow discharge for every grid point within the perturbation. Hence, the velocity

*As readily determined from the computer printout.

Table 4. Characteristics of the Attenuated +10 Percent Perturbation for Two Time Levels for Case AS9

Time Level T=32.31 sec				Time Level T=100.4 sec			
Location ft	Depth ft	Velocity ft/sec	Discharge cfs	Location ft	Depth ft	Velocity ft/sec	Discharge cfs
60	0.0911 (Unif.)	2.605	0.828	240	0.0911 (Unif.)	2.605	0.828
80	0.0952	2.532	0.841	260	0.0912	2.606	0.828
100	0.0932	2.700	0.877	280	0.0912	2.606	0.829
120	0.0943	2.657	0.874	300	0.0913	2.608	0.830
140	0.0911(Unif.)	2.605	0.828	320	0.0914	2.611	0.832
				340	0.0917	2.616	0.837
				360	0.0922	2.625	0.844
				380	0.0930	2.639	0.855
				400	0.0939	2.657	0.870
				420	0.0941	2.660	0.873
				440	0.0911 (Unif.)	2.605	0.828

reversal is required to maintain a constant volume within the perturbation and does not therefore necessarily indicate a violation of continuity. Similar results were obtained for Case AS10 although this case was not as stable as Case AS9, as mentioned earlier.

The alternative perturbation methods indicated for Sets IV and V in Table 2b showed primarily that the velocity reversal was not a function of the manner in which the flow was perturbed. For Set IV the depth was perturbed by +10 percent after the interpolation, but the velocity rather than the discharge was held constant. This method is, however, quite similar to that for Set III in as much as a 0.635 ft^3 volume is added to the flow and the net volume inflow (or outflow) should be zero. A check of the program output for Case AS9 reveals that although the net inflows remain zero, the volume of storage within the perturbation has increased by 29 percent at T=103 sec. This volume increase is more than three times that for Set III which suggests that this perturbation method is perhaps undesirable. When the depth was perturbed by +10 percent prior to the interpolation (Table 2b, Set V), while keeping the velocity constant, the volume of storage within the perturbation had increased by 31 percent at T=103 sec. Sets XII and XIII of Table 2a were run using this method in order to obtain graphs for a comparison of methods. In Figure 20 the depth hydrographs by the two perturbation methods are compared for Case AS10. The characteristics of the propagation are considerably different when the depth is perturbed prior to the interpolation (holding the velocity constant) as compared to the condition for which the depth is perturbed after the interpolation (holding the discharge constant). The hydrograph at x=80 ft does not rise to the peak of 10

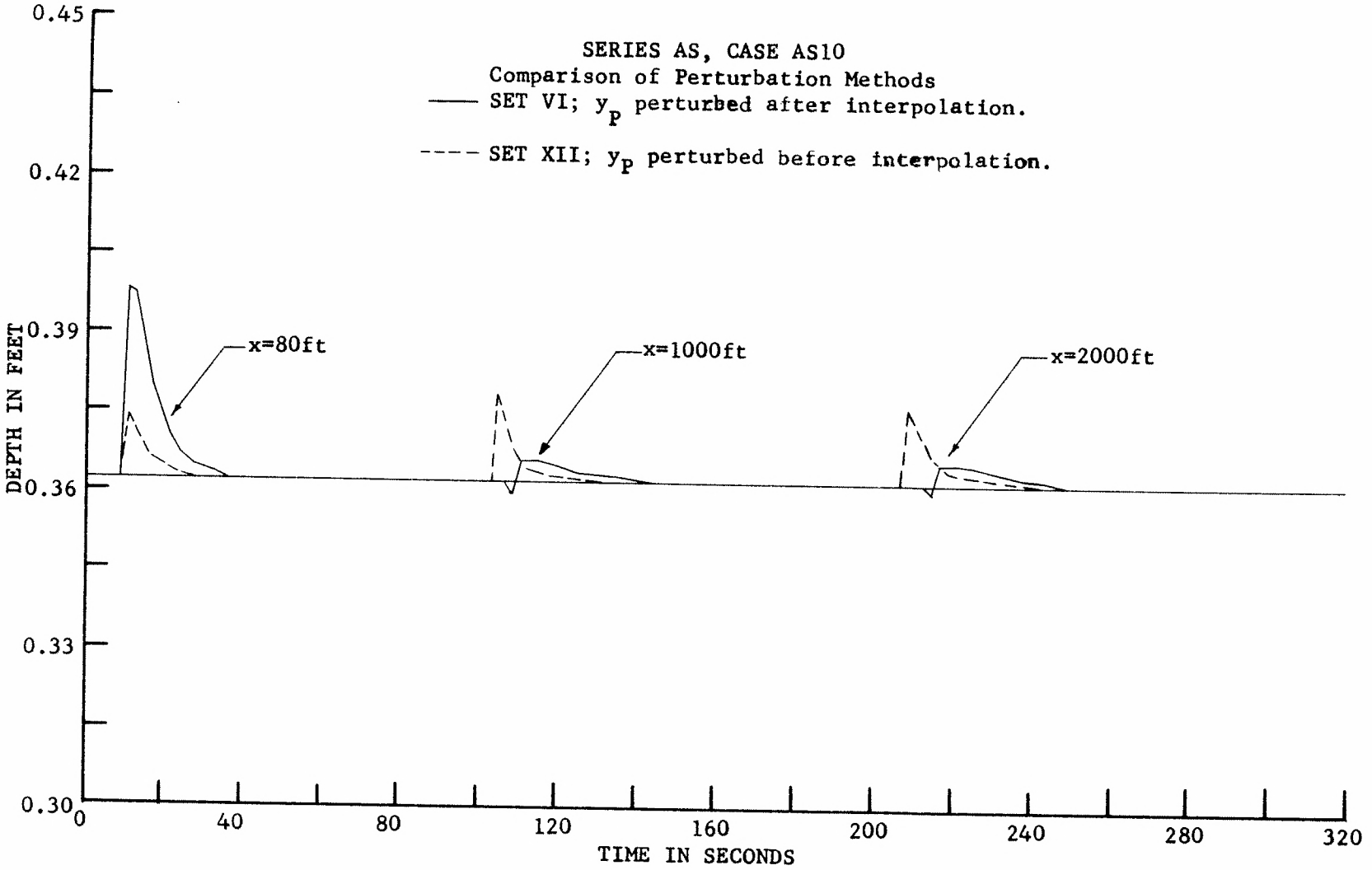

Figure 20. Comparison of Two Perturbation Methods for Case AS10

percent for Set XII because the depth is perturbed just prior to the interpolation. A peak of only about plus three percent is shown for this hydrograph. The peak then inexplicably rises (x=1000 ft) before it begins to attenuate (x=2000 ft). A similar comparison between methods for the unstable Case AS11 (Fig. 21) shows that the instability is apparently more severe when y is perturbed prior to interpolation. These results suggest this method of perturbing the depth is also undesirable.

Regardless of the perturbation method used the results pertaining to the stability and the velocity reversals were at least qualitatively, if not quantitatively, the same for each case tested. That is, Cases AS9 and AS10 were always stable and the velocities always reversed while Cases AS11 and AS12 were always unstable. Although the method of perturbation had little bearing upon the major results of the stability tests, the continuity tests at least revealed that some care should be exercised in choosing a method of perturbing the flow. In the present tests the most desirable method was to perturb the depth after the interpolation while holding the discharge constant.

Results of the Linearly Rising Hydrograph Runs (Series AL)

The initial and final uniform flows of the Series AL runs are listed in Table 5. When the upstream depth and discharge hydrographs rise linearly from the initial to the final flow, a positive wave propagates downstream. The odd-numbered Cases AL5, AL7, AL9, and AL11 (Table 5) are of this type. The even-numbered Cases AL6, AL8, AL10, and AL12 are of the type for which the hydrographs decrease from the initial to the final flow and a negative wave results. Note that the final uniform

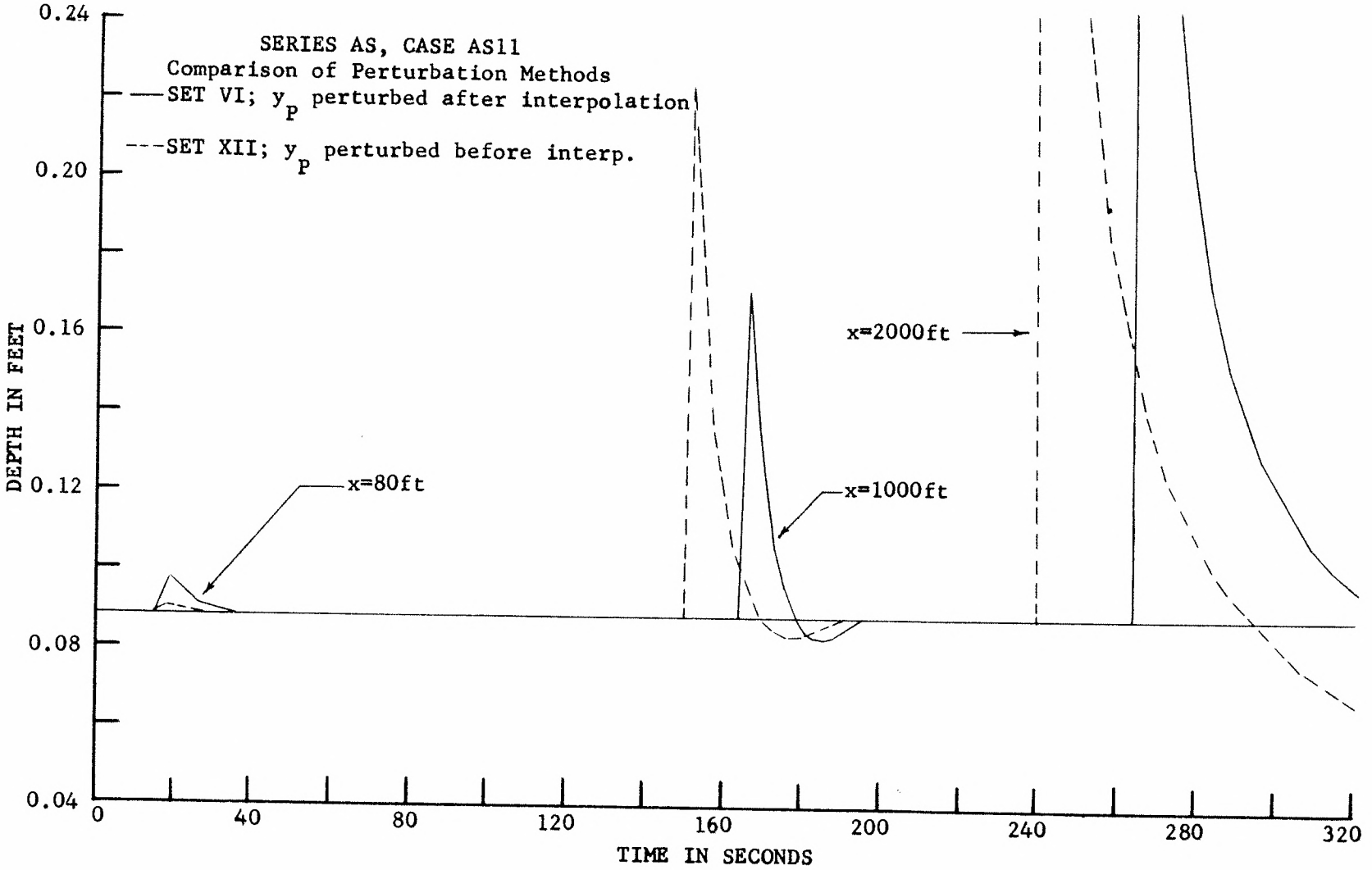

Figure 21. Comparison of Two Perturbation Methods for Case AS11

Table 5. Table of Initial and Final Uniform Flows Used in Linear Hydrograph Tests

Case No.	Initial Uniform Flow Parameters					Final Uniform Flow Parameters					Slope	ν	B
	y_u	V_u	F	R	f	y_u	V_u	F	R	f	S_o	$\frac{ft^2}{sec} \times 10^5$	
	ft.	fps		$\times 10^{-5}$		ft	fps		$\times 10^{-5}$				ft
5	0.0911	2.605	1.522	1.006	0.0197	0.3614	5.958	1.748	7.953	0.0130	0.0060	0.897	3.487
6	0.3614	5.958	1.748	7.953	0.0130	0.0911	2.605	1.522	1.006	0.0197	0.0060	0.897	3.487
7	0.0889	3.869	2.288	1.460	0.0182	0.1964	6.322	2.515	4.976	0.0142	0.0125	0.897	3.487
8	0.1964	6.322	2.515	4.976	0.0142	0.0889	3.869	2.288	1.460	0.0182	0.0125	0.897	3.487
9	0.0785	1.828	1.150	0.497	0.0231	0.3226	4.404	1.361	4.378	0.0146	0.0040	1.104	3.487
10	0.3256	4.404	1.361	4.378	0.0146	0.0785	1.828	1.150	0.497	0.0213	0.0040	1.104	3.487
11	0.0915	6.271	3.656	1.97	0.0171	0.1048	6.838	3.724	2.45	0.0163	0.030	1.104	3.487
12	0.1048	6.838	3.724	2.45	0.0163	0.0915	6.271	3.656	1.97	0.0171	0.030	1.104	3.487

flow of Case AL5 is the same as the initial uniform flow of Case AL6 which is true of the other Case pairs AL7-AL8, AL9-AL10, and AL11-AL12. Furthermore, the initial uniform flows of Cases AL5-AL10 correspond respectively to the uniform flows of the stability Cases AS9-AS14 (Table 1).

Wave Propagation Tests. The 66 runs of the Series AL tests are listed in Tables 6 and 7. In the sets of Table 6 the Cases AL5-AL8 were compared for the response of the wave propagation to changes in Δx, ΔT, and the method of solution. Only the simple two-point interpolation and the two-point interpolation with averaged friction slopes methods were used. The stability runs essentially proved that the three-point interpolation method of solution was unwarranted because of the large increase in computer time required for solution. The results of these preliminary runs are stated in Table 6.

The results of the preliminary runs initially suggested the necessity of conducting the stability tests because Cases AL7 and AL8 were consistently unstable whereas Cases AL5 and AL6 were consistently stable. Consequently, the uniform flows of Cases AL5-AL10 were checked for stability (Cases AS9-AS14, Table 1). After the stability tests, it became quite clear that the preliminary Series AL Cases AL5 and AL6 should have been stable, whereas Cases AL7 and AL8 should have been unstable.

The final Series AL runs (Table 7) were designed to give more information about the effect of grid spacing, Δx, the severity of the hydrograph rise time, ΔT, and the total length of the channel in question, L, upon the solution. Cases AL5, AL6, AL7, and AL8 of Set I were run to determine whether or not a greater distance of propagation (2000 ft as opposed to 1000 ft) would in any way alter the results of the preliminary

Table 6. Series AL Preliminary Runs List

Set*	Type	Case Nos.	Δx, ft	L, ft	ΔT, sec **	Approx. comp. time per run, min	Comments
VII	1	5,6,7,8	20	1000	5	0.6	These were preliminary runs to check the program and plot routines, varying the input parameters. For all Sets, Cases AL5 and AL6 were stable and Cases AL7 and AL8 were unstable. Varying Δx and ΔT and averaging the friction slopes did not stabilize Cases AL7 and AL8.
VIII	1	5,6,7,8	10	1000	5	2.0	
X	2	5,6,7,8	20	1000	5	0.7	
IX	2	5,6,7,8	10	1000	5	2.4	
III	1	5,6,7,8	20	1000	50	0.3	
XI	2	5,6,7,8	20	1000	50	---	
XIV	2	5,6,7,8	10	1000	50	2.4	
VI	1	5,6,7,8	20	1000	100	0.7	
XIII	1	5,6,7,8	10	1000	100	2.2	
XII	2	5,6,7,8	20	1000	100	1.5	
XV	2	5,6,7,8	10	1000	100	2.5	
I	1	5,6	20	2000	50	0.4	Continuity checks; stable solutions.
II	1	7,8	20	2000	50	1.1	Continuity checks; unstable solutions.

*Sets I,II, IV and V are not listed. In these, different methods of computing the input hydrographs and friction factor were tried. The sets listed are grouped according to the ΔT used.

** ΔT, the total time duration of the linear hydrograph should not be confused with Δt, the time increment of the transient solution as determined by the Courant condition.

Table 7. Series AL Final Runs List

Set	Type	Case Nos.	Δx, ft	L, ft	ΔT, sec	Approx. Comp. time/run, sec	Comments
I	2	5,6,7,8	20	2000	50	90	Used to obtain the final small plot representation for direct comparison.
II	2	8	40	4000	50	----	The instability continues to grow out to 4000 ft.
III	2	8	40	6000	50	----	The instability continues to grow with time and distance.
IV	1	9,10	20	2000	20	----	These runs with low F were very stable.
V	1	11,12	20	2000	100	90	These runs with high F were very stable.
VI	1	9,10	80	2000	20	16	These runs stable with larger spacing.
VII	1	9,10	200	2000	100	6	These runs unstable because of very large spacing.
VIII	1	9,10	100	2000	100	11	These runs stable. The 100 ft. spacing is optimal.
IX	1	9,10	20	2000	100	83	These runs compare favorably with set VIII.

runs. The Calcomp graphs for these runs were designed so that the results could be traced directly onto $8\frac{1}{2}$ by 11 paper. Some of the graphs for the sets listed in Table 7 are shown in Figures 22 to 26.

In Figure 22 the depth and velocity hydrographs are plotted for Case AL5. The depth and the velocity hydrograph at x=0 are the two specified boundary conditions. The velocity hydrograph is nonlinear because it is computed from the continuity relation, Q=ByV, in which the discharge and depth are linear with time. The depth profiles of Case AL5 shown in Figure 23 exhibit several important characteristics of the wave propagation. First, the profiles show very stable behavior from the standpoint of numerical stability. That is, the profiles have a continuous smooth transition from the initial uniform flow to the final uniform flow and there is no sign of the growth of numerical instabilities as shown previously for the stability runs. Both the initial and final uniform flows of this run are below the stability Froude numbers for these flows. Second, the wave front for the positive wave of Case AL5 becomes steeper with distance (or time) of propagation. This positive wave is a result of the rising hydrograph boundary conditions shown in Figure 22 and the fact that the C1 characteristics tend to form a shock discontinuity, as shown in Figure 7. That the numerical solution remains stable even though the wave front is steepening is certainly one of the more remarkable qualities of the Fixed Grid method of solution.

The wave of Case AL6 (Fig. 24) is negative. The attenuation (elongation) of this wave with time is a result of dampening provided by the friction term in the momentum equation. Since the form of the wave front is changing with time, this type of wave is sometimes termed as being

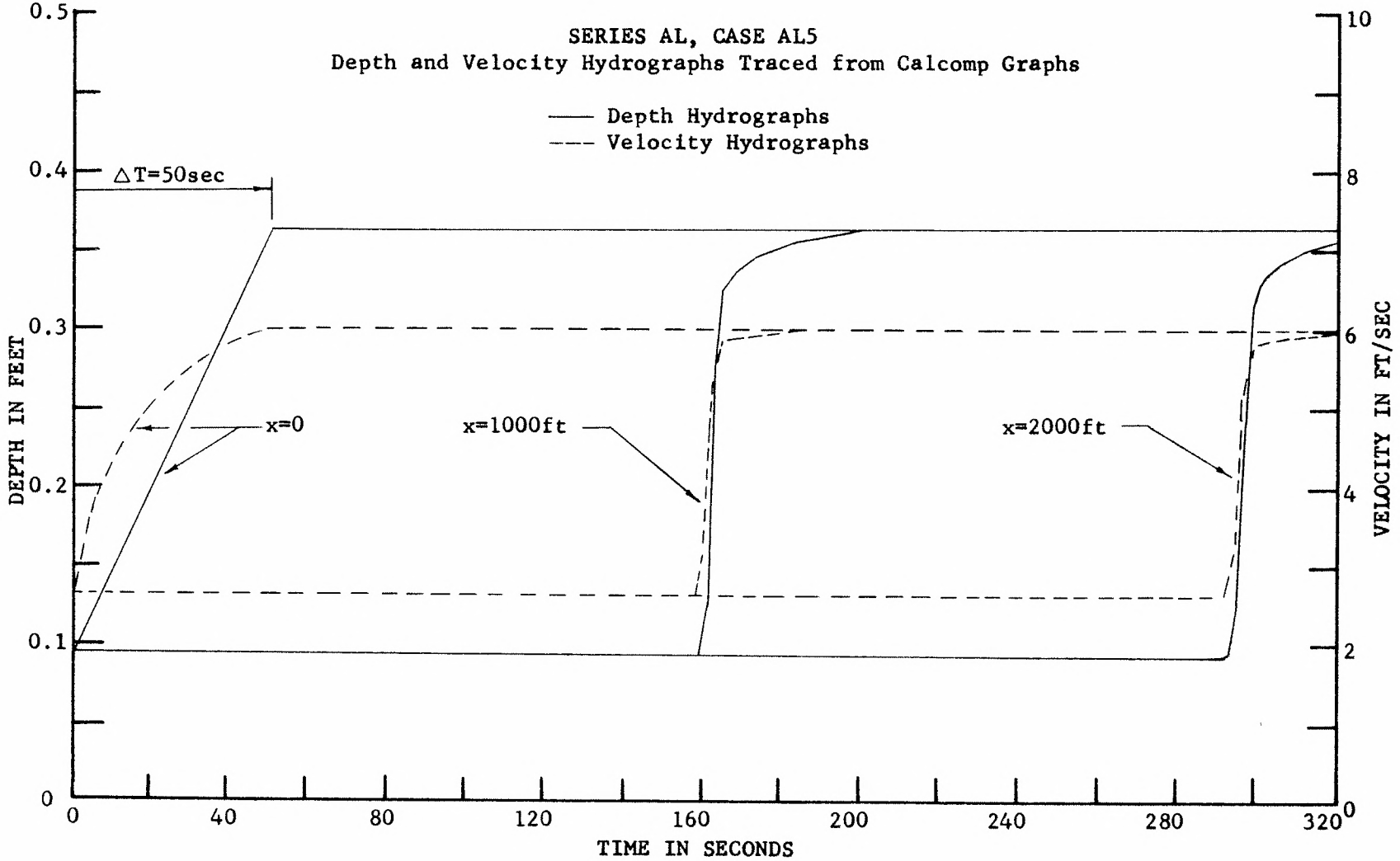

Figure 22. Typical Hydrographs for Case AL5

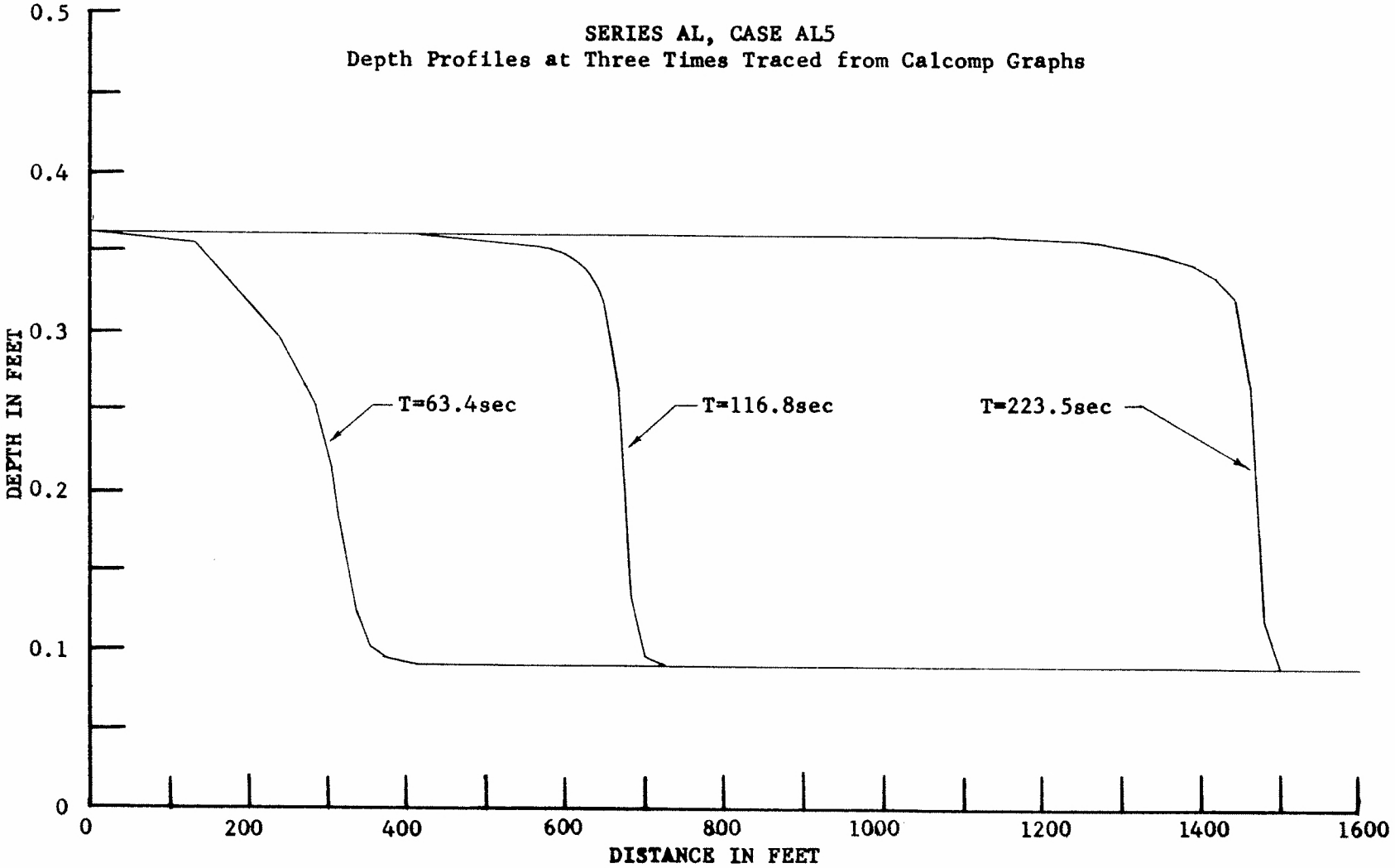

Figure 23. Typical Profiles for Case AL5

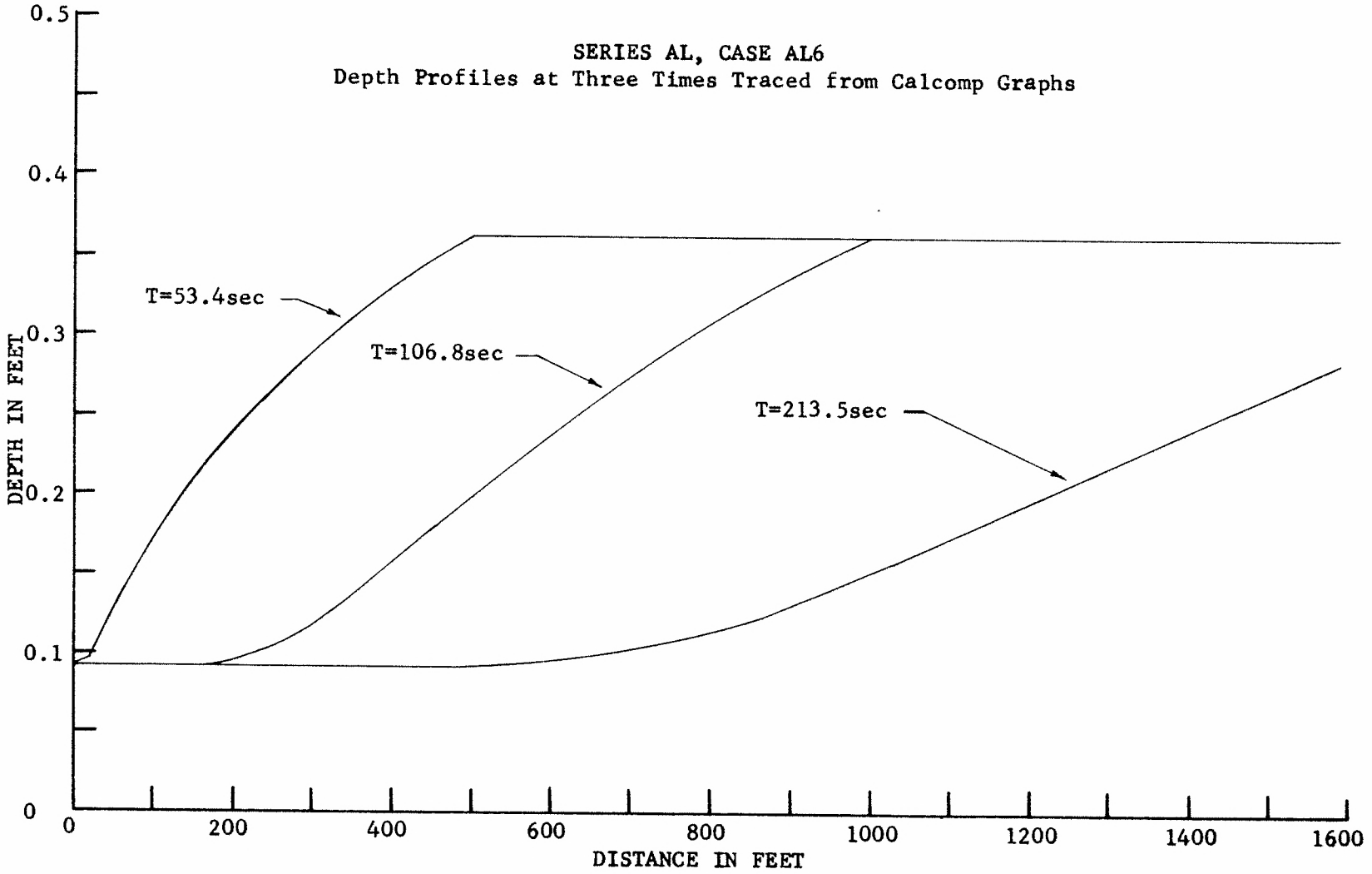

Figure 24. Typical Profiles for Case AL6

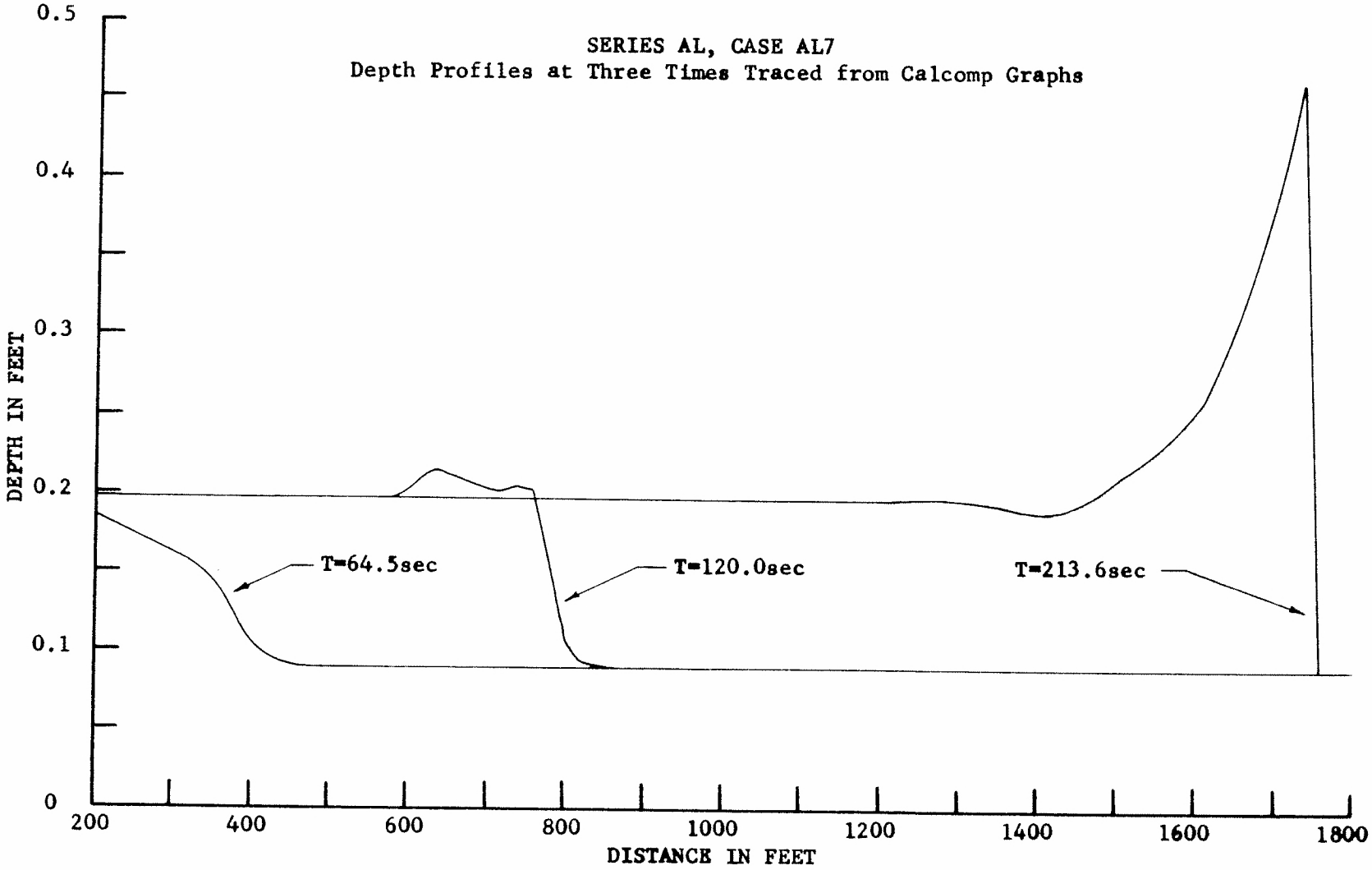

Figure 25. Typical Profiles for Case AL7

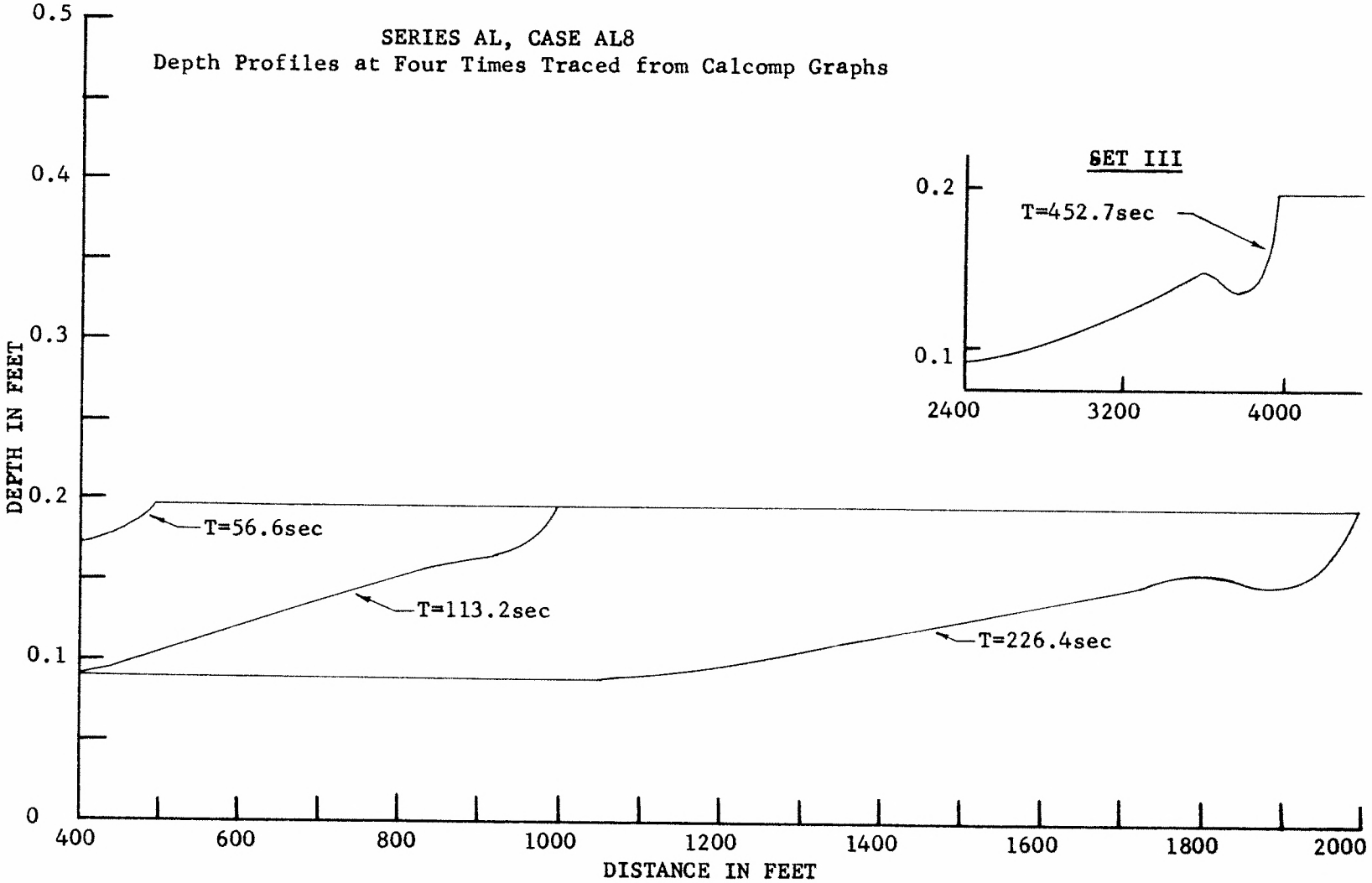

Figure 26. Typical Profiles for Case AL8

unstable (see Rouse [1949]). Based upon the criteria for stability set forth in this study, however, the numerical solution for Case AL6 is apparently quite stable. Inasmuch as the falling hydrographs yield diverging C1 characteristics, a shock discontinuity cannot occur for this case.

In comparison to Case AL5, the Case AL7 solution (Fig. 25) was markedly different. In Case AL7, as in Case AL5, the rising hydrograph boundary conditions would indicate the formation of a shock discontinuity. Since the wave front for Case AL7 is apparently steepening to reflect the formation of the shock, the exponential growth of the depth at the wave front indicates that this solution is also numerically unstable. The origin of the instability is thought to be a result of the fact that the Froude numbers of both the initial and final uniform flows for Case AL7 are above the stability Froude numbers for these flows. Since Case AL5 was numerically stable for similar shock formation conditions, the origin of the instability for Case AL7 is thought not to be a result of a shock formation condition.

Case AL8 (Fig. 26) is similar to Case AL6 in that a negative wave results when the hydrographs are reversed from those in Case AL7. As for Case AL6, the negative wave attenuates with time and distance and in the sense of the previous discussions of stability it is apparently numerically stable. There is within the wave front, however, an unexplained reversal of curvature which grows with time and distance. Sets II and III of Table 7 were run to observe the growth of this "wrinkle" in the wave. The insert of Figure 26 shows the "wrinkle" for Set III at T=452.7 sec. Although the solution at this time does not show a severe breakdown of the solution, a tendency toward instability is clear.

In Cases AL9 and AL10 of Sets IV, VI, VII, VIII, and IX the mesh size, Δx, was varied for two different ΔT's to determine the largest mesh size that could be used while still maintaining a stable solution. A comparison of Sets VIII and IX in Table 7 shows that a fivefold increase in mesh size results in a sevenfold decrease in computer time. Since the computer times listed in the table include some time for program compilation ($\approx$ five seconds), the savings in execution time are actually somewhat larger than the sevenfold decrease shown. In Figures 27 to 30 the depth hydrographs for Cases AL9 and AL10 are directly compared to determine the effect of the mesh size upon the solution. In Figure 27 the hydrographs for Case AL9 (ΔT=20 sec) show that there is very little difference in the solution whether Δx=20 ft or Δx=80 ft is used. A similar result is apparent for Case AL10 in Figure 28.

In Figure 29 the results for mesh sizes of 20, 100, and 200 ft are compared for Case AL9 (ΔT=100 sec). Although the depth hydrographs for these runs compare favorably, the insert of part of the velocity hydrograph at x=2000 ft for Δx=200 ft shows that the solution is becoming unstable for the large 200 ft mesh size. In Figure 30 the results for the mesh sizes of 20 and 100 ft are compared for Case AL10 (ΔT=100 sec). For this run the solution for the mesh size Δx=200 ft became unstable and the run terminated before the Calcomp graph was obtained. The printed output for this run showed, however, that the solution became unstable very rapidly. Clearly, for both Cases AL9 and AL10 the 200 ft mesh size was too large. The mesh size Δx=100 ft is a practical, if not optimal, limit for these runs since a very rapid solution is obtained on the computer (11 sec) with fair accuracy.

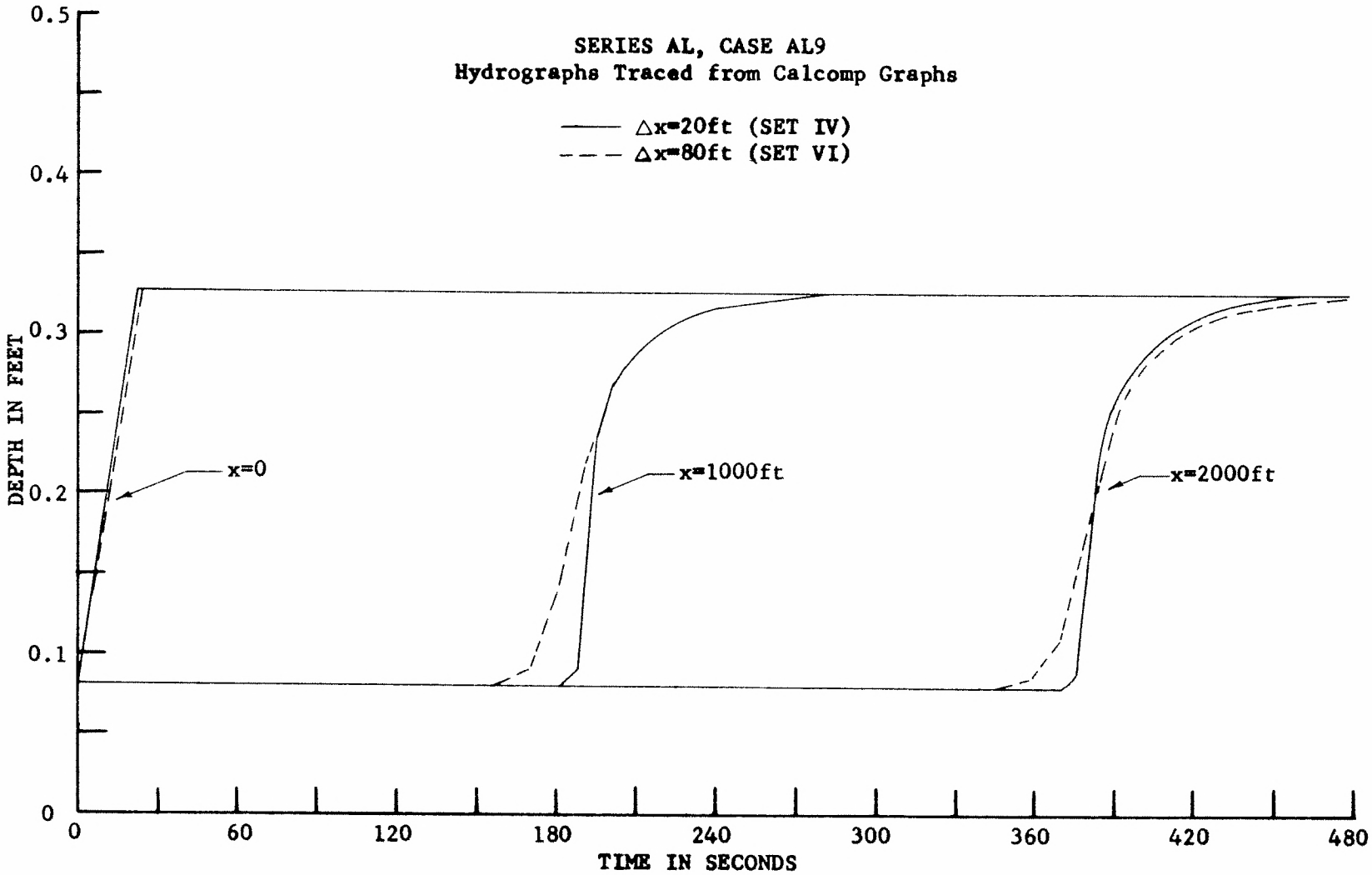

Figure 27. Effect of Mesh Size upon Solution for Case AL9 (ΔT=20 sec)

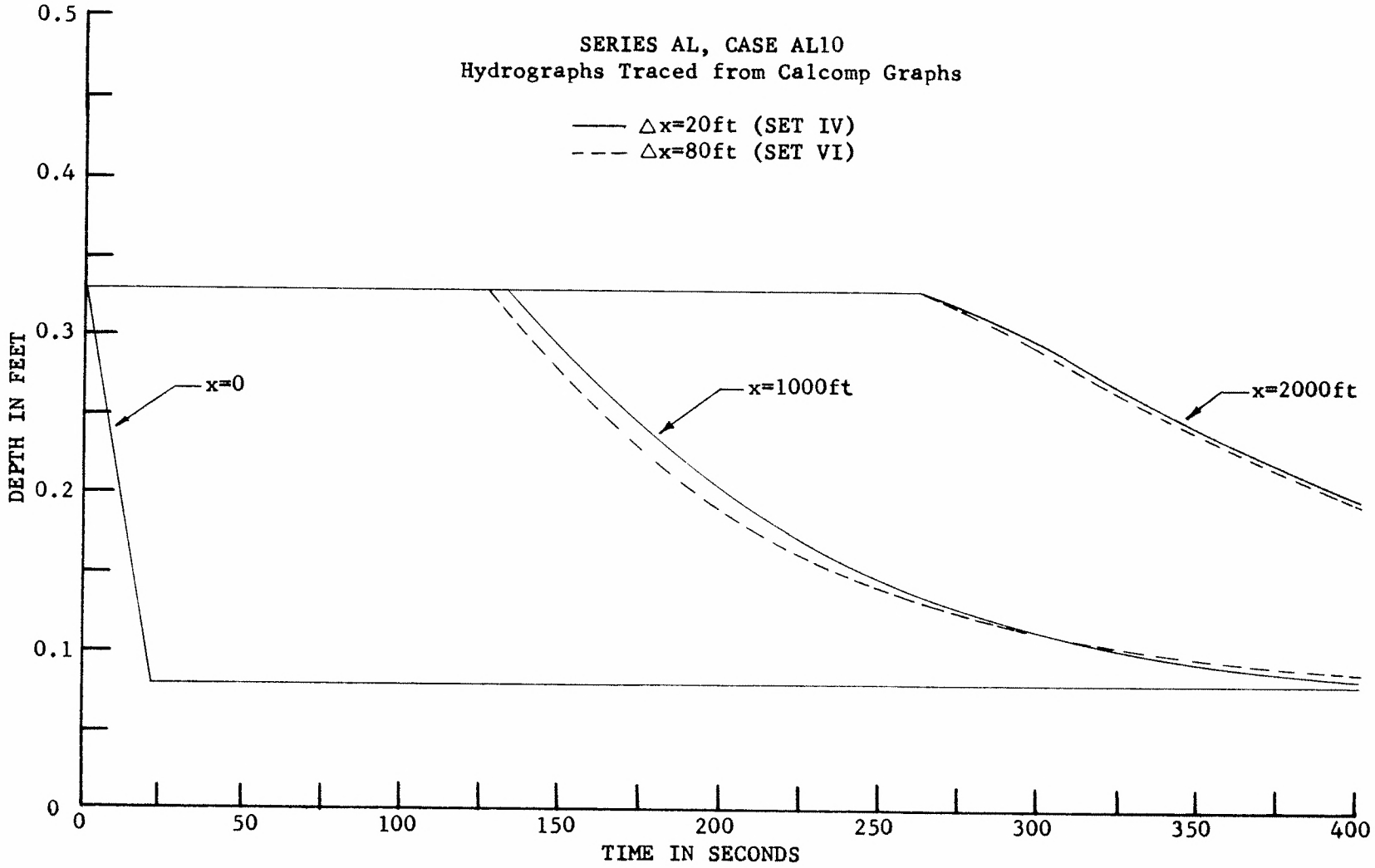

Figure 28. Effect of Mesh Size upon Solution for Case AL10 (ΔT=20 sec)

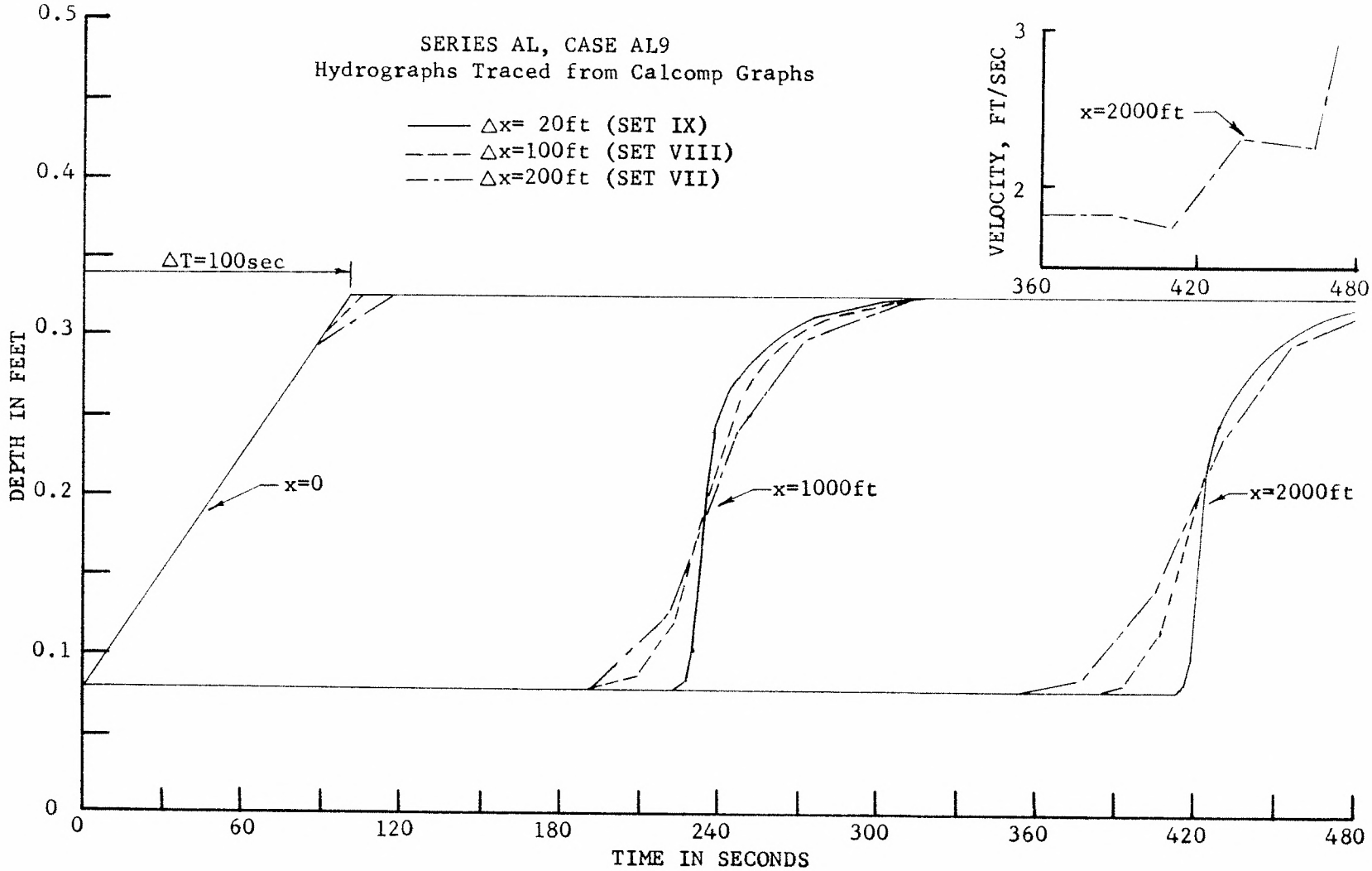

Figure 29. Effect of Mesh Size upon Solution for Case AL9 (ΔT=100 sec)

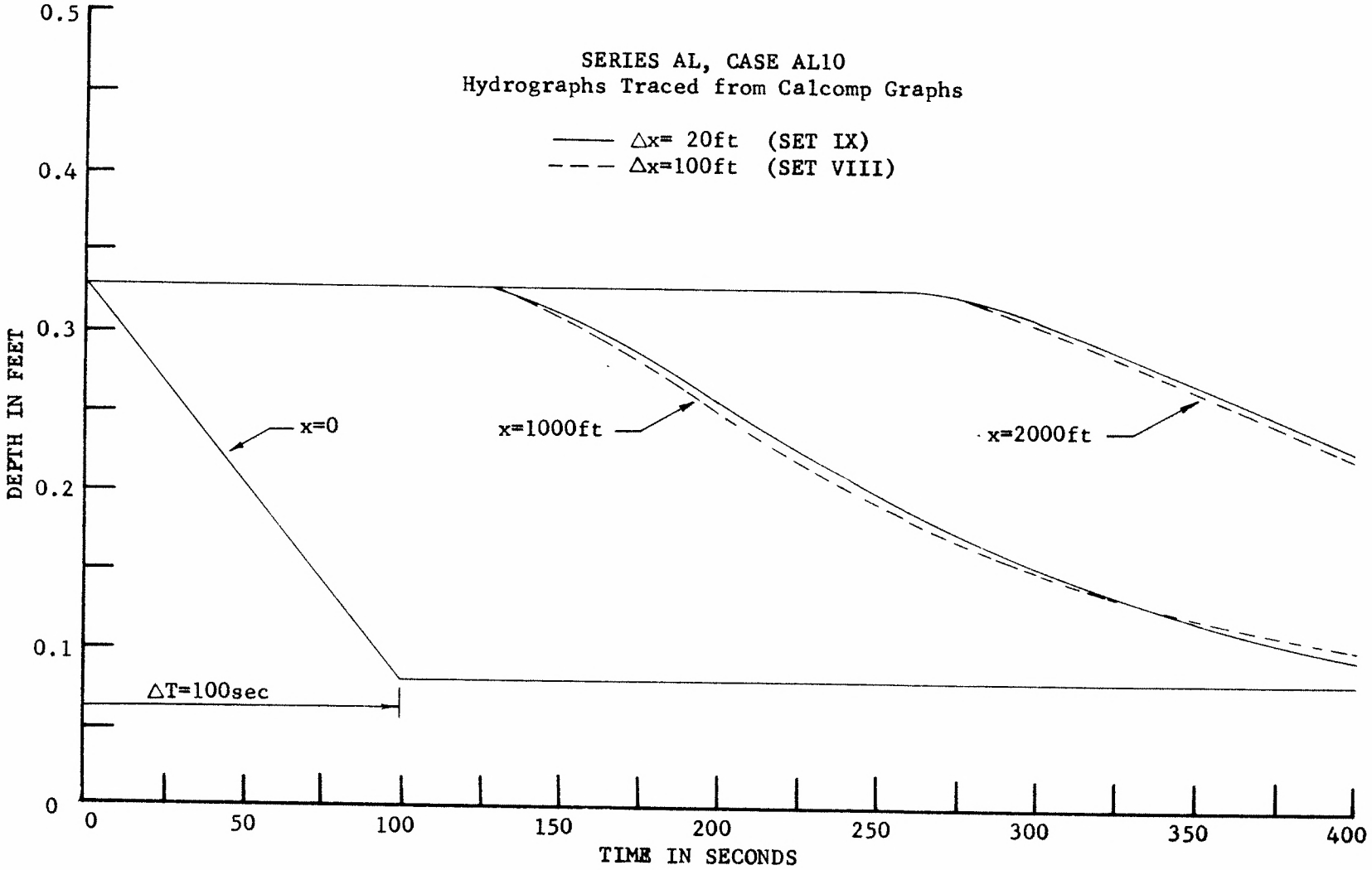

Figure 30. Effect of Mesh Size upon Solution for Case AL10 (ΔT=100 sec)

Cases AL11 and AL12 of Set V in Table 7 had Froude numbers (see Table 5) considerably larger than the theoretical stability limit ($F_S \approx 2$). As anticipated, these runs were very unstable.

In Tables 6 and 7, the ΔT values are shown to have been varied from five to 100 sec. In no case did the ΔT values affect the solution regarding stability. Although no problems with $\Delta T=0$ were run, it is thought that even this abrupt step type of boundary condition would not cause the solution to become unstable. Since the solution tolerates very sharp discontinuities in the hydrograph boundary conditions, a great deal of flexibility is allowed in the manner in which these boundary conditions are specified.

Continuity Tests. As indicated in Table 6, Sets I and II were run specifically to check Cases AL5, AL6, AL7, and AL8 for continuity. The results of these tests are analyzed for Case AL5 for which the input hydrographs rise linearly in y and Q from the initial uniform flow to the final uniform flow. The net volume inflow during the duration of the rising hydrograph at x=0 can be computed exactly for the wave to be:

Total Wave Input Volume (44)

$$= \left(\frac{7.5085 \text{ cfs} - 0.8276 \text{ cfs}}{2} - 0.8276 \text{ cfs}\right) 50 \text{ sec}$$

$$= 125.9 \text{ ft}^3$$

After 50 seconds, the entire wave is in the channel. In fact, for this run the forerunner of the wave is at x=360 ft. The profile of the wave at time T=50 sec is shown in Figure 31.

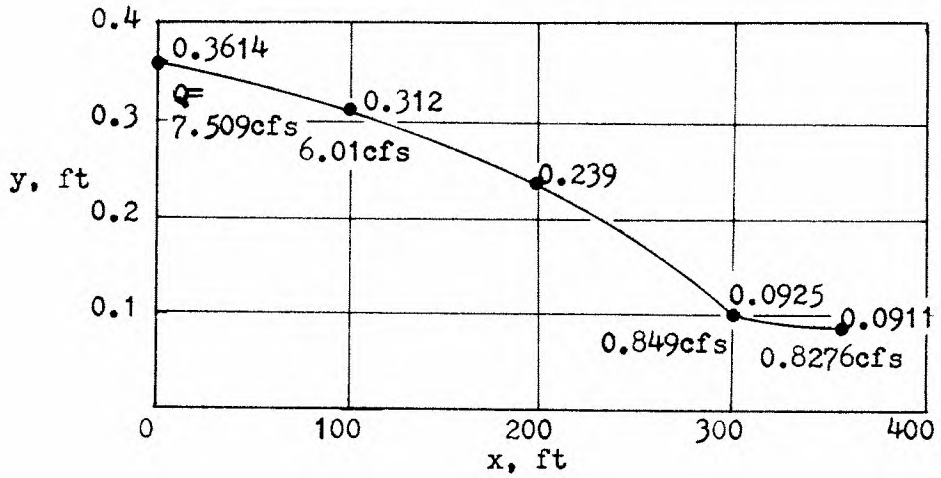

Figure 31. Wave Profile of Case AL5 at T=50 sec

Although the positive wave steepens gradually as it propagates downstream, the total volume storage (adding the accumulated storages for all reaches between x=0 and 360 ft at 50 sec) in the wave should be approximately equal to the input volume. From the program output the total volume storage is 128.5 ft^3, which is only 2.1 percent greater than the input volume. Similarly, the total net inflow (adding the accumulated net inflows for all reaches between x=0 and 360 ft) is 127.5 ft^3, which is only 1.3 percent greater than the input volume. Note also that the total net inflow is less than one percent greater than the total storage. These results indicate the continuity is being satisfied.

The continuity data for Case AL5 can be analyzed in another way to provide additional support for the conclusion that continuity is satisfied. The analysis is based upon that fact that the depth must rise from the initial uniform depth (0.0911 ft) to the final uniform depth (0.3614 ft) as the entire wave passes a given reach. The exact volume storage for

this reach, after the wave has passed by, can be computed by the relation,

$$\text{Total Storage/Reach} = B\Delta x\ (\text{Final Depth} - \text{Initial Depth}) \qquad (45)$$

Using Δx=20 ft and B=3.487 ft, the total storage per reach for Case AL5 is 18.88 ft^3. In the numerical solution the total storage per reach (and the total net inflow/reach, as well) is obtained by accumulating the values for each Δt increment for the duration of the run. The printed output for Case AL5 reveals that no storage is accumulated until the wave arrives at the reach under question. As the wave passes by, some storage and some net inflow are accumulated for each Δt time increment until the final uniform flow is reached at both ends of the reach. When this occurs, the wave has passed and the total accumulated storage and net inflow should remain constant for the remainder of the run. The total storage, and net inflow accumulated by Δt increments, should compare favorably with the exact value given by Equation (45) for continuity to be satisfied in the numerical solution. The total storage and net inflow for three different reaches of Case AL5, with Δx=20 ft and B=3.487 ft, are listed in Table 8.

Table 8. Typical Values of Storage and Net Inflow for Case AL5

Reach, ft	Total Storage/Reach, ft^3	Total Net Inflow/Reach, ft^3
20-40	18.85	19.08
100-120	18.85	18.82
200-220	18.85	18.77

Thus, the storages and net inflows compare quite favorably to each other and to the exact value computed by Equation (45). For the duration of the run, there was no detectable percentage increase of storage over net inflow, or vice versa, which adds further support to the conclusion that the continuity requirements were satisfied for this run, although the wave front steepens to a rather abrupt discontinuity by the time it reaches x=1000 ft.

Recalling that the Case AL6 input hydrographs are the exact reverse of those for Case AL5, the total input wave volume is therefore -125.9 ft^3 and the total storage per reach after the wave has passed is -18.88 ft^3. At T=50 sec, when the entire wave is in the channel, the forerunner of the wave is at 480 ft, and the total accumulated storage is -133.0 ft^3 (5.6 percent less than the input volume) and the total accumulated net inflow is -129.7 ft^3 (3.0 percent less than the input volume). Although these values do not substantiate continuity, they also do not necessarily invalidate the solution since the negative wave elongates as it propagates downstream.* Continuity was actually satisfied for Case AL6 according to the accumulated values of total storage and net inflow per reach which were typically -18.84 ft^3 and -18.90 ft^3, respectively.

Although the runs for Cases AL7 and AL8 were numerically unstable, continuity checks showed that continuity was satisfied for Case AL8, but not for Case AL7. This discrepancy is probably because the insta-

---

*The elongating wave contains ever increasing amounts of negative storage.

bility was considerably more severe for Case AL7 than for Case AL8 (see Figs. 25 and 26). In the vicinity of the location of the instability of Case AL7, the storage and net inflow values were much larger than the anticipated values.

Summary of Fixed Grid Results

The foregoing presentation of results of the Fixed Grid method as a whole proved that this method of simulating unsteady, supercritical flow is stable, efficient, and accurate, provided the Froude number of the flow is below the stability limit. There was perhaps some increase in accuracy if friction slopes were averaged or if the three-point interpolation equations were used, but the large increase in computer time required for these refinements in the solution technique limits their use in general. Furthermore, the continuity tests showed that the simple two-point interpolation equations at least were sufficiently accurate regarding the conservation of volume equation.

The Fixed Grid method operated far better than expected through a shock discontinuity inasmuch as the solution did not terminate or become unstable as a result of intersecting C1 characteristics. The method also operated without difficulty through all three of the separate zones of influence for supercritical flow. An advantage is that it is not even necessary that these zones be outlined for a given problem when the Fixed Grid method is used. A disadvantage of this method is that the maximum recommended grid spacing to maintain stability is 100 ft. For the problems solved in this study, a $\Delta x = 100$ ft yields a $\Delta t \approx 20$ sec by the Courant condition. It would take considerable machine time to simulate unsteady supercritical flows up to distances of several miles, such as

has been done for unsteady subcritical flow, using these values of Δx and Δt. On the other hand, cases of supercritical flow occurring in natural or man-made channels for many miles are rarely encountered. Another disadvantage of the method is that it does not cover the x,t-plane very efficiently inasmuch as the Courant condition must be satisfied for each grid point for each Δt increment.

Characteristics Grid Method (Series CL)

The Characteristics Grid method of solution was programmed in order to compare solutions by this method with solutions obtained by the Fixed Grid method. Although there were great difficulties involved in programming this method, a limited number of solutions were obtained for comparison with Cases AL6 and AL8. Since the solution by this method propagates along the actual characteristics, difficulties are anticipated when a shock discontinuity arises during solution because the solution should not be carried beyond the crossing of like characteristics without specifying the bore conservation equations at the point of crossing. Comparisons were obtained therefore only for the negative waves of Cases AL6 and AL8, for which no shock discontinuities can occur.

The other primary difficulty with the Characteristics Grid method is that the solutions in zones 1 and 2 (see Fig. 6) are completely independent of each other. The initial boundary conditions or the upstream hydrograph boundary conditions can therefore be specified independently and separate solutions can be obtained in zones 1 and 2, respectively.

Hence, some artificial method must be employed to connect zones 1 and 2 in order to obtain a solution in zone 3. Several methods were attempted for the Characteristics Grid method; however, none of them was uniformly successful. The one described in the following was used to obtain the comparisons for Cases AL6 and AL8.

The ordering of the grid points for this method is shown in Figure 32. The initial conditions are specified at an evenly spaced set of grid points (points 1-10) on the x-axis as shown. Since for Cases AL6 and AL8 the initial conditions are uniform flows, the y and V values are constant for all points 1-10 and, in fact, for the entire zone 1 domain bounded by the straight C1 characteristic from the origin. The upstream boundary conditions are specified at an evenly spaced set of grid points (1,1',1'', etc.) on the t-axis. Point 2' is then the intersection of the C2 characteristic from point 1 and the C1 characteristic from point 1'. The values of y and V for 2' are determined by solving the difference equations for the intersecting characteristics. The values of y and V for points 3'-10' are obtained consecutively in the same manner as for point 2'. The next solution level is then begun using points 1' and 1'' to determine point 2'', and so forth. By using this method most of the zone 3 solution is obtained, and much of the zone 2 solution is obtained. The zone 1 solution is purposely skipped since the flow in this region is known from the specified initial boundary conditions. The entire zone 2 solution could be obtained easily by a separate solution, although this was not done here because the zone 3 solution yielded enough information for a comparison with the Fixed Grid results.

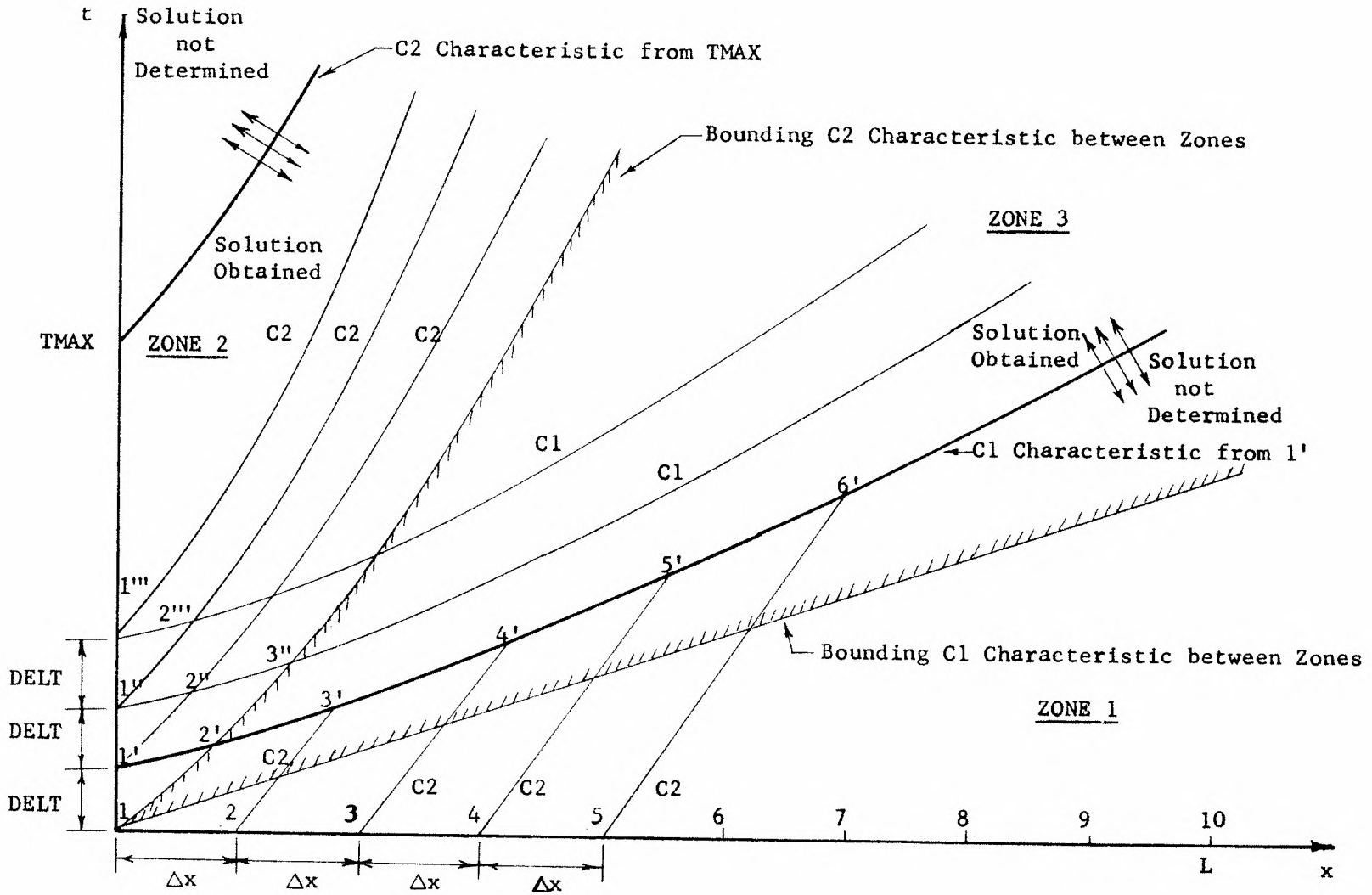

Figure 32. Ordering of Grid Points for Solution by Characteristics Grid Method

The amount of coverage of zone 3 is dependent upon the selection of DELT* since the C1 characteristic from point 1' is the bounding C1 characteristic between the known and unknown values, as shown in Figure 32. The density of spacing of grid points in zone 3 is dependent upon not only the choice of DELT but also upon the choice of Δx. In general, for the negative wave Cases AL6 and AL8, the family of C1 characteristics will diverge in zone 3. The spacing of grid points therefore becomes quite large as the solution progresses and the approximation of the friction slope can become grossly inaccurate.

Another essential difficulty with this solution arises because the last grid point, as for instance point 10' in Figure 33, is not used to obtain the last grid point for the next level, such as point 10''. As shown, point 10'' is determined from points 9 and 9'. The solution therefore marches somewhat backwards in zone 3, reflecting the fact that the C1 characteristics are diverging for the negative wave. Because of this marching back, part of the zone 3 solution is inadvertently skipped. The amount of the solution that is skipped is seen to be very much dependent upon the choices of DELT and Δx. The values of DELT and Δx therefore significantly affect the outcome of the solution although it is most difficult to know a priori what the effect will be. The programmer is left with the highly undesirable situation of determining the proper values of DELT and Δx by trial-and-error so that a maximum area of the x,t-plane is covered.

---

*DELT is the specified time increment of the input upstream hydrographs for the computer solution (see Fig. 32).

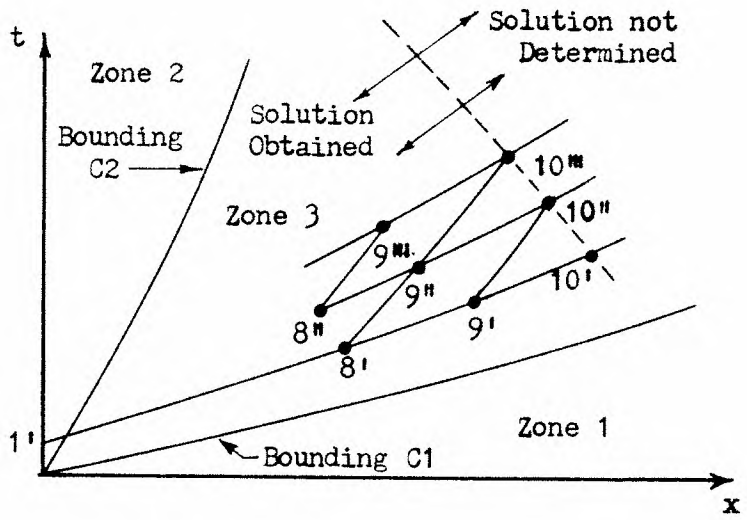

Figure 33. Showing the Area of Zone 3 that is Skipped because of the Marching Back of the Characteristics Grid Solution

In order to obtain an adequate comparison of Case CL6 with AL6, it took 12 trials of varying Δx and/or DELT. A list of these trials is given in Table 9. From six of these 12 trials the depth hydrograph at x=1000 ft was interpolated from the unevenly distributed grid points and compared to the hydrograph at x=1000 ft of the Case AL6 solution. Trial 12 finally yielded enough information so that the hydrograph at x=2000 ft could also be computed and compared. The interpolation method is shown in Figure 34.

As indicated in Figure 34, the value of y at x=1000 ft for the n^{th} level of iteration is interpolated linearly from the values of y at the grid points that fall on either side of the 1000 ft line. A cross-interpolation in time was not deemed necessary for these runs because the C1 characteristics have a very small slope (hence a small Δt for points on the same characteristic).

Table 9. List of Trials of Case CL6 to Obtain Comparison with the Case AL6 Solution

Trial*	Δx, ft	DELT, sec	Comparison Number	Comments
1	20	4		Run terminated early.
2	20	2	I	Comparison at x=1000 ft good. Spacing too large at end of hydrograph.
3	10	2		Same as trial 2.
4	5	2		Same as trial 2.
5	2.5	2		Same as trial 2.
6	0.8	2	II	Comparison at x=1000 ft shows no change. Δx does not effect solution greatly.
7**	0.8	2	III	Averaging friction slope does not improve solution.
8**	20	1		Solution does not march back as severely.
9**	20	0.5		Slightly improved over trial 8.
10	10	0.5	IV	Slightly improved over trial 9.
11	10	0.25	V	Slightly improved over trial 10.
12	5	0.25	VI	Marching back spacing improved enough to also obtain hydrograph at x=2000 ft.

*For all trials ΔT=50 sec.

**For these trials the friction slopes were averaged (Appendix A).

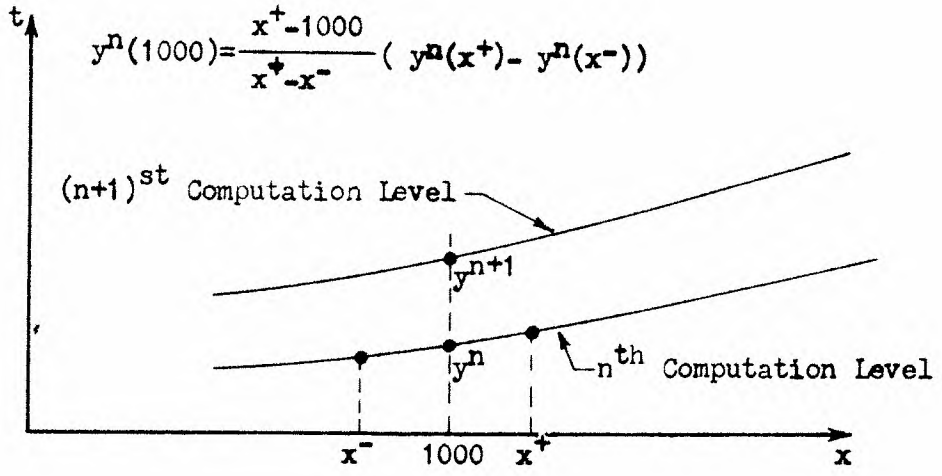

Figure 34. Interpolation Method for Obtaining the x=1000 ft Depth Hydrograph

Reducing the Δx spacing in Trials 2-7 for Case CL6 did not improve the solution as regards the marching back of the solution. Thus, the x=2000 ft hydrograph could not be obtained for these trials. By reducing DELT as well as Δx for Trials 8-12 the marching back was eliminated enough so that Comparison VI yielded a 2000 ft hydrograph as well. The solution for Case CL6 is compared with that of Case AL6 in Figure 35. All of the points are plotted for Comparison I, but only a few are plotted for Comparison VI because the points were so closely spaced for Trial 12. The comparison shows that the solutions are virtually identical for the two methods of solution.

The trials to obtain a comparison between Cases CL8 and AL8 are listed in Table 10. This case is numerically unstable which accounts for much of the difficulty in obtaining a comparison for this run. As indicated in Table 10, Trial 11 finally yielded enough data for a comparison. This comparison is shown in Figure 36. The solution for Trial 11 yielded

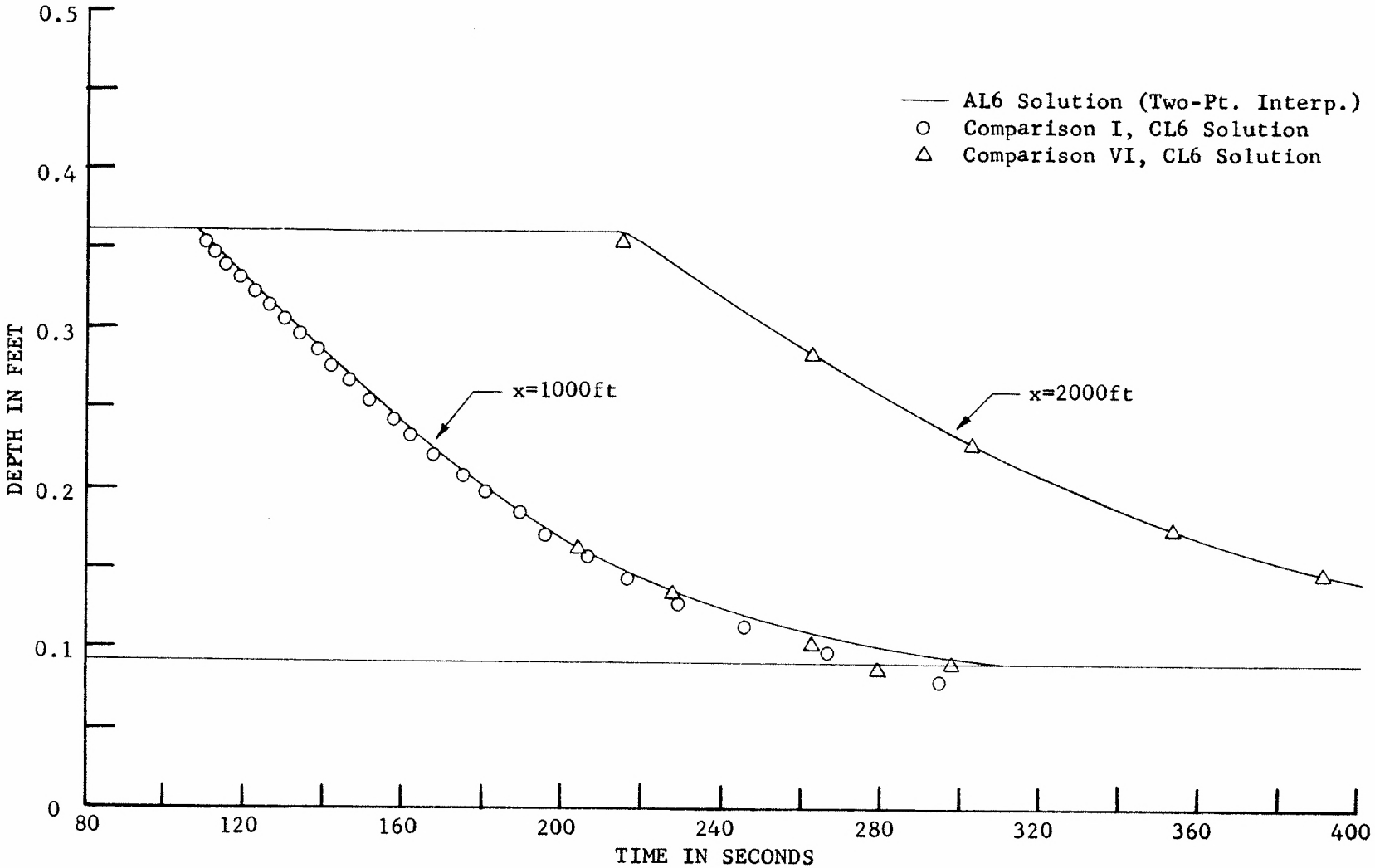

Figure 35. Comparison of Case AL6 and Case CL6 Solutions

Table 10. List of Trials of Case CL8 to Obtain Comparisons with Case AL8 Solution

Trial*	△x, ft	DELT, sec	Comparison Number	Comments
1	20	2		Terminated in first computation level.
2**	10	2		Terminated in second computation level.
3**	10	2		Terminated in second computation level.
4**	10	2		Terminated in second computation level.
5	20	1		Terminated in first computation level.
6	20	0.5		Terminated in first computation level.
7**	20	0.5		Terminated in second computation level.
8**	10	0.25		Terminated in second computation level.
9	5	0.25		Terminated in first computation level.
10	4	0.25		Good run but marched back severely.
11	3.75	0.25	I	Good enough for comparison at x=1000 ft.

*For all trials △T= 50 sec.
**For these trials the friction slopes were averaged.

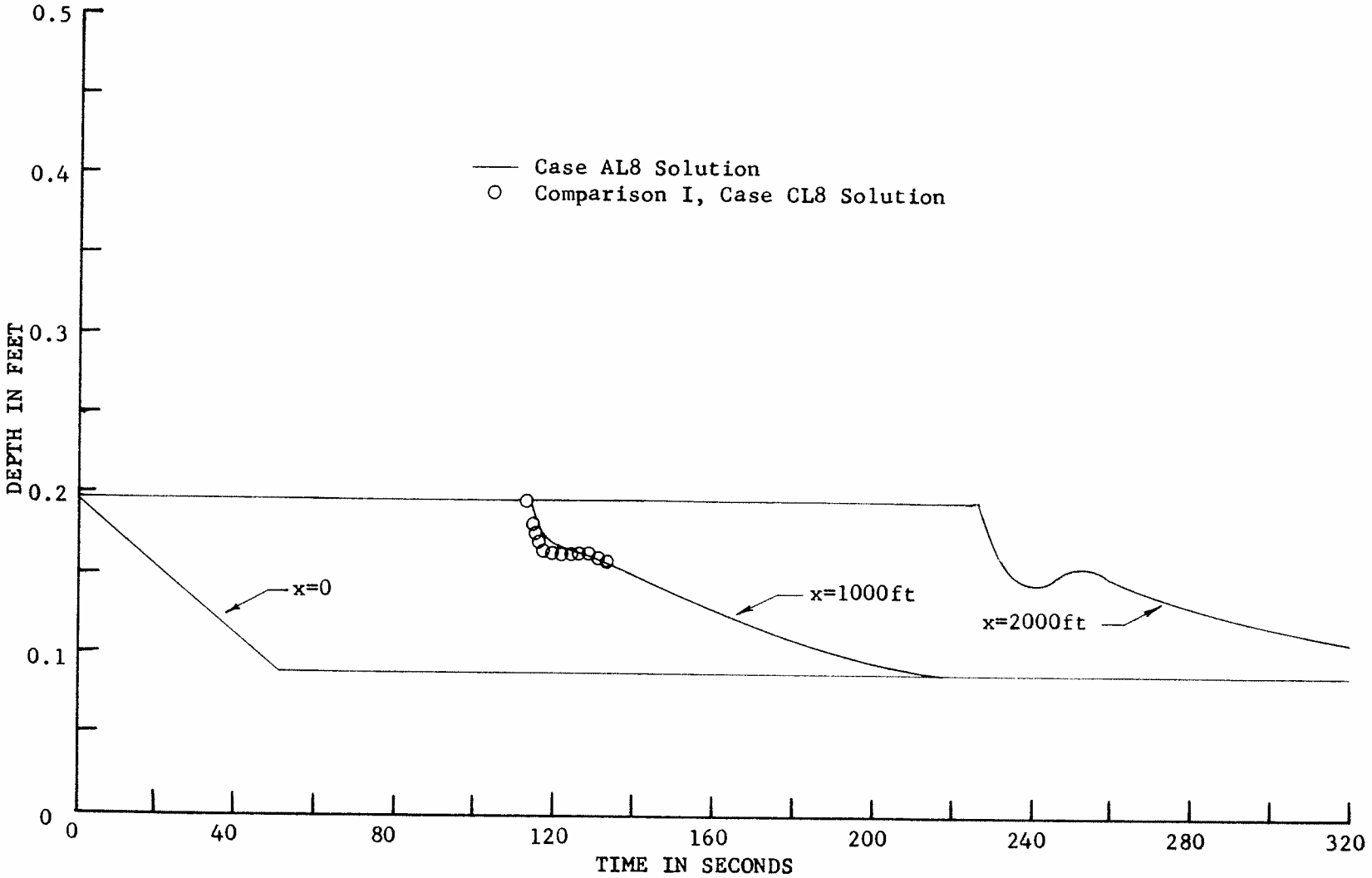

Figure 36. Comparison of Case AL8 and Case CL8 Solutions

only enough data to interpolate values for part of the x=1000 ft hydrograph. This portion of the hydrograph, however, reveals the same tendency of the solution toward instability as did the Case AL8 solution. The "wrinkle" in the CL8 solution, as shown in Figure 36, is equivalent to a rising hydrograph. As a result of the rising hydrograph, a small family of Cl characteristics would tend to intersect, which in turn would lead to a rapid termination of the solution.

Although great difficulties were encountered in obtaining solutions by the Characteristics Grid method, the few solutions that were obtained were essentially equivalent to the solutions obtained by the Fixed Grid method. This support for the Fixed Grid method is welcomed since the Characteristics Grid method is generally thought to be the more accurate one. This accuracy is mainly due to the fact that the solution is propagated along the characteristics themselves. Although the difficulties associated with the Characteristics Grid method for unsteady, supercritical flow simulations are perhaps not insurmountable, this method cannot be recommended over the Fixed Grid method for the types of problems solved in this investigation.

CHAPTER V

RESULTS OF THE NUMERICAL SIMULATION OF AN EXPERIMENTAL BORE

Description of the Experiment

The laboratory experiments were conducted in a rectangular steel tilting flume 3½ feet wide, 1½ feet deep, and 80 feet long. An overall view of this flume is shown, looking upstream, in Figure 37. The structural details of the flume are given in Tracy and Lester [1961]. The flume is tilted by means of two pairs of jacks which are driven simultaneously by an electric motor. The number of turns made by the jacks is recorded automatically by a counter device which is calibrated to give an immediate determination of slope. The flume is also equipped with a head gate and tail gate which provide for control of the flow. These gates are driven by electric motors and their positions can be located relatively by means of radio compasses.

Water is supplied to the flume by the laboratory reservoir system either through a 12 inch or a 6 inch pipe line. The discharges are measured either by a Venturi meter located in the 12 inch line or by an orifice meter located in the 6 inch line. These meters were calibrated gravimetrically.

The floor and sides of the flume are hydraulically smooth. The logarithmic friction factor relation (Eqn. 5) for this flume, which was originally established experimentally by Tracy and Lester [1961], was verified by the writer. The results of the verification are shown in

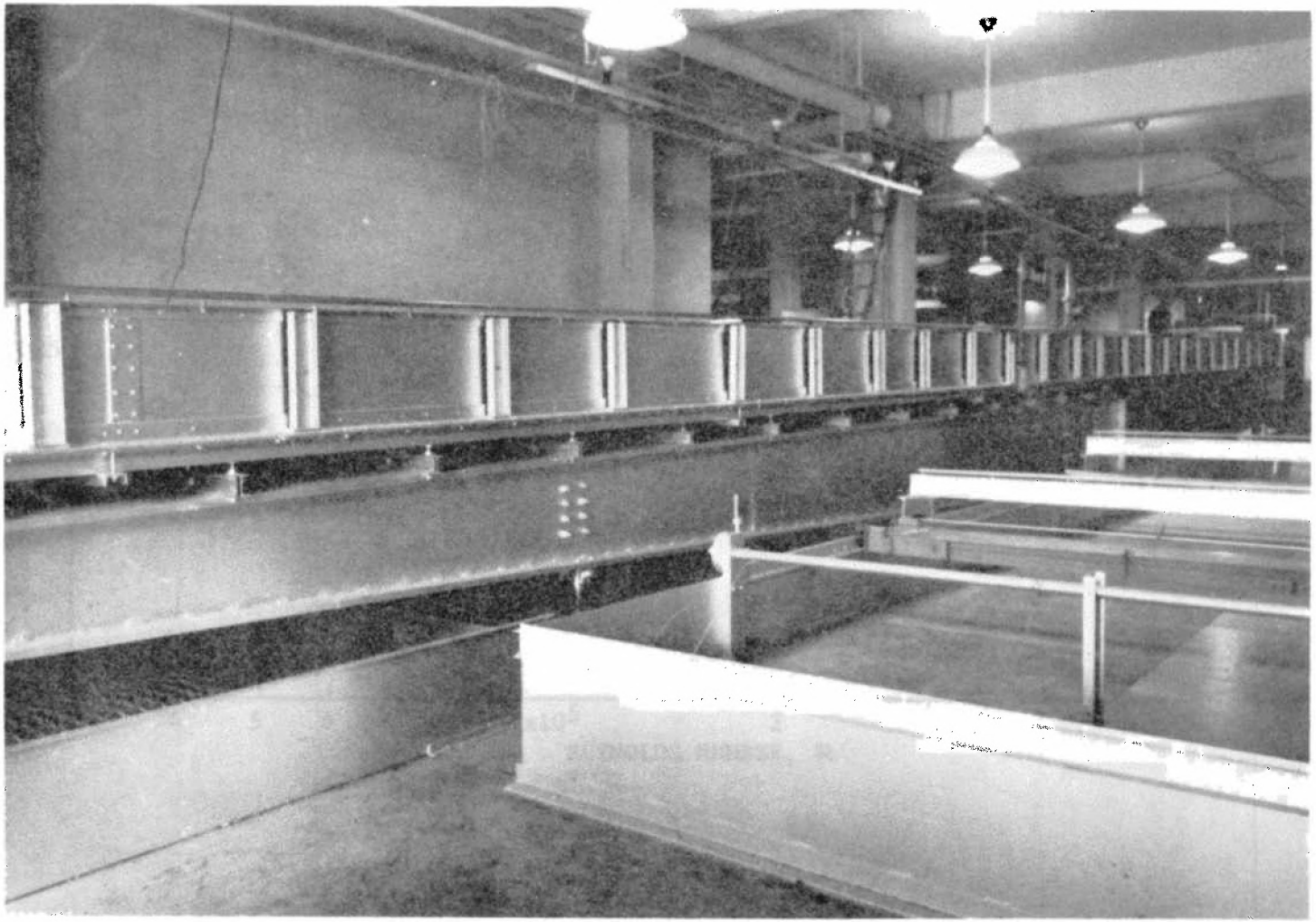

Figure 37. View of the Flume Used in the Bore Propagation Experiments

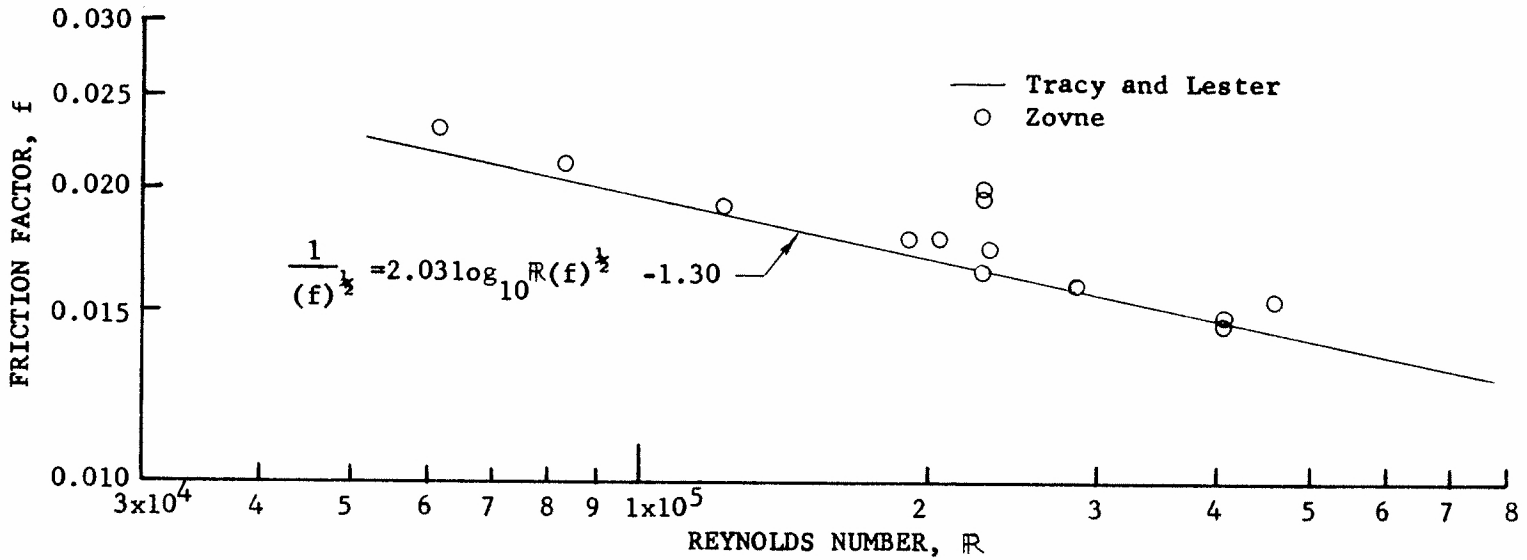

Figure 38. Variation of the Friction Factor in Supercritical Flow

Figure 38. The solid line in Figure 38 represents Equation (5), while the data points shown were obtained by the writer for verification. These data points were obtained as follows:

1) A steady supercritical was established in the flume. The discharge was measured using either the Venturi meter or the orifice meter and the slope was determined from the counter reading.

2) The uniform flow depth was determined from the convergence of the S2 and S3 profiles for this discharge and slope, as shown schematically in Figure 39. The flow profiles were determined by point gage readings spaced at 10 ft intervals from 20 ft to 40 ft and at 5 ft intervals from 40 ft to 75 ft downstream.

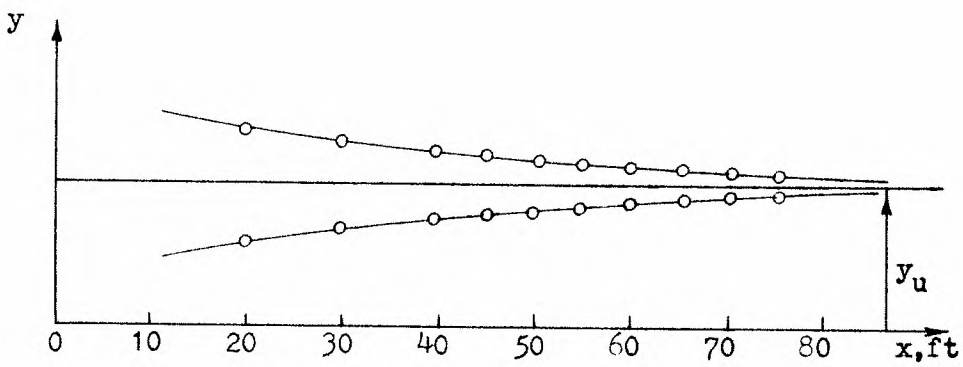

Figure 39. Schematic Representation of Surface Profiles in Supercritical Flow

3) The average velocity is computed from V=Q/By, in which B is the average width, which was determined by Tracy and Lester [1961]. (B=3.487 ft)

4) The friction factor is computed from the Darcy-Weisbach relation (Eqn. 4).

5) The Reynolds number is computed from $R = 4RV/\nu$.

A considerable experimental error is associated with the determination of the uniform depth because of the surface waves associated with supercritical flows and because the depths are relatively small. On the other hand, subcritical uniform depths were even more difficult to obtain because of the slow convergence of subcritical flow profiles to uniform flow. In spite of the experimental error, the points shown in Figure 38 are considered to be a good verification of the relation determined by Tracy and Lester [1961].

Four experimental bores were generated and observed in the flume. A bore was generated in the following manner:

1) A steady supercritical flow was initially established in the flume.

2) A hydraulic jump was created by gradually raising the tail gate downstream. Once the jump reached approximately the 70 ft station the tail gate motion was stopped.

3) After the jump had stabilized, the steady state discharge and the slope were recorded. At the same time, the depth upstream (x=0) was measured with a point gage and the depth downstream (x=79 ft) was measured using a large piezometer tube immersed at mid-point of the channel and connected to a manometer at the side of the flume.

4) The jump was then forced to propagate upstream by raising the motor-driven tail gate at a constant rate. The rate of propagation of the bore was obtained by recording its location every 20 seconds. The location of the moving bore front was obtained by sighting across a scale which was fixed to the side of the flume. The scale runs the length of the flume with the zero station located at the head gate and the 80 ft station located at the tail gate. The downstream depth was also recorded by reading the manometer every 20 seconds. Since the gate is mechanically operated, these runs can be duplicated an indefinite number of times in order to obtain average values of the bore propagation and rate of rise downstream. All of the required data can be obtained by a single observer by simply duplicating runs. Usually a run was repeated once or twice in order to obtain the rate of propagation and the rate of rise, while the discharge, temperature, and depth upstream were checked before and after the unsteady data were collected.

A summary of the data for the four bores tested is given in Appendix E. The bottom slopes used in the runs varied from 0.005 to 0.02 and the upstream supercritical Froude numbers varied from 1.29 to 2.92. Two physical factors limited the range of slopes and Froude numbers that could be used in this flume. First, the Froude number of 1.29 (Bore No. 5) produced a very small undular bore which was just barely discernible in the flume. Below this Froude number the bore could not be observed. Second, the Froude number of 2.92 (Bore No. 4) produced a very abrupt bore front and a large depth downstream. While still containing the water within the flume, this bore could only be forced to propagate a distance of 21.5 feet to the 46 ft station. At higher Froude numbers, the downstream flow overtopped the flume very quickly, while the distance of propagation was too small for numerical simulation.

Photographs of two of the experimental bores are shown in Figures 40 and 41. The profile view of Bore No. 3 reveals the oscillating character of the water surface in the subcritical region behind the bore front (Fig. 40a). The front of this bore was skewed because the flume became skewed near the downstream end at the greater slopes. As can be seen in Figure 40b, an eddy system develops downstream as a result of the angular bore front. The point gage staff to which the piezometer tube was attached can also be seen in this figure. The profile of Bore No. 5 was undular, as shown in Figure 41a. The regular appearance of the undular wave train is quite apparent in Figure 41b. In each of the bore experiments the bore front was initially located at least 10 feet upstream of the piezometer in order that the depth readings downstream would not be severely affected by the erratic flow conditions in the vicinity of the

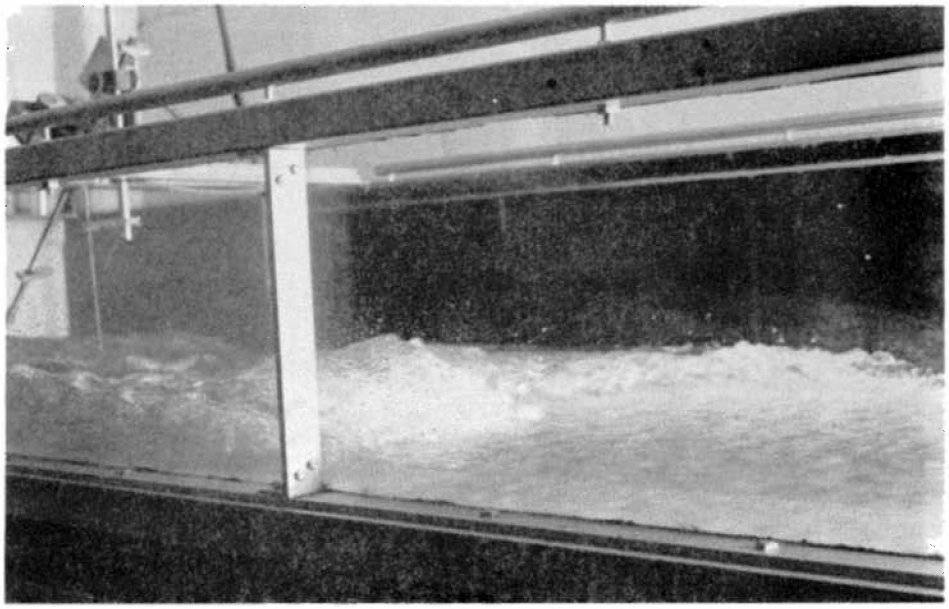

a) PROFILE

b) LOOKING DOWNSTREAM

Figure 40. Photographs of Bore No. 3

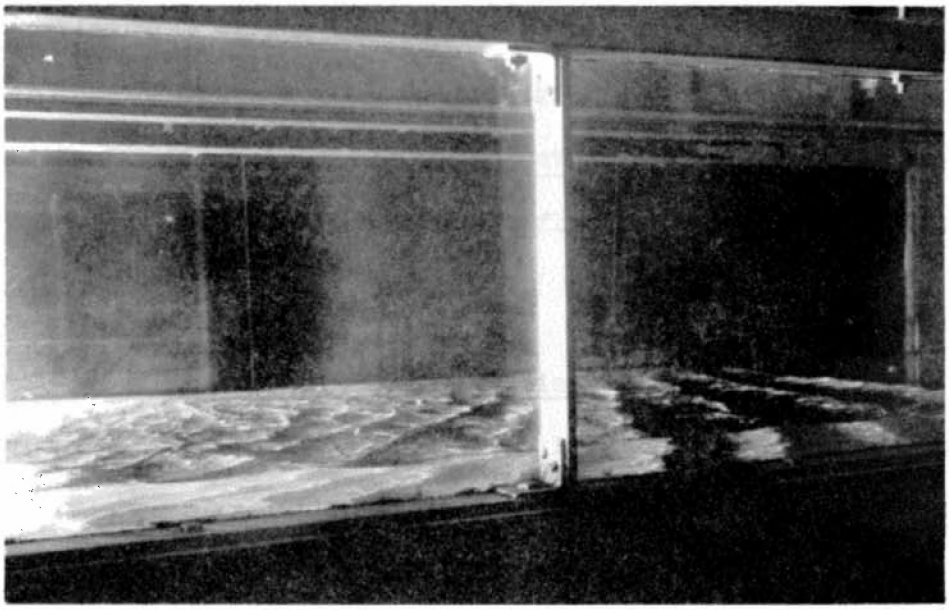

a) PROFILE

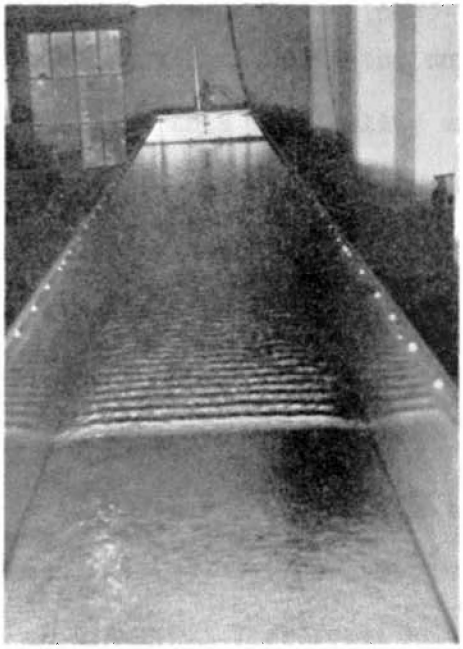

b) LOOKING DOWNSTREAM

Figure 41. Photographs of Bore No. 5

bore. Particularly during the earlier stages of the propagation, the manometer readings were still somewhat erratic for Bores No. 1, 3, and 4, however. Hence, the readings were subject to some judgment on the part of the observer. The magnitudes of the fluctuations are given with the data in Appendix E.

Description of the Numerical Simulation

The four experimental bores were simulated numerically using the Fixed Grid method of solution. The presence of the abrupt transition from supercritical flow to subcritical flow at the bore front, however, required extensive modifications and additions to the basic method of solution. In subcritical flow a shallow-water wave can propagate upstream as well as downstream. The interpolation technique in the unsteady solution must therefore be revised to include this possibility and the program must contain a method of switching to the proper interpolation equations depending upon the Froude number. The subcritical case is shown in Figure 12, in which the negatively sloped C2 characteristic intersects the T level at point S'. If the Froude numbers at points A, B, and C are less than unity, the values of $x_{S'}$, $y_{S'}$, and $V_{S'}$ must be determined rather than the values of x_S, y_S, and V_S. The three equations used to determine the values at S' are similar to Equations (34) - (36) except that the grid points C and B are used instead of A and C. Therefore,

$$x_{S'} = x_P - (V_{S'} - c_{S'})\,\Delta t \tag{46}$$

$$\frac{y_{S'} - y_C}{y_B - y_C} = \frac{x_{S'} - x_C}{x_B - x_C} \tag{47}$$

$$\frac{V_{S'} - V_C}{V_B - V_C} = \frac{x_{S'} - x_C}{x_B - x_C} \tag{48}$$

which are solved simultaneously for $y_{S'}$ to yield the root of the quadratic equation,

$$y_{S'} = \frac{X'^2}{2} + \psi' + X' \left| \left(\frac{X'^2}{4} + \psi' \right)^{\frac{1}{2}} \right| \tag{49}$$

where,

$$X' = g^{\frac{1}{2}} \left[\frac{\theta \, (y_B - y_C)}{1 + \theta \, (V_B - V_C)} \right] \tag{50}$$

and

$$\psi' = y_C - \frac{\theta V_C \, (y_B - y_C)}{1 + \theta \, (V_B - V_C)} \tag{51}$$

Then $V_{S'}$ is computed from

$$V_{S'} = \frac{V_C + (V_B - V_C) \, \theta \, (g y_{S'})^{\frac{1}{2}}}{1 + \theta \, (V_B - V_C)} \tag{52}$$

and $x_{S'}$ is computed from Equation (46).

The features of the experimental bore as described previously are shown in Figure 42.

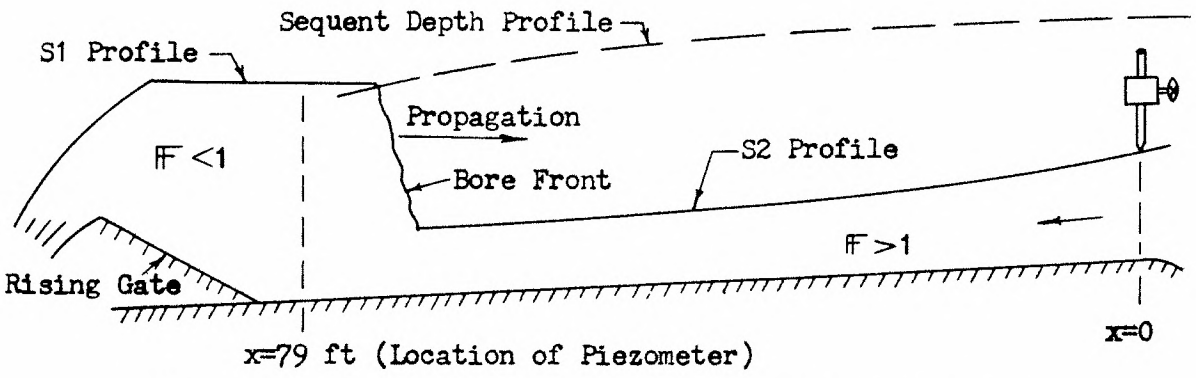

Figure 42. Schematic Diagram of the Experimental Bore

In order to simulate the bore numerically, the following features must be incorporated into the numerical solution in addition to the changes in the interpolation equations already described:

1) The initial steady state upstream S2 profile must be calculated using the depth at x=0 as a starting value.

2) The initial steady state downstream S1 profile must be calculated using the depth at x=79 ft as a starting value.

3) The initial location of the hydraulic jump must be determined.

4) A method must be devised to keep track of the location of the bore front during the transient.

5) An additional boundary condition is required downstream; namely, the experimentally determined depth hydrograph at the 79 ft station.

Profile Computations

The profile computations mentioned in items (1) and (2) above were programmed in subroutine STEADY of the Fixed Grid program (see Appendix F). The calculation of the profiles is based upon the direct application of the energy equation for steady, gradually-varied open-channel flow in a rectangular channel. The energy head relation for two points spaced a distance Δx apart, as in Figure 43, is given by:

$$\frac{V_L^2}{2g} + y_L + S_o \Delta x = \frac{V_R^2}{2g} + y_R + (H_\ell)_{L-R} \Delta x \qquad (53)$$

where $(H_\ell)_{L-R}$ is assumed to be the average of the energy slopes at L and R. Thus

$$(H_\ell)_{L-R} = \tfrac{1}{2}(S_L + S_R) \qquad (54)$$

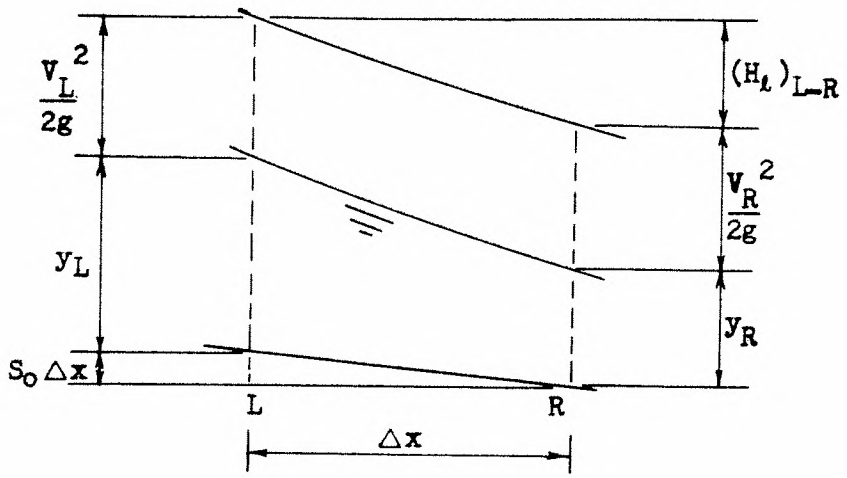

Figure 43. Sketch of the Energy Head Relation for Open-Channel Flow

If the profile is supercritical (i.e. S2), the quantities are known at L and must be determined at R. Solving for y_R in Equation (53) gives the implicit relation

$$y_R = y_L + \frac{V_L^2}{2g} - \frac{V_R^2}{2g} - \Delta x \left[\tfrac{1}{2}(S_L + S_R) - S_o\right] \qquad (55)$$

which is solved iteratively for y_R by Newton's method, holding V_R temporarily constant. When y_R converges to a constant value, V_R is computed by

$$V_R = \frac{Q}{By_R} \qquad (56)$$

This value of V_R is compared with the V_R used in Equation (55). If the difference between them is larger than the specified error bound, a new y_R is computed from Equation (55) using the V_R from Equation (56). This process is continued until V_R converges to within the error bound. The

solution for $y(n\Delta x,0)$ and $V(n\Delta x,0)$, n=1,2,3...N, is progressed in the positive x-direction starting from the known values $y(0,0)$ and $V(0,0)$.

For the subcritical reach in the channel (i.e. S1), the quantities are known at R but desired at L. The implicit relation in Equation (53) gives

$$y_L = y_R + \frac{V_R^2}{2g} - \frac{V_L^2}{2g} + \Delta x \left[\tfrac{1}{2}(S_R + S_L) - S_o\right] \qquad (57)$$

The values y_L and V_L are determined by the same procedure as described for the supercritical profile, however, in this case the solution for $y(n\Delta x,0)$ and $V(n\Delta x,0)$ is progressed in the negative x-direction starting from the known values $y(N\Delta x,0)$ and $V(N\Delta x,0)$.*

Method of Locating the Bore and Predicting the Propagation

The initial location of the hydraulic jump is determined by the sequent depth equation

$$\frac{y_2}{y_1} = \tfrac{1}{2}\left(\sqrt{1 + 8F_1^2} - 1\right) \qquad (58)$$

where y_2 is the sequent depth and y_1 is the supercritical depth. Equation (58) is derived from simple momentum considerations of a hydraulic jump neglecting the weight force of the fluid in the jump as well as the boundary shear force (see Chow [1959]). In the computer program the sequent depth is computed for each grid point of the S2 profile, resulting in a sequent depth profile as shown in Figure 42. The intersection of

*In this case the $y(N\Delta x,0)$ is known from the manometer reading at x=79 ft and $V(79,0) = Q/By(79,0)$.

the sequent depth profile and the S1 profile is assumed to be the location of the jump. Since the profiles are known only at a finite number of grid points, however, the jump is actually located at the grid point for which the difference between the sequent depth and the S1 depth is smallest. The jump is therefore represented as a step discontinuity in the numerical solution although it may physically be of the undular type or it may span several grid points.

The sequent depth calculation offers a means to predict the propagation of the bore as the tail gate is raised. The rising tail gate is represented numerically by the depth hydrograph which is measured just upstream (at x=79 ft) of it. Because of the nature of supercritical flow, the conditions upstream of the jump, including the upstream boundary conditions, remain independent of the downstream boundary condition, and thus remain invariant. On the other hand, the subcritical flow downstream of the jump is definitely affected by the tail gate motion. In the analytical solution, the S1 depth at the jump eventually will be greater than the sequent depth for that station. When this occurs, the location of the jump is arbitrarily moved upstream one station in the numerical solution. This procedure is repeated whenever the S1 depth exceeds the sequent depth for the station at which the bore is currently located.

In the numerical solution, the bore is actually a moving finite discontinuity which is the dividing point between supercritical and subcritical flow and thus represents a so-called internal boundary condition. The method of solution, however, is different for the two regions separated by the internal boundary condition. Upstream of the discontinuity

the supercritical interpolation equations are used while downstream of the discontinuity the subcritical interpolation equations are used.

The computations to locate the initial position of the jump are carried out in the STEADY subroutine (Appendix F) while the unsteady computations, including the bore propagation, are carried out in the UNSTD subroutine.

Results of the Numerical Simulation

In Figures 44 to 47 the results of the numerical simulations are compared with the observed bore propagations. In each numerical simulation the progress of the bore was stored in two arrays. One array is filled by the times at which the bore is moved up one station while the other is filled by the locations of the bore at the respective times. When these arrays are plotted on an x,t-plane, the slope of the line joining the points represents the velocity of propagation of the bore. Generally, the simulations were surprisingly accurate considering the somewhat crude method in which the downstream boundary condition was specified in the numerical solution. That is, the particular value of YDATA(I)* downstream was held constant for the five second interval until the time corresponding to YDATA(I+1) was reached in the numerical solution. At that time, the depth was stepped from YDATA(I) to YDATA(I+1). Since the Δt time intervals are small fractions of one second ($\approx \frac{1}{4}$ sec), the depth downstream is held constant through as many as 25 iterations, which accounts

---

*YDATA(I) is the array in which the downstream depth hydrograph is stored in the computer program. The array is filled with the depths at five second intervals, which are interpolated from the average manometer readings (see Appendix E for the average manometer readings).

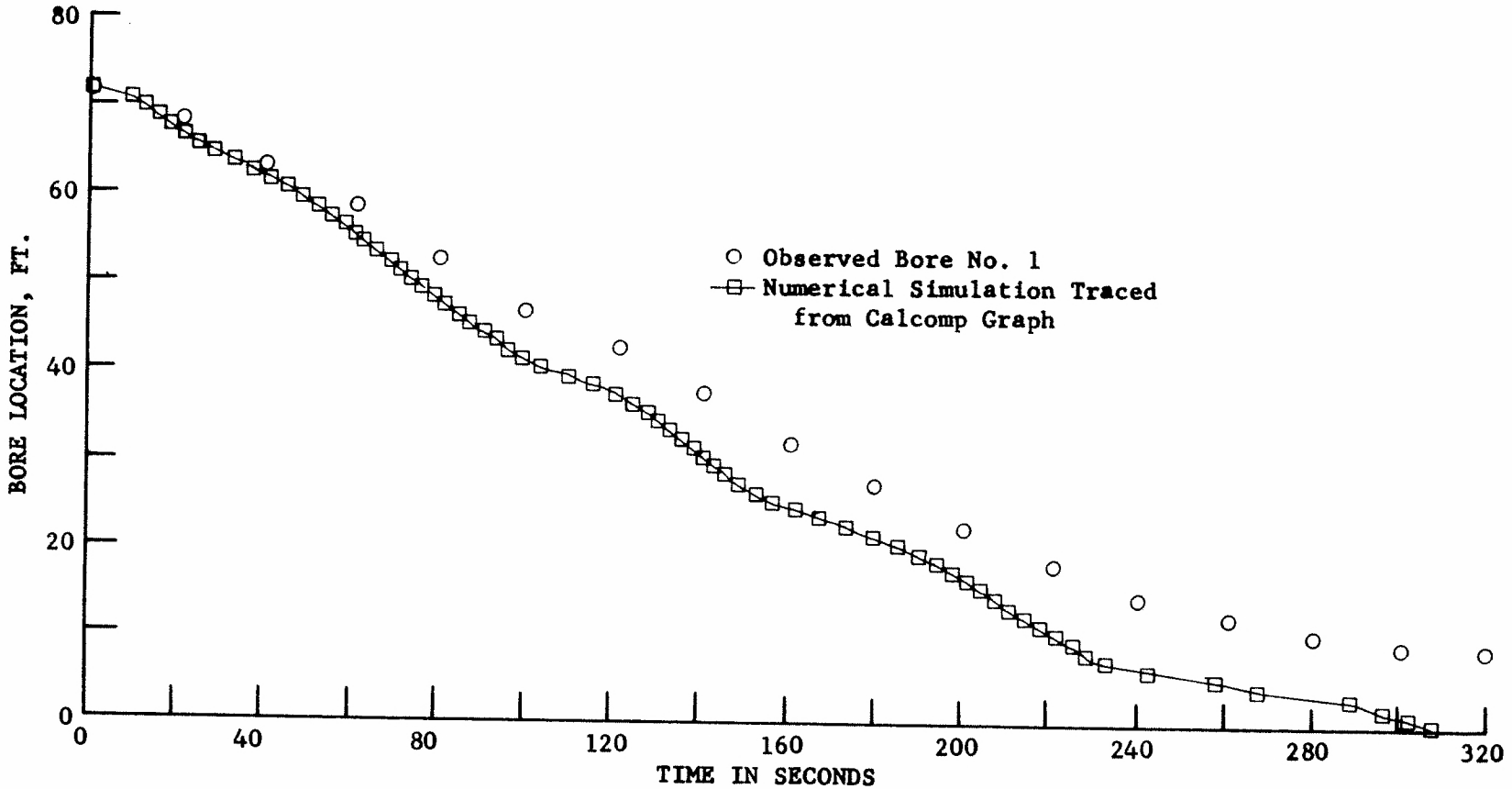

Figure 44. The Numerical Simulation Compared to the Observed Bore No. 1

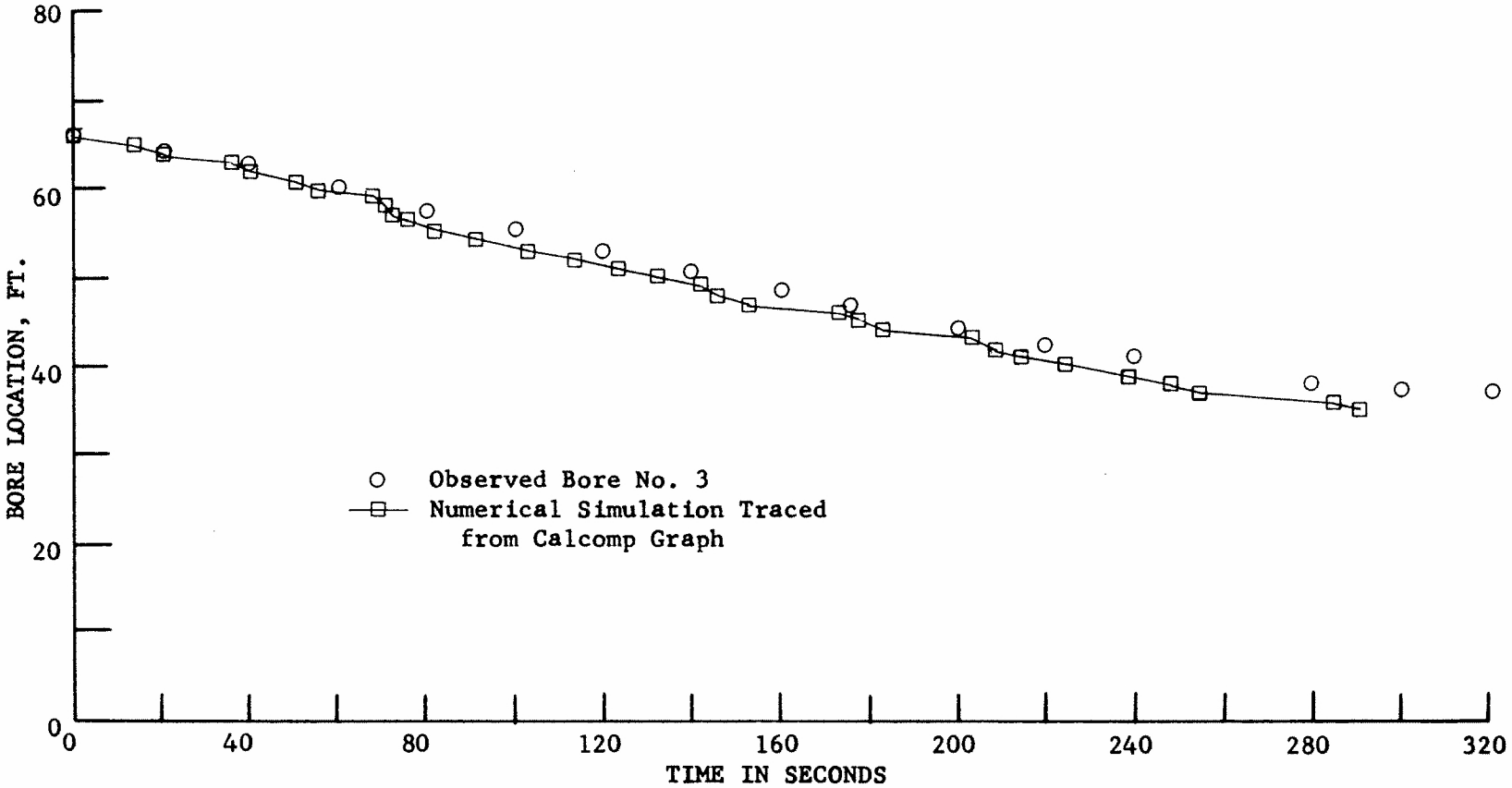

Figure 45. The Numerical Simulation Compared to the Observed Bore No. 3

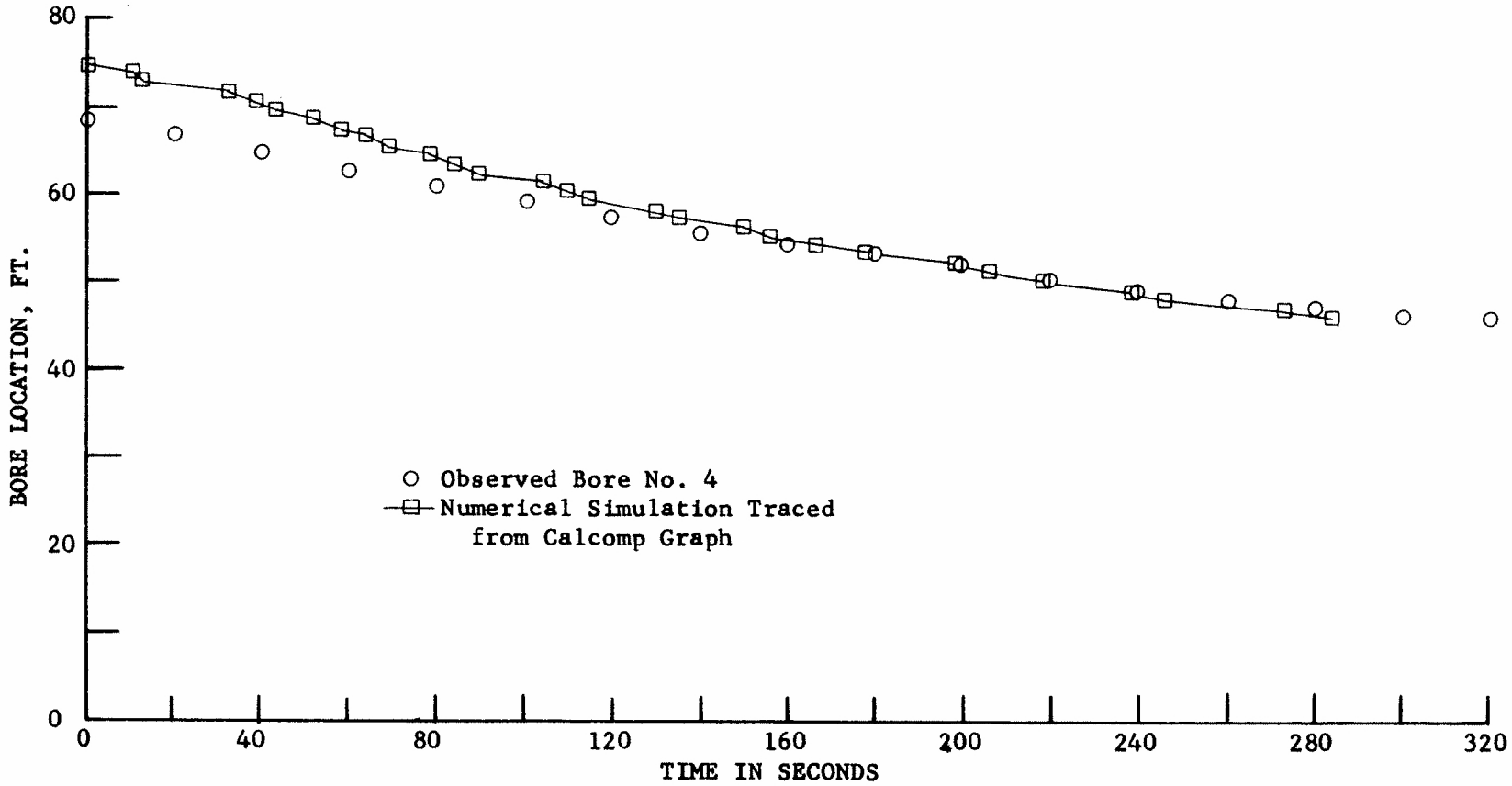

Figure 46. The Numerical Simulation Compared to the Observed Bore No. 4

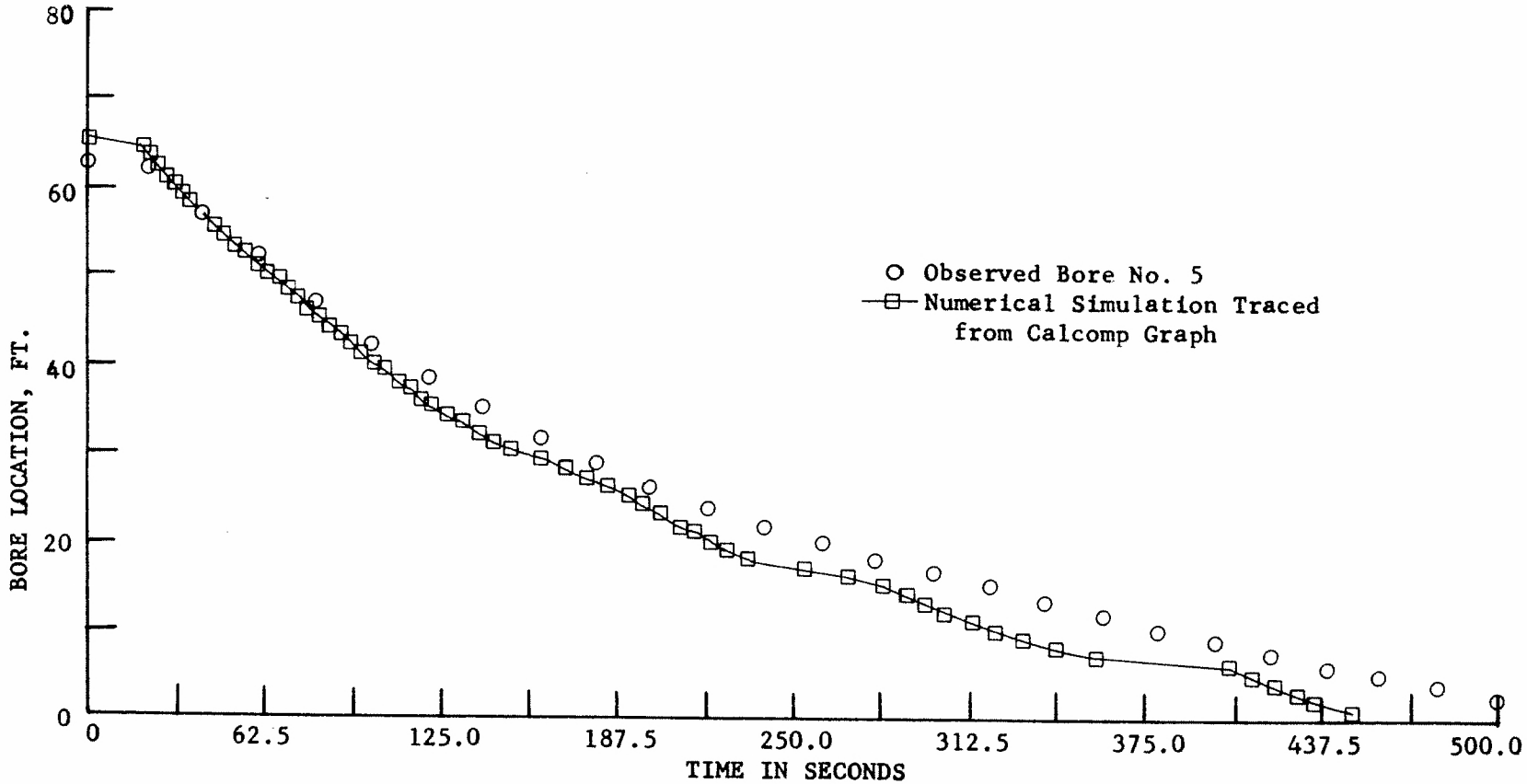

Figure 47. The Numerical Simulation Compared to the Observed Bore No. 5

in part for the "plateauing" of the points in the numerical simulations shown in Figures 44 to 47. It is quite probable that these curves could be smoothed either by specifying YDATA(I) at smaller time intervals or by interpolating between YDATA(I) values for each Δt time step. These refinements in the numerical solution should not, however, cause radical changes in the general trend of the propagation curves.

Bore No. 1

This was the trial bore in which the initial value of YDATA(I) was adjusted so that the numerical location of the stationary hydraulic jump corresponded more favorably to the experimental location. This jump, with $F \approx 1.5$ upstream, was of the undular type. The 79 ft station was located in the undular tail water of the jump and the manometer readings fluctuated ± 0.015 foot. Because of the fluctuations the adjustment of the initial depth from the experimental value of 0.20 ± 0.015 ft to the numerical value of 0.215 ft was considered justifiable. The increase in the initial depth from 0.20 ft to 0.215 ft moved the initial location of the numerical bore from 74 ft to 71 ft, as compared to the experimental location at 69.5 feet.

The manometer readings fluctuated for this bore until the bore propagated upstream to at least x=60 ft, at which time the piezometer tube was no longer in the undular tail water of the bore. The manometer then stabilized and more accurate readings were henceforth obtained. The input YDATA(I) values were adjusted so that the depth rise was uniform as compared to the average manometer readings. Even though these compensating adjustments were made in the YDATA(I) array, the comparison between the numerical and the experimental propagation was the poorest of the four

bores tested. In the other tests no particular attempt was made to adjust the numerical location of the jump nor to significantly alter the average manometer readings, yet in each case the numerical simulation was better.

Bore No. 3

As shown in Figure 45, there is almost an identical correspondence between the observed and numerical bore in this case. Chow [1959] describes the initial hydraulic jump for this case, with an upstream $F \approx 2.6$, as being an "oscillating" jump which produces a large wave of irregular period which propagates great distances downstream (see Fig. 40). Hence the depths at the downstream manometer were subject to considerable fluctuation from surface wave action as was the case for Bore No. 1. The readings were also affected by the large eddy system, as previously mentioned. These two experimental difficulties however disappeared quite rapidly as the bore propagated upstream from its initial location of x=66 ft. Although the YDATA(I) values for the first 60 sec of the propagation were adjusted only slightly for this bore, the simulation was somewhat better than that for Bore No. 1, in which the values were significantly altered.

This bore propagated more slowly ($\approx$ 0.10 ft/sec) than did Bore No. 1 ($\approx$ 0.23 ft/sec) because of the fixed mechanical speed of tail gate rise. That is, the total depth change for this bore in 260 seconds of gate rise was only 0.4 foot for a total relative depth increase of 67 percent, while for Bore No. 1 the total depth change in 200 seconds of gate rise was 0.35 foot for a total relative depth increase of 165 percent. Since the rate of relative depth rise is considerably smaller for this bore as

compared to Bore No. 1, the rate of propagation is naturally slower.

Bore No. 4

This bore was similar to Bore No. 3 except for the greater slope (two percent) and the larger upstream Froude number (≈ 2.9). Although the downstream manometer readings were subject to the same fluctuations as described for Bore No. 3, the YDATA(I) values were not adjusted to account for these variations. The initial location of the jump was observed to be at x=67.5 ft while the numerical solution placed it at x=74 ft. However, the numerical solution converged to the observed bore propagation within 80 seconds (Fig. 46).

Bore No. 5

This bore had the smallest slope (0.5 percent) and the smallest upstream Froude number (≈ 1.3) of all runs. It was an undular bore, being only barely perceptible in the flume. According to previous discussion, it would be expected to propagate more rapidly than the other three bores. The simulation was excellent (Fig. 47) although the initial location of the jump was placed at x=65 ft as compared to the observed location at x=62 ft. Again, the YDATA(I) values corresponded identically to the average manometer readings.

Other graphs, such as depth profiles and hydrographs were plotted for each of the four bores. The profiles which were plotted for Bore No. 3 are shown in Figure 48. Recalling that the upstream Froude number for this run is well above the stability limit, it would be reasonable to expect that the upstream S2 profile as computed by the method described might become unstable in the unsteady solution. In Figure 48, no such instabilities are apparent and there is no detectable change in the upstream

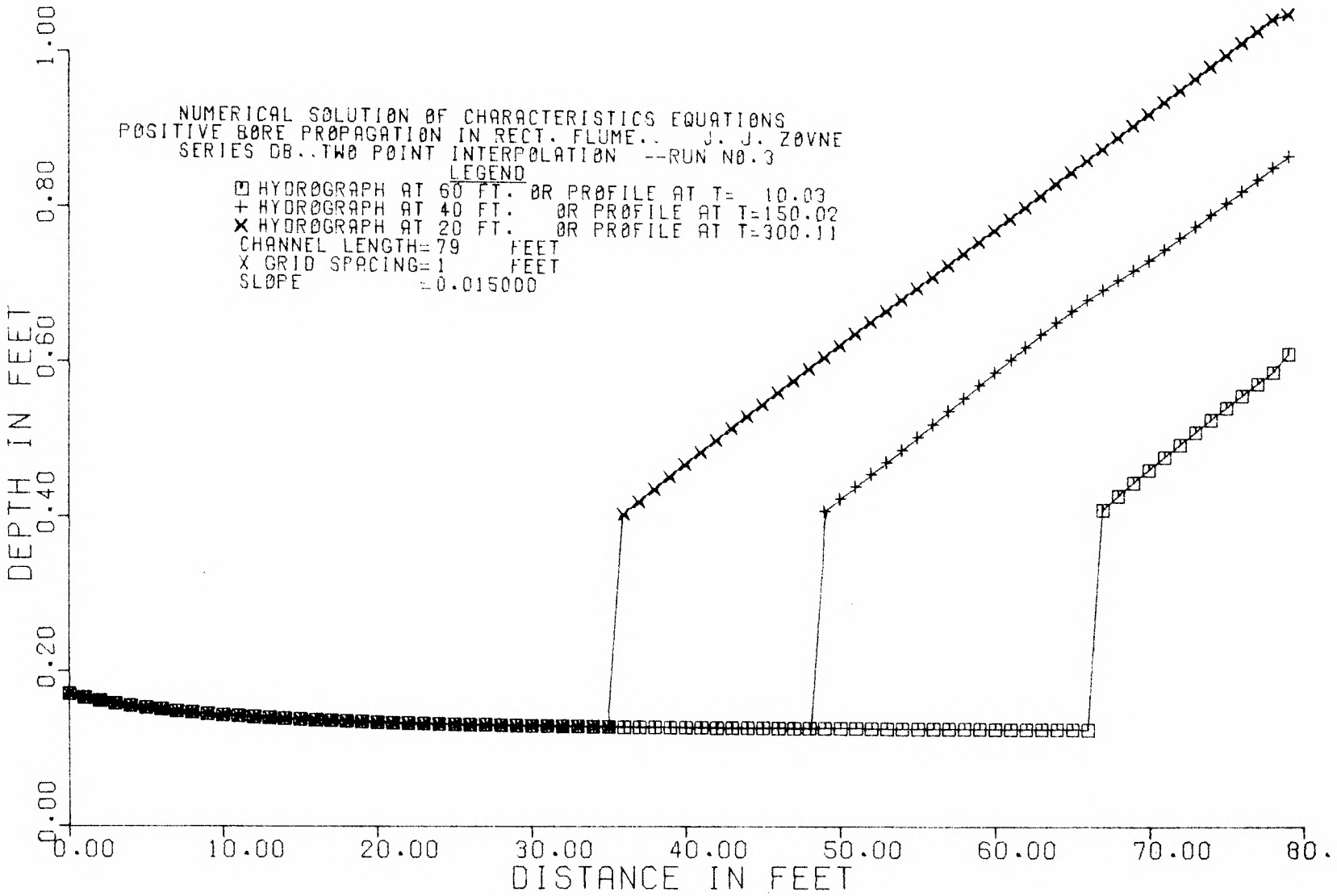

Figure 48. Profiles of Bore No. 3 Plotted by Calcomp Plotter

profile for up to 300 seconds of simulation. The method of computing the steady state profile must therefore be accurate, since according to previous analyses, any initial deviation in the profile would result in the rapid growth of an instability. Similar results were obtained for Bore No. 4 which had an even higher Froude number upstream.

The computer time required for each of these runs was inordinately large (from seven to 12 minutes) due to the small spacing (Δx=1 ft) and the fact that the Δt as determined by the Courant condition was very small. Since the Courant condition must be satisfied at every grid point, the resulting Δt is much smaller than would be required for the subcritical flow (S1 profile) alone. To reduce this computer time significantly, either the Δx can be increased or the unsteady solution for the upstream steady flow can be eliminated. The latter suggestion would apply, of course, only to the present case of a steady flow upstream.

Summary of Results

The bore propagation study presented herein was meant primarily to provide additional support for the numerical techniques developed earlier. There has been no attempt as yet to refine the methods for numerically simulating the propagation of the bore since the results were satisfactory and adequately served the purpose without additional refinements.

It is possible that some more general bore propagation problems could be solved numerically using the basic method developed herein. For instance, the program could be altered to simulate the propagation of a negative bore and an unsteady discharge could be allowed to enter the channel upstream. The negative bores obtained by lowering the tail gate

were observed and recorded for the four cases studied here; however, the program has not yet been altered to include this case. Furthermore, since unsteady upstream discharges are difficult to measure accurately for the flume used in this study, this type of flow was not studied either experimentally or numerically. These relatively simple refinements and additions to the numerical technique are therefore reserved for future investigation. It is pointed out, however, that whenever unsteady, supercritical flow is encountered, the Froude number of this flow should be below the theoretical stability limit, as previously mentioned.

The comparisons between the experimental and the numerical propagations of the four bores tested were surprisingly good in view of the experimental difficulties encountered. Although the computer programming for the numerical simulation was the simplest imaginable, the sequent depth proved adequate as a device for locating and propagating the bore front in the numerical solution. Of course, the simulation of the water surface profile downstream of the bore front was not an objective of this investigation. This might, once again, require a two- or three-dimensional representation of the flow equations.

It is quite probable that this basic computer program could be expanded into a more general program which could solve for several interconnecting channels with a variety of boundary conditions and channel cross sections. General programs such as this for flows restricted to the subcritical regime are presently available [see Martin and DeFazio, 1969]. To the writer's knowledge there are none as yet available which can handle both subcritical and supercritical flow where the possibility

of bore inception is present. There appears to be a practical need for this type of program as indicated to the writer by personnel of the Tennessee Valley Authority.

CHAPTER VI

CONCLUSIONS AND RECOMMENDATIONS

The major conclusions of this investigation are:

1) It is possible to simulate numerically unsteady, supercritical, open-channel flow using the method of characteristics by relying heavily upon the numerical techniques developed for subcritical flow. It is, however, necessary to be aware of problems which are unique to supercritical flow, such as the change in the boundary conditions and the nature of the occurrence of discontinuities.

2) Of the two finite-difference methods applied to the characteristic equations that are used in this study, namely, the Fixed Grid method and the Characteristics Grid method, the Fixed Grid method was found to be the more reliable for supercritical flow simulation. Although the Characteristics Grid method is perhaps the more accurate and efficient of the two, it was found to be considerably more difficult to program for supercritical flow.

3) When a solution obtained by the Fixed Grid method was compared with one obtained by the Characteristics Grid method, it was revealed that the wave propagation characteristics were very nearly identical. Since the Characteristics Grid method is often used as a standard for accuracy, at least for the much studied subcritical case, additional support was therefore gained for the recommendation of the Fixed Grid method over the Characteristics Grid method.

4) An advantage of the Fixed Grid method for the engineering type of solutions sought here is that the method itself precludes the formation

of a shock. That is, the crossing of characteristics of the same family is not allowed by the interpolation technique although the boundary conditions may indicate that such a crossing is likely to occur. Instead, the solution yields a continuous smooth surge profile in the vicinity of the discontinuity which may be adequate for engineering purposes, since the profile behind the surge then gradually attains the maximum anticipated depth which is often of primary interest to the engineer.

5) Both the Fixed Grid method and the Characteristics Grid method were found to be numerically unstable when the Froude number was above the theoretical stability limit for turbulent supercritical flow in a rectangular, hydraulically smooth channel. Conversely, both methods were found to be numerically stable when the Froude number was below the theoretical stability Froude number.

6) The Fixed Grid method satisfied a continuity test devised for this method of solution whenever the upstream boundary condition was either a linearly rising or a linearly falling hydrograph.

7) The simple two-point interpolation type of solution used in the Fixed Grid method was found to be very rapid yet sufficiently accurate to warrant its use over the considerably less efficient, although perhaps somewhat more accurate, three-point interpolation type of solution. On the other hand, the device of averaging friction slopes increased the accuracy somewhat without significantly increasing the time required for solution.

8) By using the Fixed Grid method with an additional internal boundary condition it was possible to numerically simulate the propagation of an experimental bore. The relatively simple technique of employing the sequent depth equation as a means to follow the propagation of the bore

front was found to be an adequate specification of the internal boundary condition. Although the Fixed Grid method had to be programmed to operate in both the subcritical and the supercritical regimes, no other special finite-difference equations were required to simulate the rapidly-varied flow in the vicinity of the bore front.

9) A disadvantage of using the Fixed Grid method to simulate the bore propagation is that inordinately large amounts of computer time are required for solution. This is basically a result of the necessity of using small grid spacings to adequately simulate the bore propagation, which in turn results in the specification of very small time increments to satisfy the Courant condition for stability.

In this investigation only two finite-difference methods were singled out for extensive analysis pertaining to the numerical simulation of supercritical flow. Presumably other finite-difference methods such as the second-order method of characteristics as proposed by Liggett and Woolhiser [1967], the Lax-Wendroff method, and the leap-frog method would work equally as well as the Fixed Grid method. A comparison of these methods would be an interesting future investigation. Future research could also be directed toward defining more clearly the role of friction in causing numerical instability in supercritical flow.

A practical outgrowth of this investigation would be to develop a more general computer program to simulate a wider variety of open-channel flow problems. This program could be devised to solve problems in subcritical and/or supercritical flow for a variety of boundary conditions and channel cross sections and for a number of interconnecting channels.

APPENDIX A

METHOD OF AVERAGING FRICTION SLOPES FOR THE CHARACTERISTICS GRID SOLUTION

In Equations (24) and (25) the friction slopes from R to P and S to P were approximately given by their respective values at R and S, that is, S_R and S_S. Another somewhat more accurate approximation is to use average friction slopes from R to P and S to P. Using the average slopes, $\frac{1}{2}(S_R + S_P)$ and $\frac{1}{2}(S_S + S_P)$, the difference Equations (13) and (15) can be rewritten as:

$$V_P - V_R + \lambda\,(y_P - y_R) + g\left(\frac{S_R + S_P}{2} - S_o\right)(t_P - t_R) = 0 \qquad (59)$$

$$= G\,(y_P, V_P)$$

$$V_P - V_S - \lambda\,(y_P - y_S) + g\left(\frac{S_S + S_P}{2} - S_o\right)(t_P - t_S) = 0 \qquad (60)$$

$$= H\,(y_P, V_P)$$

These two equations can no longer be solved directly as were Equations (24) and (25) because they are nonlinear in y_P and V_P (Eqn. 4). An iterative scheme is therefore employed to solve the equations using Newton's method for a system of equations [Conte, 1965]. The iterative scheme is given as follows,

$$y_{P(k+1)} = y_{P(k)} - \left[\frac{GH_{V_P} - HG_{V_P}}{G_{y_P} H_{V_P} - H_{y_P} H_{V_P}}\right]_k \tag{61}$$

$$V_{P(k+1)} = V_{P(k)} - \left[\frac{HG_{y_P} - GH_{y_P}}{G_{y_P} H_{V_P} - H_{y_P} G_{V_P}}\right]_k \tag{62}$$

where G and H denote the functions given by Equations (59) and (60), G_{y_P} is the partial derivative of G with respect to y_P, etc., and the subscript k denotes the iteration level. The initial values of y_P and V_P are obtained from Equations (24) and (25) and the new values $y_{P(k+1)}$ and $V_{P(k+1)}$ are computed using Equations (61) and (62). The new values are then used for the next iteration and the process is continued until $\left|y_{P(k+1)} - y_{P(k)}\right| \leqq \epsilon_1$ and $\left|V_{P(k+1)} - V_{P(k)}\right| \leqq \epsilon_2$, where ϵ_1 and ϵ_2 are predetermined error bounds. The partial derivatives are given as:

$$G_{y_P} = \left(\frac{g}{y_R}\right)^{\frac{1}{2}} + \frac{g}{2}\left[\frac{fV_P^2}{8gB^3}\left(\frac{-4\,y_P^3 - 3\,y_P^2 B}{y_P^6}\right)\right](t_P - t_R) \tag{63}$$

$$G_{V_P} = 1 + \frac{g}{2}\left[\frac{f}{8g}\left(\frac{3V_P}{y_P} + \frac{4V_P}{B}\right)\right](t_P - t_R) \tag{64}$$

$$H_{y_P} = -\left(\frac{g}{y_S}\right)^{\frac{1}{2}} + \frac{g}{2}\left[\frac{fV_P^2}{8gB^3}\left(\frac{-4\,y_P^3 - 3\,y_P^2 B}{y_P^6}\right)\right](t_P - t_S) \tag{65}$$

$$H_{V_P} = 1 + \frac{g}{2}\left[\frac{f}{8g}\left(\frac{3V_P}{y_P} + \frac{4V_P}{B}\right)\right](t_P - t_S) \tag{66}$$

where the friction factor f is taken to be constant. This is a reasonable assumption since f varies approximately inversely to the 1/5 power of both y_p and V_p and thus remains nearly constant throughout an entire iteration.*

*For the range of $\mathfrak{R}$ used in this study, $f \approx 0.236/\mathfrak{R}^{0.21}$.

APPENDIX B

THREE-POINT INTERPOLATION FOR THE FIXED GRID SOLUTION

A three-point interpolation using the known grid points D, A, C in Figure 12 can be used to obtain a more refined second-order approximation of y_R, V_R, y_S, and V_S. The linear interpolation Equations (27) and (28) are replaced by the second-order interpolation equations,

$$y_R = r_1 x_R^2 + r_2 x_R + r_3 \tag{67}$$

$$V_R = r_4 x_R^2 + r_5 x_R + r_6 \tag{68}$$

where r_1, r_2,...r_6 are coefficients resulting from a three-point Lagrange interpolating polynomial given as:

$$r_1 = \frac{1}{2\Delta x^2} (y_D - 2y_A + y_C) \tag{69}$$

$$r_2 = \frac{1}{2\Delta x^2} [- y_D(2x_C-\Delta x) + 4y_A(x_C-\Delta x) - y_C(2x_C-3\Delta x)] \tag{70}$$

$$r_3 = \frac{1}{2\Delta x^2} [- y_D x_C(x_C-\Delta x) - 2y_A x_C(x_C-2\Delta x) + y_C(x_C-\Delta x)(x_C-2\Delta x)] \tag{71}$$

$$r_4 = \frac{1}{2\Delta x^2} (V_D - 2V_A + V_C) \tag{72}$$

$$r_5 = \frac{1}{2\Delta x^2} [- V_D(2x_C-\Delta x) + 4V_A(x_C-\Delta x) - V_C(2x_C-3\Delta x)] \tag{73}$$

$$r_6 = \frac{1}{2\Delta x^2}\left[- V_D x_C(x_C-\Delta x) - 2V_A x_C(x_C-2\Delta x) + V_C(x_C-\Delta x)(x_C-2\Delta x)\right] \quad (74)$$

As before, Equations (26), (67), and (68) can be solved simultaneously for x_R, y_R, and V_R. However, in this case, the solution requires an iterative scheme. In all, three iterative techniques were tried. The first two were based upon Newton's method and were neither as efficient nor as consistent as the third method which was a simple trial-and-error method. In the trial-and-error method the initial estimate of x_R is computed from the equation:

$$x_{Ro} = x_C - (V_A + c_A)\,\Delta t \quad (75)$$

The y_R and V_R are then computed from Equations (67) and (68). A new x_R is then computed using Equation (26) and is compared to the old value. This process is continued until $\left|x_{R(k+1)} - x_{R(k)}\right| \leqq \epsilon$.

The values of x_S, y_S, and V_S are obtained in the same manner using Equation (34) and the following interpolation equations,

$$y_S = r_1 x_S^2 + r_2 x_S + r_3 \quad (76)$$

$$V_S = r_4 x_S^2 + r_5 x_S + r_6 \quad (77)$$

in which the initial estimate of x_S is obtained from the equation,

$$x_{So} = x_C - (V_A - c_A)\Delta t \quad (78)$$

The values of y_p and V_p can then be determined from Equations (39) and (40) or Equations (79) and (80).

APPENDIX C

METHOD OF AVERAGING FRICTION SLOPES FOR THE FIXED GRID SOLUTION

Averaging the friction slopes for this method results in a somewhat simpler set of equations than those given in Appendix A for the Characteristics Grid (Eqn. 59 and 60). Replacing S_S and S_R in Equation (39) by $\frac{1}{2}(S_R + S_P)$ and $\frac{1}{2}(S_S + S_P)$ results in a direct determination of y_P

$$y_P = \frac{V_R - V_S + g(S_S - S_R)\frac{\Delta t}{2} + c_R + c_S}{(g/y_R)^{\frac{1}{2}} + (g/y_S)^{\frac{1}{2}}} \tag{79}$$

From Equation (40) V_P becomes:

$$V_P - V_R + \left(\frac{g}{y_R}\right)^{\frac{1}{2}}(y_P - y_R) + g\left(\frac{S_R + S_P}{2} - S_o\right)\Delta t = 0 = F(V_P) \tag{80}$$

An iterative procedure is necessary to determine V_P. In this study Newton's method for a single equation is used:

$$V_{P(k+1)} = V_{P(k)} - \frac{F(V_{P(k)})}{F'(V_{P(k)})} \tag{81}$$

Assuming again that f is constant the resulting iterative equation is:

$$V_{P(k+1)} = V_{P(k)} - \frac{V_{P(k)} - V_R + \left(\frac{g}{y_R}\right)^{\frac{1}{2}}(y_P - y_R) + g\left(\frac{S_R + S_{P(k)}}{2} - S_o\right)\Delta t}{1 + \frac{f}{8}\frac{V_{P(k)}}{R_P}\Delta t} \tag{82}$$

The initial value of V_P for this equation is given by Equation (40) and the iteration is performed until $\left|V_{P(k+1)} - V_{P(k)}\right| \leq \epsilon$.

APPENDIX D

SERIES AS AND SERIES AL COMPUTER PROGRAMS

Series AS Program (Two-Point Interpolation)

Nomenclature by Subroutine

1) SUBROUTINE MAIN
   K - Index parameter.
   NPROB - Number of problems to be solved.

2) SUBROUTINE UNSTD (Unsteady Solution)
   I, IPLOT, K, M, N - Index parameters.
   NM - Integer corresponding to the mid-gridpoint of the channel.
   NP - Integer corresponding to the total number grid points.
   NPLT - Integer corresponding to the total number of points in a hydrograph plot.
   NX - Input integer corresponding to the total number of channel reaches; = NP-1
   XL - Input channel length.
   S - Input channel slope.
   B - Input channel width.
   GNU - Input kinematic viscosity.
   TL - Input time of hydrograph rise (used in Series AL solution).
   TMAX - Input total time duration of solution.
   RUNNO - Input run number for plot legend.
   TITLE (I) - Input alphanumeric title field for printed output.
   GR - Gravitational constant.
   T - Current time level in unsteady solution.
   X(I) - Array of channel locations corresponding to grid points.
   Y(I) - Array of flow depths corresponding to grid points.
   V(I) - Array of flow velocities corresponding to grid points.
   FR - Froude number.
   REY - Reynolds number.
   FRICF - Friction factor.
   TPL(I) - Array of times corresponding to depths or velocities for hydrograph plots.
   Y1N(I) - Array of depths for hydrograph plot at 5^{th} gridpoint.
   Y2N(I) - Array of depths for hydrograph plot at mid-gridpoint.
   Y3N(I) - Array of depths for hydrograph plot at end-gridpoint.
   V1N(I) - Array of velocities for hydrograph plot at 5^{th} gridpoint.
   V2N(I) - Array of velocities for hydrograph plot at mid-gridpoint.
   V3N(I) - Array of velocities for hydrograph plot at end-gridpoint.

DTINV - Inverse of Δt time interval.
DTT - Inverse Δt time interval for current gridpoint from Courant condition.
DT - Minimum Δt for entire channel for next iteration.
YP(I) - Array of depths for T+DT time level.
VP(I) - Array of velocities for T+DT time level.
DX - Length of a channel reach between gridpoints.
TH - Ratio DT/DX.
A1 - Function used in interpolation (corresponds to χ in text).
B1 - Function used in interpolation (corresponds to ψ in text).
YR - Interpolated value of y at point R (Fig. 12).
CR - Celerity at point R.
VR - Interpolated value of V at point R (Fig. 12).
XR - Location of point R (Fig. 10).
YS - Interpolated value of y at point S (Fig. 12).
CS - Celerity at point S.
VS - Interpolated value of V at point S (Fig. 12).
XS - Location of point S.
SFR - Friction slope at point R.
YFIN - Average depth for a reach at T+DT.
YBEG - Average depth for a reach at T.
DELY - Average increase in depth for a reach during DT.
DSTR(I) - Increment of reach storage during DT, for each reach.
QINTO - Average flow rate into reach during DT.
QOUT - Average flow rate out of reach during DT.
DQSTR(I) - Net volume flowing into reach during DT, for each reach.
CUMSTR(I) - Cumulative storage for each reach to T+DT.
CUMQ(I) - Cumulative net volume flowing into each reach to T+DT.
YPR1(I) - Array of depth values for profile plot at time TPR1.
YPR2(I) - Array of depth values for profile plot at time TPR2.
YPR3(I) - Array of depth values for profile plot at time TPR3.

2) SUBROUTINE STEADY (Uniform flow computation by trial-and-error).
YSTART - Input value of y(0,0).
QI - Input constant value of discharge.
D(I) - Current value of uniform flow depth.
U(I) - Current value of uniform flow velocity.
SA - Current value of friction slope.

3) FUNCTION C(D) (Computation of celerity for a depth, D).
C - Celerity.

4) FUNCTION SF(D,U,FRICF) (Computation of friction slope for a depth D, a velocity U, and a friction factor, FRICF).
SF - Friction slope using Darcy equation.

5) FUNCTION F(D,U) (Computation of friction factor for a depth D and a velocity U).
F1 - Initial estimate of friction factor.
F - Friction factor computed by Newton's method from Eqn. (5).

6) FUNCTION R(D) (Computation of hydraulic radius for a depth D).
R - Hydraulic radius.

7) SUBROUTINE MAXMIN (D,V,TT,NPP,XX,TTMAX) (Computation of maximum and minimum values of y and V at each grid point for duration of run).

D(I) - Input array of depths at each grid point for a time level T.
U(I) - Input array of velocities at each grid for a time level T.
DMAX(I) - Current maximum depth at each grid point.
TDMAX(I) - Time at which current DMAX(I) occurred at each grid point.
DMIN(I) - Current minimum depth at each grid point.
TDMIN(I) - Time at which current DMIN(I) occurred at each grid point.
UMAX(I) - Current maximum velocity at each grid point.
TUMAX(I) - Time at which current UMAX(I) occurred at each grid point.
UMIN(I) - Current minimum velocity of each grid point.
TUMIN(I) - Time at which current UMIN(I) occurred at each grid point.

8) SUBROUTINE GRAPHS (Assembles and organizes plot data for plotting by Calcomp plotter).

ZEROY - Input initial value of depth scale.
DELY - Input depth scale increment/inch.
ZEROV - Input initial value of velocity scale.
DELV - Input velocity scale increment/inch.
CALL PLOT - Calls machine subroutine to command movement of plotter pen.
CALL LINE - Calls machine subroutine to command the plotting of arrays of points.
CALL SYMBOL - Calls machine subroutine to plot titles and legends.
CALL AXIS - Calls machine subroutine to command the plotting of axes.

```
-FOR,IS  MAIN
         K=0
    5    READ(5,10) NPROB
   10    FORMAT(I2)
   15 CALL UNSTD
         CALL GRAPHS
         K=K+1
         IF(K.NE.NPROB) GO TO 15
         CALL PLOT(16.0,0.0,999)
      STOP
      END
-FOR,IS  UNSTD
      SUBROUTINE UNSTD
      DIMENSION TITLE(160),Q(200),VP(200),YP(200)
         DIMENSION STOR(999),QSTOR(999),DSTR(999),DQSTR(999),CUMSTR(999)
     1           ,CUMQ(999)
      COMMON/Z1/Y(200),V(200),X(200),NX,XL,S,B,GR,GNU,DX,
     1         YSTART,QI,NP,M
      COMMON/Z2/TPL(500),Y1N(500),Y2N(500),Y3N(500),V1N(500),V2N(500),
     1 V3N(500),NPLT,RUNNO,YPR1(200),YPR2(200),YPR3(200),TPR1,TPR2,TPR3,
     2         TMAX
      NAMELIST/INPUT/NX,XL,S,B,          GNU,TL    ,TMAX,M,RUNNO
         READ(5,31) K
   31    FORMAT(I2)
         K=K*16
         READ(5,32) (TITLE(I),I=1,K)
   32    FORMAT(16A5)
         WRITE(6,33) (TITLE(I),I=1,K)
   33    FORMAT(1H1////////////(25X,16A5/))
         READ(5,INPUT)
         GR=32.166
         N=1
         T=0.0
         DO 250 I=1,NX
         STOR(I)=0.
  250    QSTOR(I)=0.
      CALL STEADY(Y,V)
         CALL MAXMIN(Y,V,T,NP,X,TMAX)
         WRITE(6,10) RUNNO
   10    FORMAT(25X,8HRUN NO. ,F4.1)
         WRITE(6,34) XL,S,B,GNU,QI,YSTART,TMAX,NX,TL
   34    FORMAT(1H1,10HINPUT DATA//5X,7HLENGTH=F7.1,10X,6HSLOPE=,F10.8,
     1         10X,6HWIDTH=,F5.2,10X,15HKIN. VISCOSITY=,F10.9/5X,
     212HINI. DISCH.=,F9.6,5X,11HINI. DEPTH=,F8.4,   10X,12HTIME OF RUN=
     3,        F7.1,3HSEC/5X,3HNX=,I3,5X,3HTL=,F6.2/)
         WRITE(6,76)
   76    FORMAT(5X,51HINITIAL STEADY STATE SURFACE PROFILE AND VELOCITIE
     1S/5X,13HDISTANCE, FT.,10X,10HDEPTH, FT.,10X,16HVELOCITY, FT/SEC,
     2   10X,13HDISCHARGE,CFS)
         WRITE(6,77) X(1),Y(1),V(1),QI
   77    FORMAT(10X,F6.0,13X,F8.6,13X,F9.6,16X,F9.6/)
```

```
      FR=V(1)/C(Y(1))
      REY=4.*R(Y(1))*V(1)/GNU
      FRICF=F(Y(1),V(1))
      WRITE(6,78) FR,REY,FRICF
   78 FORMAT(5X,11HFROUDE NO.=,F5.3,5X,13HREYNOLDS NO.=,E12.6,5X,
     1       12HFRIC. FACT.=,F8.7//)
      IPLOT=1
      TPL(1)=0.
      NM=NX/2.+1
      Y1N(1)=Y(5)
      V1N(1)=V(5)
      Y2N(1)=Y(NM)
      V2N(1)=V(NM)
      Y3N(1)=Y(NP)
      V3N(1)=V(NP)
C     OBTAIN THE MAXIMUM VALUE OF DT FOR LAST INTERVAL
   35 DTINV=0.
      DO 50 I=1,NP
   45 DTT=(V(I)+C(Y(I)))/DX
      IF(DTT.GT.DTINV) DTINV=DTT
   50 CONTINUE
      DT=1.0/DTINV
   60 T=T+DT
C     COMPUTE VALUES AT UPSTREAM BOUNDARY FO TIME T
      YP(1)=Y(1)
      VP(1)=V(1)
C     COMPUTE INTERMEDIATE VALUES
  150 DO 180 I=2,NP
      IF(IPLOT.NE. 5) GO TO 160
      IF(I.NE.5) GO TO 160
      Y(I)=1.1*Y(I)
  160 TH=DT/DX
      A1=SQRT(GR)*TH*(Y(I)-Y(I-1))/(1.+TH*(V(I)- V(I-1)))
      B1=TH*V(I)*(Y(I)-Y(I-1))/(1.+TH*(V(I)-V(I-1)))-Y(I)
C     LOCATION OF C PLUS CHARACTERISTIC
      YR=.5*A1*A1-B1-A1*SQRT(.25*A1*A1-B1)
      CR=C(YR)
      VR=(V(I)-(V(I)-V(I-1))*TH*CR)/(1.+TH*(V(I)-V(I-1)))
      XR=X(I)-DT*(VR+CR)
C     LOCATION OF C MINUS CHARACTERISTIC
      YS=.5*A1*A1-B1+A1*SQRT(.25*A1*A1-B1)
      CS=C(YS)
      VS=(V(I)+(V(I)-V(I-1))*TH*CS)/(1.+TH*(V(I)-V(I-1)))
      XS=X(I)-DT*(VS-CS)
C     COMPUTATION ALONG CHARACTERISTICS TO T+DT
      AR=SQRT(GR/YR)
      AS=SQRT(GR/YS)
C     COMPUTATION ALONG CHARACTERISTICS TO T+DT
      AR=SQRT(GR/YR)
      AS=SQRT(GR/YS)
      SFR=SF(YR,VR,F(YR,VR))
      YP(I)=(VR-VS+GR*(SF(YS,VS,F(YS,VS))-SFR)*DT/2.+AR
```

```
     1          *YR+AS*YS)/(AR+AS)
           VP(I)=VR-AR*(YP(I)-YR)-GR*(SFR-S)*DT
  180 CONTINUE
           DO 182 I=1,NX
           YFIN=(YP(I)+YP(I+1))/2.
           YBEG=(Y(I)+Y(I+1))/2.
           DELY=YFIN-YBEG
           DSTR(I)=DELY*B*DX
           QINTO=B*(VP(I)*YP(I)+V(I)*Y(I))/2.
           QOUT=B*(VP(I+1)*YP(I+1)+V(I+1)*Y(I+1))/2.
  182      DQSTR(I)=(QINTO-QOUT)*DT
           DO 183  I=1,NX
           STOR(I)=STOR(I)+DSTR(I)
  183      QSTOR(I)=QSTOR(I)+DQSTR(I)
           CUMSTR(1)=STOR(1)
           CUMQ(1)=QSTOR(1)
           DO 184  I=2,NX
           CUMSTR(I)=CUMSTR(I-1)+STOR(I)
           CUMQ(I)=CUMQ(I-1)+QSTOR(I)
  184      CONTINUE
  185 DO 190 I=1,NP
           Y(I)=YP(I)
           V(I)=VP(I)
           IF(IPLOT.NE. 5) GO TO 186
           YPR1(I)=YP(I)
           TPR1=T
           GO TO 19.
  186      IF(IPLOT.NE. 40) GO TO 187
           YPR2(I)=YP(I)
           TPR2=T
           GO TO 190
  187      IF(IPLOT.NE. 70) GO TO 190
           YPR3(I)=YP(I)
           TPR3=T
  190      Q(I)=V(I)*Y(I)*B
           CALL MAXMIN(Y,V,T,NP,X,TMAX)
           IF(T.LT.FLOAT(N)*10.) GO TO 195
  189      WRITE(6,191) T
  191      FORMAT( 5X,5HTIME=,F9.3,3HSEC//)
           WRITE(6,192)
  192      FORMAT(5X,11HDISTANCE,FT,2X,                8HDEPTH,FT,2X,
     1          15HVELOCITY,FT/SEC,2X,13HDISCHARGE,CFS,2X,22HSTORAGE VS.
     2INFLOW,FT3,5X,30HCUM. WAVE STOR. VS. NET INFLOW)
           DO 193 I=1,NP,1
  193      WRITE(6,93) X(I),Y(I),V(I),Q(I),STOR(I),QSTOR(I),CUMSTR(I),
     1          CUMQ(I),I
   93      FORMAT(5X,F8.2,4X,F7.4, 4X,F9.4,10X,F8.4,5X,F10.6,2X,F10.6,8X,
     1          F10.6,2X,F10.6,2X,I5)
           IPLOT=IPLOT+1
           TPL(IPLOT)=T
           Y1N(IPLOT)=Y(5)
           V1N(IPLOT)=V(5)
```

```
          Y2N(IPLOT)=Y(NM)
          V2N(IPLOT)=V(NM)
          Y3N(IPLOT)=Y(NP)
          V3N(IPLOT)=V(NP)
  195     IF(T.GE.TMAX) GO TO 200
          GO TO 35
  200     NPLT=IPLOT
          N=N+1
          RETURN
        END
-FOR,IS  STEADY
        SUBROUTINE STEADY(D,U)
        DIMENSION D(55),U(55)
        COMMON/Z1/Y(200),V(200),X(200),NX,XL,S,B,GR,GNU,DX,
       1         YSTART,QI,NP,M
        NAMELIST/INPUT2/YSTART,QI
           READ(5,INPUT2)
           DX=XL/FLOAT(NX)
           X(1)=0.0
           D(1)=YSTART
           U(1)=QI/(B*D(1))
           NP=NX+1
   20      SA=SF(D(1),U(1),F(D(1),U(1)))
           IF(ABS(SA-S).LT.0.000000001) GO TO 30
           U(1)=SQRT(8.*GR*R(D(1))*S/ F(D(1),U(1)))
           D(1)=QI/(B*U(1))
           GO TO 20
   30      DO 40 J=2,NP
           D(J)=D(J-1)
           U(J)=U(J-1)
   40      X(J)=X(J-1)+DX
           RETURN
        END
-FOR,IS  CELER
        FUNCTION C(D)
        COMMON/Z1/Y(200),V(200),X(200),NX,XL,S,B,GR,GNU,DX,
       1         YSTART,QI,NP,M
           C=SQRT(GR*D)
        RETURN
        END
-FOR,IS  FSLOPE
        FUNCTION SF(D,U,FRICF)
        COMMON/Z1/Y(200),V(200),X(200),NX,XL,S,B,GR,GNU,DX,
       1         YSTART,QI,NP,M
           SF=U*ABS(U)*FRICF/(8.*R(D)*GR)
           IF(M.EQ.2) SF=0.
        RETURN
        END
-FOR,IS  FFACT
        FUNCTION F(D,U)
        COMMON/Z1/Y(200),V(200),X(200),NX,XL,S,B,GR,GNU,DX,
       1         YSTART,QI,NP,M
```

```
      F1=0.236/((4.*U*R(D)/GNU)**(0.2126))
10    F=F1-((2.03*ALOG10(4.*R(D)*U*(F1**0.5)/GNU)-1./(F1**0.5)-1.30)/
     1  (1.015*ALOG10(EXP(1.))/F1+0.5/(F1**1.5)))
      IF(ABS(F-F1).LT.0.000001) GO TO 20
      F1=F
      GO TO 10
20    RETURN
      END
-FOR,IS  HYDRAD
      FUNCTION R(D)
      COMMON/Z1/Y(200),V(200),X(200),NX,XL,S,B,GR,GNU,DX,
     1        YSTART,QI,NP,M
      R=B*D/(B+2.*D)
      RETURN
      END
-FOR,IS  MM
      SUBROUTINE MAXMIN(D,U,TT,NPP,XX,TTMAX)
      DIMENSION D(200),U(200),DMAX(200),TDMAX(200),DMIN(200),TDMIN(200),
     1  UMAX(200),TUMAX(200),UMIN(200),TUMIN(200),XX(200)
      IF(TT.GT.0.01) GO TO 20
      DO 10 I=1,NPP
      DMAX(I)=D(I)
      TDMAX(I)=TT
      DMIN(I)=D(I)
      TDMIN(I)=TT
      UMAX(I)=U(I)
      TUMAX(I)=TT
      UMIN(I)=U(I)
10    TUMIN(I)=TT
      GO TO 100
20    DO 60 I=1,NPP
      IF(DMAX(I)-D(I).GE.0.) GO TO 30
      DMAX(I)=D(I)
      TDMAX(I)=TT
30    IF(DMIN(I)-D(I).LE.0.) GO TO 40
      DMIN(I)=D(I)
      TDMIN(I)=TT
40    IF(UMAX(I)-U(I).GE.0.) GO TO 50
      UMAX(I)=U(I)
      TUMAX(I)=TT
50    IF(UMIN(I)-U(I).LE.0.) GO TO 60
      UMIN(I)=U(I)
      TUMIN(I)=TT
60 CONTINUE
      IF(TT.LT.TTMAX) GO TO 100
      WRITE(6,70)
70    FORMAT(10X,58HMAXIMUM AND MINIMUM VALUES FOR EACH STATION FOR E
     1NTIRE RUN///)
      WRITE(6,80)
80    FORMAT(5X,10H  DIST.,FT,5X,7HYMAX,FT,5X,7HYMIN,FT,5X,8HVMAX,FPS
     1  ,5X,8HVMIN,FPS/19X,9HTYMAX,SEC,3X,9HTYMIN,SEC,4X,9HTVMAX,SEC,4X
     2  ,9HTVMIN,SEC///)
```

```
      WRITE(6,90) (XX(I),DMAX(I),DMIN(I),UMAX(I),UMIN(I),TDMAX(I),
     1   TDMIN(I),TUMAX(I),TUMIN(I), I=1,NPP)
   90    FORMAT(7X,F9.2,4X,F8.5,4X,F8.5,5X,F8.4,5X,F8.4/21X,F7.2,5X,F7.2
     1   ,6X,F7.2,6X,F7.2)
  100    RETURN
       END
-FOR,IS  GRAPHS
       SUBROUTINE GRAPHS
       DIMENSION TOPLOT(4000)
       COMMON/Z1/Y(200),V(200),X(200),NX,XL,S,B,GR,GNU,DX,
     1         YSTART,QI,NP,M
       COMMON/Z2/TPL(500),Y1N(500),Y2N(500),Y3N(500),V1N(500),V2N(500),
     1 V3N(500),NPLT,RUNNO,YPR1(200),YPR2(200),YPR3(200),TPR1,TPR2,TPR3,
     2         TMAX
       NAMELIST/INPLOT/ZEROY,ZEROV,DELY,DELV
          READ(5,INPLOT)
          CALL PLOTS(TOPLOT,4000,2)
          CALL FACTOR(1.0)
          TPL(NPLT+1)=0.
          TPL(NPLT+2)=TMAX/8.
          Y1N(NPLT+1)=ZEROY
          Y2N(NPLT+1)=ZEROY
          Y3N(NPLT+1)=ZEROY
          V1N(NPLT+1)=ZEROV
          V2N(NPLT+1)=ZEROV
          V3N(NPLT+1)=ZEROV
          Y1N(NPLT+2)=DELY
          Y2N(NPLT+2)=DELY
          Y3N(NPLT+2)=DELY
          V1N(NPLT+2)=DELV
          V2N(NPLT+2)=DELV
          V3N(NPLT+2)=DELV
          YPR1(NP+1)=ZEROY
          YPR2(NP+1)=ZEROY
          YPR3(NP+1)=ZEROY
          YPR1(NP+2)=DELY
          YPR2(NP+2)=DELY
          YPR3(NP+2)=DELY
          X(NP+1)=0.
          X(NP+2)=XL/8.
          CALL PLOT(0.0,-30.0,-3)
          CALL PLOT(0.0,1.0,-3)
          CALL PLOT( 9.0,0.0,-3)
          CALL AXIS(0.0,0.0,15HTIME IN SECONDS,-15, 8.0,0.0,TPL(NPLT+1),
     1              TPL(NPLT+2))
          CALL AXIS(0.0,0.0,13HDEPTH IN FEET,+13, 5.0,90.0,Y1N(NPLT+1),
     1              Y1N(NPLT+2))
          CALL LINE(TPL,Y1N,NPLT,1,+1,0)
          CALL LINE(TPL,Y2N,NPLT,1,+1,3)
          CALL LINE(TPL,Y3N,NPLT,1,+1,4)
          CALL PLOT(0.0,-30.0,-3)
          CALL PLOT(9.0,1.0,-3)
```

```
      CALL AXIS(0.0,0.0,15HTIME IN SECONDS,-15, 8.0,0.0,TPL(NPLT+1),
     1            TPL(NPLT+2))
      CALL AXIS(0.0,0.0,18HVELOCITY IN FT/SEC,+18, 5.0,90.0,V1N(NPLT+
     1            1),V1N(NPLT+2))
      CALL LINE(TPL,V1N,NPLT,1,+1,0)
      CALL LINE(TPL,V2N,NPLT,1,+1,3)
      CALL LINE(TPL,V3N,NPLT,1,+1,4)
      CALL PLOT(0.0,-30.0,-3)
      CALL PLOT(0.0,1.0,-3)
      CALL PLOT( 9.0,0.0,-3)
      CALL AXIS(0.0, 0.0,16HDISTANCE IN FEET,-16, 8.0,0.0,X(NP+1),
     1   X(NP+2))
      CALL AXIS(0.0,0.0,13HDEPTH IN FEET,+13, 5.0,90.0,Y1N(NPLT+1),
     1            Y1N(NPLT+2))
      CALL LINE(X,YPR1,NP,1,+1,0)
      CALL LINE(X,YPR2,NP,1,+1,3)
      CALL LINE(X,YPR3,NP,1,+1,4)
      CALL FACTOR(0.4)
      CALL SYMBOL(2.0,16.,0.21,47HNUMERICAL SOLUTION OF CHARACTERISTI
     1CS EQUATIONS,0.0,47)
      CALL SYMBOL(1.05,15.7,.21,56HUNSTEADY, SUPERCRITICAL, OPEN-CHAN
     1NEL FLOW   J. J. ZOVNE,0.0,56)
      CALL SYMBOL(2.,15.4,.21  ,48HSERIES AS1--TWO POINT INTERPOLATIO
     1N --RUN NO.    ,0.0,48)
      CALL NUMBER(11.5,15.4,.21 ,RUNNO,0.0,-1)
      CALL SYMBOL(6.4,15.1,.21  ,6HLEGEND,0.0,6)
      CALL PLOT(6.4,15.05,+3)
      CALL PLOT(7.6,15.05 ,+2)
      CALL SYMBOL(3.,14.9,.21    ,0,Q.0,-1)
      CALL SYMBOL(3.3,14.8,.21,  37HHYDROGRAPH AT X=     OR PROFILE A
     1T T=,0.0,37)
      CALL NUMBER(6.7,14.8,.21,X(5),0.0,1)
      CALL NUMBER(11.5,14.8,.21 ,TPR1,0.0,2)
      CALL SYMBOL(3.,14.6,.21,     3,0.0,-1)
      CALL SYMBOL(3.3,14.5,.21  ,39HHYDROGRAPH AT MIDPOINT OR PROFILE
     1 AT T=,0.0,39)
      CALL NUMBER(11.5,14.5,.21 ,TPR2,0.0,2)
      CALL SYMBOL(3.,14.3,.21    ,4,0.0,-1)
      CALL SYMBOL(3.3,14.2,.21  ,39HHYDROGRAPH AT ENDPOINT OR PROFILE
     1 AT T=,0.0,39)
      CALL NUMBER(11.5,14.2,.21 ,TPR3,0.0,2)
      CALL SYMBOL(3.,13.9,.21  ,25HCHANNEL LENGTH=       FEET,0.0,25)
      CALL NUMBER(6.2,13.9,.21  ,XL,0.0,-1)
      CALL SYMBOL(3.,13.6,.21   ,25HX GRID SPACING=       FEET,0.0,25)
      CALL NUMBER(6.2,13.6,.21   ,DX,0.0,-1)
      CALL SYMBOL(3.,13.3,.21   ,15HSLOPE          =,0.0,15)
      CALL NUMBER(6.2,13.3,.21   ,S,0.0,6)
      RETURN
      END
-HDG,P  TWO POINT INTERPOLATION
-XQT
```

```
 1
 2
SERIES A---RUNS TO CHECK STABILITY OF NUMERICAL SOLUTION WITH VARYING SLOPE,
          FRICTION, AND BOUNDARY CONDITIONS.
 $INPUT   NX=176,
          XL=5280.,
          S=0.0060,
          B=3.487  ,
          GNU=.00000897,
          TL=150.,
          TMAX=1500.,
          M=1,
          RUNNO=9.,
 $END
 $INPUT2  YSTART=0.0911,
          QI=0.82761,
 $END
 $END
 $INPLOT  ZEROY=.070,ZEROV=2.1,DELY=.004,DELV=0.1,
```

Series AL Program (Two-Point Interpolation with Averaged Friction Slopes)

This program differs from the Series AS program only in the subroutine UNSTD where the linear hydrograph boundary conditions are specified and where the friction slopes are averaged. Only the UNSTD subroutine is therefore listed in the following. The set of input data for Case AL5 is listed following UNSTD.

```
-FOR,IS  UNSTD
      SUBROUTINE UNSTD
      DIMENSION TITLE(160),Q(999),VP(999),YP(999)
         DIMENSION STOR(999),QSTOR(999),DSTR(999),DQSTR(999),CUMSTR(999)
     1             ,CUMQ(999)
      COMMON/Z1/Y(999),V(999),X(999),NX,XL,S,B,GR,GNU,DX,
     1         YSTART,QI,NP,M
      COMMON/Z2/TPL(999),Y1N(999),Y2N(999),Y3N(999),V1N(999),V2N(999),
     1 V3N(999),NPLT,RUNNO,YPR1(999),YPR2(999),YPR3(999),TPR1,TPR2,TPR3,
     2         TMAX
      NAMELIST/INPUT/NX,XL,S,B,YEND,QEND,GNU,TL    ,TMAX,M,RUNNO
         READ(5,31) K
   31    FORMAT(I2)
         K=K*16
         READ(5,32) (TITLE(I),I=1,K)
   32    FORMAT(16A5)
         WRITE(6,33) (TITLE(I),I=1,K)
   33    FORMAT(1H1//////////////(25X,16A5/))
         READ(5,INPUT)
         GR=32.166
         N=1
         T=0.0
         DO 250 I=1,NX
         STOR(I)=0.
  250    QSTOR(I)=0.
      CALL STEADY(Y,V)
         WRITE(6,10) RUNNO
   10    FORMAT(25X,8HRUN NO. ,F4.1)
         WRITE(6,34) XL,S,B,GNU,QI,YSTART,TMAX,QEND,YEND,NX,TL
   34    FORMAT(1H1,10HINPUT DATA//5X,7HLENGTH=F7.1,10X,6HSLOPE=,F10.8,
     1         10X,6HWIDTH=,F5.2,10X,15HKIN. VISCOSITY=,F10.9/5X,
     212HINI. DISCH.=,F9.6,5X,11HINI. DEPTH=,F8.4,   10X,12HTIME OF RUN=
     3,        F7.1,3HSEC/5X,12HFIN. DISCH.=,F9.6,5X,11HFIN. DEPTH=,F8.4,
     4    5X,3HNX=,I3,5X,3HTL=,F6.2//)
         WRITE(6,76)
   76    FORMAT(5X,51HINITIAL STEADY STATE SURFACE PROFILE AND VELOCITIE
     1S/5X,13HDISTANCE, FT.,10X,10HDEPTH, FT.,10X,16HVELOCITY, FT/SEC)
         WRITE(6,77) X(1),Y(1),V(1)
   77    FORMAT(10X,F6.0,13X,F8.6,19X,F9.6)
         FR=V(1)/C(Y(1))
         REY=4.*R(Y(1))*V(1)/GNU
         FRICF=F(Y(1),V(1))
         WRITE(6,78) FR,REY,FRICF
   78    FORMAT(5X,11HFROUDE NO.=,F5.3,5X,13HREYNOLDS NO.=,E12.6,5X,
     1         12HFRIC. FACT.=,F8.7//)
         VOL=(QI+QEND)*TL/2.
         WRITE(6,80) VOL
   80    FORMAT(5X,18HTOTAL WAVE VOLUME=,F12.5,2X,3HFT3//)
         IPLOT=1
         NM=NX/2.+.1
         TPL(1)=0.
         Y1N(1)=YSTART
```

```
          V1N(1)=V(1)
          Y2N(1)=Y(NM)
          V2N(1)=V(NM)
          Y3N(1)=Y(NP)
          V3N(1)=V(NP)
C         OBTAIN THE MAXIMUM VALUE OF DT FOR LAST INTERVAL
   35     DTINV=0.0
          DO 50 I=1,NP
   45     DTT=(V(I)+C(Y(I)))/DX
          IF(DTT.GT.DTINV) DTINV=DTT
   50   CONTINUE
          DT=1.0/DTINV
   60     T=T+DT
C         COMPUTE VALUES AT UPSTREAM BOUNDARY FO TIME T
          IF(T.GT.TL) GO TO 140
          YP(1)=YSTART+(YEND-YSTART)*T/TL
          VP(1)=(QI+(QEND-QI)*T/TL)/(B*YP(1))
          GO TO 150
  140     YP(1)=YEND
          VP(1)=QEND/(B*YP(1))
C         COMPUTE INTERMEDIATE VALUES
  150   DO 180 I=2,NP
          TH=DT/DX
          A1=SQRT(GR)*TH*(Y(I)-Y(I-1))/(1.+TH*(V(I)- V(I-1)))
          B1=TH*V(I)*(Y(I)-Y(I-1))/(1.+TH*(V(I)-V(I-1)))-Y(I)
C         LOCATION OF C PLUS CHARACTERISTIC
          YR=.5*A1*A1-B1-A1*SQRT(.25*A1*A1-B1)
          CR=C(YR)
          VR=(V(I)-(V(I)-V(I-1))*TH*CR)/(1.+TH*(V(I)-V(I-1)))
          XR=X(I)-DT*(VR+CR)
C         LOCATION OF C MINUS CHARACTERISTIC
          YS=.5*A1*A1-B1+A1*SQRT(.25*A1*A1-B1)
          CS=C(YS)
          VS=(V(I)+(V(I)-V(I-1))*TH*CS)/(1.+TH*(V(I)-V(I-1)))
          XS=X(I)-DT*(VS-CS)
C         COMPUTATION ALONG CHARACTERISTICS TO T+DT
          AR=SQRT(GR/YR)
          AS=SQRT(GR/YS)
          SFR=SF(YR,VR,F(YR,VR))
          YP(I)=(VR-VS+GR*(SF(YS,VS,F(YS,VS))-SFR)*DT/2.+AR
     1          *YR+AS*YS)/(AR+AS)
          VP(I)=VR-AR*(YP(I)-YR)-GR*(SFR-S)*DT
  170     FF=F(YP(I),VP(I))
          VPK=VP(I)-(VP(I)-VR+AR*(YP(I)-YR)+GR*((SFR+SF(YP(I),VP(I),FF))/
     1          2.-S)*DT)/(1.+(FF*VP(I)*DT)/(8.*R(YP(I))))
          IF(ABS(VPK-VP(I)).LT.0.000001) GO TO 175
          VP(I)=VPK
          GO TO 170
  175     VP(I)=VPK
  180   CONTINUE
          DO 182 I=1,NX
```

```
      YFIN=(YP(I)+YP(I+1))/2.
      YBEG=(Y(I)+Y(I+1))/2.
      DELY=YFIN-YBEG
      DSTR(I)=DELY*B*DX
      QINTO=B*(VP(I)*YP(I)+V(I)*Y(I))/2.
      QOUT=B*(VP(I+1)*YP(I+1)+V(I+1)*Y(I+1))/2.
182   DQSTR(I)=(QINTO-QOUT)*DT
      DO 183  I=1,NX
      STOR(I)=STOR(I)+DSTR(I)
183   QSTOR(I)=QSTOR(I)+DQSTR(I)
      CUMSTR(1)=STOR(1)
      CUMQ(1)=QSTOR(1)
      DO 184  I=2,NX
      CUMSTR(I)=CUMSTR(I-1)+STOR(I)
      CUMQ(I)=CUMQ(I-1)+QSTOR(I)
184   CONTINUE
185 DO 190 I=1,NP
      Y(I)=YP(I)
      V(I)=VP(I)
      Q(I)=Y(I)*V(I)*B
      IF(IPLOT.NE.40) GO TO 186
      YPR1(I)=YP(I)
      TPR1=T
      GO TO 190
186   IF(IPLOT.NE. 80) GO TO 187
      YPR2(I)=YP(I)
      TPR2=T
      GO TO 19^
187   IF(IPLOT.NE.120) GO TO 190
      YPR3(I)=YP(I)
      TPR3=T
190   Q(I)=V(I)*Y(I)*B
      IPLOT=IPLOT+1
      TPL(IPLOT)=T
      Y1N(IPLOT)=Y(1)
      V1N(IPLOT)=V(1)
      Y2N(IPLOT)=Y(NM)
      V2N(IPLOT)=V(NM)
      Y3N(IPLOT)=Y(NP)
      V3N(IPLOT)=V(NP)
      IF(T.LT.FLOAT(N)*10.) GO TO 195
189   WRITE(6,191) T
191   FORMAT( 5X,5HTIME=,F9.3,3HSEC//)
      WRITE(6,192)
192   FORMAT(5X,11HDISTANCE,FT,2X,                8HDEPTH,FT,2X,
     1        15HVELOCITY,FT/SEC,2X,13HDISCHARGE,CFS,2X,22HSTORAGE VS.
     2INFLOW,FT3,5X,30HCUM. WAVE STOR. VS. NET INFLOW)
      DO 193 I=1,NP,2
193   WRITE(6,93) X(I),Y(I),V(I),Q(I),STOR(I),QSTOR(I),CUMSTR(I),
     1       CUMQ(I),I
```

```
   93     FORMAT(5X,F8.2,4X,F7.4, 4X,F9.4,10X,F8.4,5X,F10.4,2X,F10.4,8X,
     1         F10.4,2X,F10.4,2X,I5)
          N=N+1
  195     IF(T.GE.TMAX) GO TO 200
          GO TO 35
  200     NPLT=IPLOT
          RETURN
        END
-XQT
 1
 2
SERIES A---RUNS TO CHECK STABILITY OF NUMERICAL SOLUTION WITH VARYING SLOPE,
          FRICTION, AND BOUNDARY CONDITIONS.
 $INPUT   NX=100,
          XL=2000.,
          S=0.0060
          B=3.487  ,
          YEND=0.3614,
          QEND=7.50853,
          GNU=.00000897,
          TL= 50.,
          TMAX=200.,
          M=1,
          RUNNO=5.,
 $END
 $INPUT2 YSTART=0.0911,
          QI=0.82761,
 $END
 $INPLOT ZEROY=0.,ZEROV=0.,DELY=0.05,DELV=1.,
 $END
- FIN
```

Table 11. A Portion of the Series AL, Case AL5 Printed Output Showing Continuity Checks at T=91.131 Seconds

TWO POINT INTERPOLATION

TIME= 91.131SEC

DISTANCE,FT	DEPTH,FT	VELOCITY,FT/SEC	DISCHARGE,CFS	STORAGE VS. INFLOW,FT3	CUM. WAVE STOR. VS. NET INFLOW	
.00	.3614	5.9582	7.5085	18.8494	19.6563	18.8494	19.6563	1
20.00	.3614	5.9583	7.5085	18.8482	19.0838	37.6975	38.7401	2
40.00	.3614	5.9586	7.5083	18.8448	18.9357	56.5423	57.6758	3
60.00	.3613	5.9591	7.5075	18.8384	18.8651	75.3807	76.5409	4
80.00	.3612	5.9599	7.5061	18.8295	18.8229	94.2102	95.3638	5
100.00	.3610	5.9605	7.5040	18.8199	18.7938	113.0302	114.1576	6
120.00	.3609	5.9606	7.5013	18.8115	18.7725	131.8417	132.9301	7
140.00	.3608	5.9606	7.4983	18.8043	18.7556	150.6460	151.6857	8
160.00	.3607	5.9589	7.4950	18.7971	18.7401	169.4431	170.4258	9
180.00	.3606	5.9577	7.4911	18.7880	18.7231	188.2312	189.1490	10
200.00	.3604	5.9565	7.4865	18.7758	18.7013	207.0070	207.8502	11
220.00	.3602	5.9553	7.4807	18.7594	18.6695	225.7664	226.5197	12
240.00	.3600	5.9540	7.4736	18.7383	18.6252	244.5047	245.1449	13
260.00	.3596	5.9525	7.4647	18.7116	18.5756	263.2163	263.7204	14
280.00	.3592	5.9508	7.4537	18.6782	18.5248	281.8946	282.2453	15
300.00	.3587	5.9486	7.4399	18.6365	18.4685	300.5311	300.7137	16
320.00	.3580	5.9459	7.4228	18.5842	18.4015	319.1153	319.1152	17
340.00	.3572	5.9426	7.4014	18.5181	18.3196	337.6334	337.4348	18
360.00	.3561	5.9385	7.3742	18.4181	18.2022	356.0514	355.6370	19
380.00	.3543	5.9289	7.3250	18.0167	17.7813	374.0682	373.4183	20
400.00	.3446	5.8451	7.0237	17.2020	16.9438	391.2702	390.3621	21
420.00	.3309	5.7230	6.6044	16.1758	15.8903	407.4461	406.2525	22
440.00	.3152	5.5793	6.1312	14.8619	14.5397	422.3071	420.7922	23
460.00	.2937	5.3715	5.4935	12.3957	11.9696	434.7027	432.7613	24
480.00	.2444	4.8497	4.1334	7.5108	6.6990	442.2136	439.4603	25
500.00	.1532	3.6477	1.9406	2.6099	1.8811	444.8235	441.3414	26
520.00	.1038	2.8376	1.0275	.5245	.3376	445.3470	441.6789	27
540.00	.0934	2.6479	.8606	.0960	.0612	445.4430	441.7402	28
560.00	.0916	2.6132	.8343	.0185	.0118	445.4616	441.7520	29
580.00	.0912	2.6065	.8288	.0036	.0023	445.4652	441.7543	30
600.00	.0911	2.6052	.8279	.0007	.0004	445.4658	441.7547	31
620.00	.0911	2.6049	.8277	.0001	.0001	445.4659	441.7547	32
640.00	.0911	2.6049	.8276	.0000	.0000	445.4659	441.7547	33
660.00	.0911	2.6048	.8276	-.0000	.0000	445.4659	441.7547	34
680.00	.0911	2.6048	.8276	-.0000	.0000	445.4659	441.7547	35
700.00	.0911	2.6048	.8276	-.0000	.0000	445.4659	441.7547	36
720.00	.0911	2.6048	.8276	-.0000	.0000	445.4659	441.7547	37
740.00	.0911	2.6048	.8276	-.0000	.0000	445.4659	441.7547	38
760.00	.0911	2.6048	.8276	-.0000	.0000	445.4659	441.7547	39
780.00	.0911	2.6048	.8276	-.0000	.0000	445.4659	441.7547	40
800.00	.0911	2.6048	.8276	-.0000	.0000	445.4659	441.7547	41
820.00	.0911	2.6048	.8276	-.0000	.0000	445.4659	441.7547	42
840.00	.0911	2.6048	.8276	-.0000	.0000	445.4659	441.7547	43
860.00	.0911	2.6048	.8276	-.0000	.0000	445.4659	441.7547	44
880.00	.0911	2.6048	.8276	-.0000	.0000	445.4659	441.7547	45
900.00	.0911	2.6048	.8276	-.0000	.0000	445.4659	441.7547	46
920.00	.0911	2.6048	.8276	-.0000	.0000	445.4659	441.7547	47
940.00	.0911	2.6048	.8276	-.0000	.0000	445.4659	441.7547	48
960.00	.0911	2.6048	.8276	-.0000	.0000	445.4659	441.7547	49
980.00	.0911	2.6048	.8276	-.0000	.0000	445.4659	441.7547	50
1000.00	.0911	2.6048	.8276	-.0000	.0000	445.4659	441.7547	51
1020.00	.0911	2.6048	.8276	-.0000	.0000	445.4659	441.7547	52

APPENDIX E

BORE PROPAGATION DATA

Experimental Data for Bore No. 1

Steady Flow Characteristics: $Q=0.8276$ cfs ; $\nu = 1.104 \times 10^{-5} ft^2/sec$; $B=3.487$ ft ; $S_o=0.006$

Normal Depth From Computer Profile = 0.0926 ft

Normal Velocity From Computer Profile = 2.564 ft/sec

Normal Froude No. From Computer Profile = 1.49

Upstream depth measured at x=0: y=0.102 ft (S2 Profile)

Downstream piezometer located at x=79 ft

Table 12. Bore Propagation Data for Bore No. 1

Time, sec	Avg. Bore Location, ft	Avg. Manometer* Readings, ft	Remarks
0	69.5 ±0.5	0.20±0.015	Initial manometer readings
20	68.0	0.250	were affected by the undu-
40	63.0	0.283	lar tailwater of the jump.
60	57.8	0.326	Readings very stable after
80	52.7	0.373	60 sec of tailgate rise.
100	47.0	0.403	Bore location could be read
120	42.3	0.443	to ±0.3 ft. Tailgate rise
140	37.2	0.473	was terminated at 200 sec.
160	32.3	0.503	
180	27.5	0.533	
200	22.7	0.563	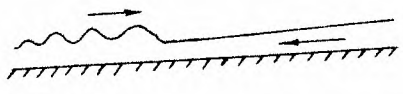
220	18.2	0.583	
240	14.5	0.603	
260	12.5	0.613	
280	10.8	0.615	Sketch of Bore Profile
300	9.8	0.628	

*These readings were obtained by averaging the readings recorded for two or three repetitions of the bore.

Experimental Data for Bore No. 3*

Steady Flow Characteristics: $Q=2.25$ cfs ; $\nu=1074\times10^{-5}$ ft^2/sec ; $B=3.487$ ft ; $S_o=0.015$

Normal Depth From Computer Profile = 0.1245 ft

Normal Velocity From Computer Profile = 5.182 ft/sec

Normal Froude No. From Computer Profile = 2.59

Upstream depth measured at x=0; 0.171 ft (S2 Profile)

Downstream piezometer located at x=79 ft

Table 13. Bore Propagation Data for Bore No. 3

Time, sec	Avg. Bore Location, ft	Avg. Manometer Readings, ft	Remarks
0	66 ± 0.5	0.58 ± 0.05	Initial manometer readings affected by waves behind the hydraulic jump. Manometer readings stabilized after 40 sec. of tailgate rise. Jump is oscillating type. Tailgate rise terminated at 260 sec. Flume skewed downstream causing large eddy system behind bore. Bore locations read to ±0.3 ft.
20	65.3	0.60	
40	62.8	0.63	
60	60.3	0.69	
80	57.8	0.745	
100	55.5	0.78	
120	53.3	0.81	
140	50.8	0.85	
160	48.8	0.88	
180	47.0	0.91	
200	44.8	0.94	
220	42.8	0.97	
240	41.3	1.00	
260	39.8	1.02	
280	38.3	1.04	
300	37.8	1.05	

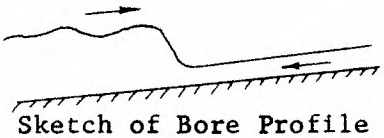

Sketch of Bore Profile

*Bore No. 2 was aborted because of equipment failure.

Experimental Data for Bore No. 4

Steady Flow Characteristics: $Q=1.565$ cfs ; $\nu = 1.074 \times 10^{-5}$ ft^2/sec ; $S_o=0.02$; $B=3.487$ ft

Normal Depth From Computer Profile = 0.09027 ft

Normal Velocity From Computer Profile = 4.972 ft/sec

Normal Froude No. From Computer Profile = 2.92

Upstream depth measured at x=0; y=0.133 ft (S2 Profile)

Downstream piezometer located at x=79 ft

Table 14. Bore Propagation Data for Bore No. 4

Time, sec	Avg. Bore Location, ft	Avg. Manometer Readings, ft	Remarks
0	67.5 ± 0.5	0.43 ± 0.05	Initial manometers seriously affected by waves downstream of jump and by the skewness of the flume downstream. Manometer fluctuates for the first 200 sec of tailgate rise. Tailgate rise terminated at 280 sec. Bore locations read to $\pm$ 0.5 ft.
20	66.3	0.45	
40	64.8	0.51	
60	62.5	0.57	
80	60.5	0.62	
100	59.0	0.70	
120	57.0	0.73	
140	55.5	0.77	
160	54.3	0.81	
180	53.0	0.84	
200	51.5	0.87	
220	50.0	0.90	
240	49.0	0.93	
260	47.8	0.95	
280	46.8	0.97	
300	46.0	0.99	

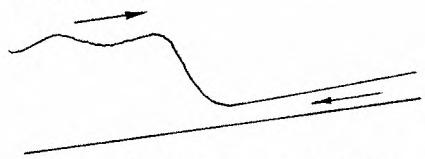

Sketch of Bore Profile

Experimental Data for Bore No. 5

Steady Flow Characteristics: $Q=0.505$ cfs ; $\nu = 1.104 \times 10^{-5} ft^2/sec$;
$B=3.487$ ft; $S_o=0.005$
Normal Depth From Computer Profile = 0.07318 ft
Normal Velocity From Computer Profile = 1.979 ft/sec
Normal Froude No. From Computer Profile = 1.29
Upstream depth measured at x=0; y=0.078 ft (S2 Profile)
Downstream piezometer located at x=79 ft

Table 15. Bore Propagation Data for Bore No. 5

Time, sec	Avg. Bore Location, ft	Avg. Manometer Readings, ft	Remarks
0	62.0±0.5	0.18 steady	This bore was just barely visible, however, the manometer readings were very stable. This bore is of the undular type. The tailgate rise was terminated at 260 sec.
20	61.5	0.21	
40	56.3	0.24	
60	51.5	0.27	
80	46.8	0.30	
100	42.0	0.32	
120	38.3	0.34	
140	34.8	0.355	
160	31.5	0.37	
180	28.8	0.385	
200	26.0	0.40	
220	23.5	0.41	
240	21.3	0.42	
260	20.0	0.43	
280	18.0	0.44	
300	16.5	0.45	
320	15.0	0.46	
340	13.0	0.465	
360	11.5	0.47	
380	10.0	0.477	
400	9.0	0.483	
420	7.5	0.49	
440	6.0	0.495	
460	5.0	0.50	
480	4.0	0.505	
500	2.5	0.51	

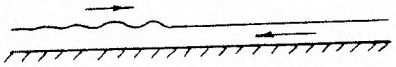

Sketch of Bore Profile

APPENDIX F

SERIES DB BORE PROPAGATION PROGRAM

This program is similar to the Series AS program in Appendix D with the exception of the computation of water surface profiles and sequent depths in the STEADY subroutine and the addition of the internal and downstream boundary conditions in the UNSTD subroutine. The nomenclature for these subroutines is the same, except for the following additions:

1) SUBROUTINE UNSTD

- YTEMP - Temporarily stored value of Y(I).
- VTEMP - Temporarily stored value of V(I).
- YJMP - Sequent depth at jump location.
- VJMP - Sequent velocity at jump location.
- YDATA(IDATA) - Depth hydrograph at x=79 ft.
- TDATA - Time increment between YDATA(IDATA) values.
- LOC - Grid point at which bore front is located.
- XJMP(LOC) - Array of values representing the locations of the bore front.
- TJMP(LOC) - Array of values representing times corresponding to the XJMP(LOC) values.

2) SUBROUTINE STEADY (Profile and Sequent Depth Computations)

- XB(M) - Grid point locations corresponding to S1 profile computations.
- DB(M) - S1 depth at M^{th} grid point.
- UB(M) - S1 velocity at M^{th} grid point.
- FRB(M) - Froude number of S1 flow at M^{th} grid point.
- SAB - Temporary value of average friction slope.
- FDB - Numerator for Newton's method.
- FPDB - Denominator for Newton's method.
- YL - Temporary left-hand depth computed by Newton's method.
- VL - Temporary left-hand velocity.
- X(J) - Grid point locations corresponding to S2 profile computations.
- D(J) - S2 depth at J^{th} grid point.
- U(J) - S2 velocity at J^{th} grid point.
- SA - Temporary value of friction slope.

Y2 - Temporary right-hand value of depth computed by Newton's method.
V2 - Temporary right-hand value of velocity.
FR(J) - Froude number of S2 flow at J^{th} grid point.
YSEQ(I) - Sequent depth of S2 flow at I^{th} grid point.
DELYL - Absolute value of the difference between sequent depth and S1 depth for a left-hand grid point.
XJMP - Location of bore front.
DJMP - S1 depth at XJMP.
UJMP - S1 velocity at XJMP.
JMP - Grid point of XJMP.
DELYR - Absolute value of the difference between sequent depth and S1 depth for a right-hand grid point.
REY1 - Reynolds number at x=0.
FF1 - Friction factor at x=0.
REY2 - Reynolds number at x=L.
FF2 - Friction factor at x=L.

```
-FOR,IS  UNSTD
      SUBROUTINE UNSTD
      DIMENSION TITLE(160),Q(200),VP(200),YP(200),YDATA(200)
      COMMON/Z1/Y(200),V(200),X(200),NX,XL,S,B,GR,GNU,DX,
     1         YSTART,QI,NP
      COMMON/Z2/TPL(500),Y1N(500),Y2N(500),Y3N(500),
     1           NPLT,RUNNO,YPR1(200),YPR2(200),YPR3(200),TPR1,TPR2,TPR3,
     2         TMAX,XJMP(100),TJMP(100),NLOC
      COMMON/Z3/YSEQ(999),VSEQ(999)
      NAMELIST/INPUT/NX,XL,S,B,           GNU,TL    ,TMAX,  RUNNO
      NAMELIST/DATA/IDATA,TDATA,YDATA
         READ(5,31) K
   31    FORMAT(I2)
         K=K*16
         READ(5,32) (TITLE(I),I=1,K)
   32    FORMAT(16A5)
         WRITE(6,33) (TITLE(I),I=1,K)
   33    FORMAT(1H1//////////(25X,16A5/))
         READ(5,INPUT)
         GR=32.166
         N=1
         T=0.0
         WRITE(6,10) RUNNO
   10    FORMAT(25X,8HRUN NO. ,F4.1)
         WRITE(6,34) XL,S,B,GNU,           TMAX,NX,TL
   34    FORMAT(1H1,10HINPUT DATA//5X,7HLENGTH=F7.1,10X,6HSLOPE=,F10.8,
     1         10X,6HWIDTH=,F5.2,10X,15HKIN. VISCOSITY=,F10.9/5X,
     2                                                  10X,12HTIME OF RUN=
     3,        F7.1,3HSEC/5X,3HNX=,I3,5X,3HTL=,F6.2/)
      CALL STEADY(Y,V,JMPB,YJMP,VJMP)
         CALL MAXMIN(Y,V,T,NP,X,TMAX)
         READ(5,DATA)
         WRITE(6,300) TDATA,IDATA
  300    FORMAT(5X,22HHYDROGRAPH AT X=79 FT.,5X,14HTIME INTERVAL=,F5.2,
     1       5X,14HNO. OF POINTS=,I3)
         WRITE(6,301) (I,YDATA(I),I=1,IDATA)
  301    FORMAT(5X,I4,3X,F9.5)
         IHYD=1
         LOC=1
         XJMP(LOC)=X(JMPB)
         TJMP(LOC)=0.
         YP(NP)=Y(NP)
         VP(NP)=V(NP)
         IPLOT=1
         TPL(1)=0.
         Y1N(1)=Y(61)
         Y2N(1)=Y(41)
         Y3N(1)=Y(20)
C     OBTAIN THE MAXIMUM VALUE OF DT FOR LAST INTERVAL
   35    DTINV=0.
      DO 50 I=1,NP
   45    DTT=(V(I)+C(Y(I)))/DX
```

```
          IF(DTT.GT.DTINV) DTINV=DTT
   50 CONTINUE
          DT=1.0/DTINV
   60     T=T+DT
C       COMPUTE VALUES AT UPSTREAM BOUNDARY FO TIME T
          YP(1)=Y(1)
          VP(1)=V(1)
C       COMPUTE INTERMEDIATE VALUES
  150   DO 180 I=2,NP
          TH=DT/DX
          A1=SQRT(GR)*TH*(Y(I)-Y(I-1))/(1.+TH*(V(I)- V(I-1)))
          B1=TH*V(I)*(Y(I)-Y(I-1))/(1.+TH*(V(I)-V(I-1)))-Y(I)
C       LOCATION OF C PLUS CHARACTERISTIC
          YR=.5*A1*A1-B1-A1*SQRT(.25*A1*A1-B1)
          CR=C(YR)
          VR=(V(I)-(V(I)-V(I-1))*TH*CR)/(1.+TH*(V(I)-V(I-1)))
          XR=X(I)-DT*(VR+CR)
          RR=CR/YR
          IF(I.EQ.NP)  GO TO 181
          IF(V(I+1).LT.C(Y(I+1)))  GO TO 155
C       LOCATION OF C MINUS CHARACTERISTIC
  154     YS=.5*A1*A1-B1+A1*SQRT(.25*A1*A1-B1)
          CS=C(YS)
          VS=(V(I)+(V(I)-V(I-1))*TH*CS)/(1.+TH*(V(I)-V(I-1)))
          XS=X(I)-DT*(VS-CS)
          GO TO 160
  155     IF(I.NE.JMPB)  GO TO 158
          YTEMP=Y(I)
          VTEMP=V(I)
          Y(I)=YJMP
          V(I)=VJMP
  158     A1=SQRT(GR)*TH*(Y(I+1)-Y(I))/(1.+TH*(V(I+1)-V(I)))
          B1=Y(I)-TH*V(I)*(Y(I+1)-Y(I))/(1.+TH*(V(I+1)-V(I)))
          YS=0.5*A1*A1+B1+A1*SQRT(A1*A1/4.+B1)
          CS=SQRT(GR*YS)
          VS=(V(I)+TH*CS*(V(I+1)-V(I)))/(1.+TH*(V(I+1)-V(I)))
          XS=X(I)-(VS-CS)*DT
  160     AR=SQRT(GR/YR)
          AS=SQRT(GR/YS)
          SFR=SF(YR,VR,F(YR,VR))
          SFS=SF(YS,VS,F(YS,VS))
          YP(I)=(VR-VS+GR*(SFS                    -SFR)*DT    +AR
     1          *YR+AS*YS)/(AR+AS)
          VP(I)=VR-AR*(YP(I)-YR)-GR*(SFR-S)*DT
          IF(I.NE.JMPB)  GO TO 180
          IF(YP(I).LE.YSEQ(I))  GO TO 170
          JMPB=JMPB-1
          YJMP=YSEQ(I-1)
          VJMP=VSEQ(I-1)
          LOC=LOC+1
          XJMP(LOC)=X(JMPB)
          TJMP(LOC)=T
```

```
      GO TO 18
170   YJMP=YP(I)
      VJMP=VP(I)
      YP(I)=YTEMP
      VP(I)=VTEMP
180 CONTINUE
181   IF(T.GT.TL) GO TO 185
      IF(T.LT.FLOAT(IHYD)*TDATA) GO TO 185
      YP(NP)=YDATA(IHYD)
      IHYD=IHYD+1
      VP(NP)=QI/(YP(NP)*B)
      IF(VP(NP).GT.C(YP(NP))) GO TO 185
      VP(NP)=VR-RR*(YP(NP)-YR)-GR*(SF(YR,VR,F(YR,VR))-S)*DT
185 DO 190 I=1,NP
      Y(I)=YP(I)
      V(I)=VP(I)
      IF(IPLOT.NE. 1) GO TO 186
      YPR1(I)=YP(I)
      TPR1=T
      GO TO 190
186   IF(IPLOT.NE. 15) GO TO 187
      YPR2(I)=YP(I)
      TPR2=T
      GO TO 19
187   IF(IPLOT.NE.  30) GO TO 190
      YPR3(I)=YP(I)
      TPR3=T
190   Q(I)=V(I)*Y(I)*B
      CALL MAXMIN(Y,V,T,NP,X,TMAX)
      IF(T.LT.FLOAT(IPLOT)*10.0)  GO TO 196
      IPLOT=IPLOT+1
      TPL(IPLOT)=T
      Y1N(IPLOT)=Y(61)
      Y2N(IPLOT)=Y(41)
      Y3N(IPLOT)=Y(21)
196   IF(T.LT.FLOAT(N)*10.)  GO TO 195
189   WRITE(6,191) T
191   FORMAT( 5X,5HTIME=,F9.3,3HSEC)
      WRITE(6,192)
192   FORMAT(5X,11HDISTANCE,FT,5X,                8HDEPTH,FT,5X,
     1        15HVELOCITY,FT/SEC,5X,13HDISCHARGE,CFS)
      DO 193 I=JMPB,NP,1
193   WRITE(6,93) X(I),Y(I),V(I),Q(I),I
 93   FORMAT(5X,F8.2,4X,F7.4,10X,F9.4,10X,F8.4,2X,I5)
      N=N+1
195   IF(T.GE.TMAX) GO TO 200
      IF(JMPB.EQ.2)  GO TO 200
      GO TO 35
200   NPLT=IPLOT
      NLOC=LOC
      RETURN
    END
```

```
-FOR,IS  STEADY
      SUBROUTINE STEADY(D,U,JMP,DJMP,UJMP)
C********CALCULATES SUPERCRITICAL AND SUBCRITICAL INITIAL FLOW PROFILES
C     AND THE LOCATION OF THE HYDRAULIC JUMP**************************
      DIMENSION D(999),U(999),DB(999),UB(999),XB(999),          FR(999),
     1          FRB(999)
      COMMON/Z1/Y(200),V(200),X(200),NX,XL,S,B,GR,GNU,DX,
     1         YSTART,QI,NP
      COMMON/Z3/YSEQ(999),VSEQ(999)
      NAMELIST/INPUT2/YSTART,QI,YDOWN
         READ(5,INPUT2)
         DX=XL/FLOAT(NX)
         X(1)=0.0
         D(1)=YSTART
         U(1)=QI/(B*D(1))
         NP=NX+1
         FR(1)=U(1)/C(D(1))
         XB(NP)=XL
         DB(NP)=YDOWN
         UB(NP)=QI/(B*DB(NP))
         FRB(NP)=UB(NP)/C(DB(NP))
      DO 30 J=2,NP
         M=NP-J+1
         XB(M)=XB(M+1)-DX
         YL=DB(M+1)
         VL=UB(M+1)
         IF(FRB(M+1).LE.1.) GO TO 10
         DB(M)=DB(M+1)
         UB(M)=UB(M+1)
         FRB(M)=FRB(M+1)
         GO TO 15
   10    SAB=(SF(DB(M+1),UB(M+1),F(DB(M+1),UB(M+1)))+SF(YL,VL,F(YL,VL)))
     1         /2.
         FDB=YL-DB(M+1)+(VL*VL-UB(M+1)*UB(M+1))/(2.*GR)-DX*(SAB-S)
         FPDB=1.-VL*VL/(YL*GR)+(F(YL,VL)*VL*VL*(4.*YL+3.*B)*DX)/
     1         (16.*GR*B*YL*YL)
         DB(M)=YL-FDB/FPDB
         UB(M)=QI/(B*DB(M))
         FRB(M)=UB(M)/C(DB(M))
         IF(FRB(M).GE.1.) GO TO 15
   11    IF(ABS(YL-DB(M)).LT.0.00001)  GO TO 15
         YL=DB(M)
         VL=UB(M)
         GO TO 10
   15    Y2=D(J-1)
         V2=U(J-1)
         X(J)=X(J-1)+DX
   20    SA=(SF(Y2,V2,F(Y2,V2))+SF(D(J-1),U(J-1),F(D(J-1),U(J-1))))/2.
         D(J)=Y2-(Y2-D(J-1)-(U(J-1)**2.-V2*V2 )/(2.*GR)+DX*(SA-S))/(1.
     1     -V2*V2 /(Y2*GR)-(DX/2.)*(F(Y2,V2)*V2*V2 )*(4.+(3.*B)/Y2)/
     2     (8.*GR*B*Y2))
         U(J)=QI/(B*D(J))
```

```
27    FR(J)=U(J)/C(D(J))
      IF(FR(J).LT.1.) D(J)=0.9*D(J)
      IF(ABS(Y2-D(J)).LT..00001)  GO TO 30
      Y2=D(J)
      V2=U(J)
      GO TO 20
30 CONTINUE
       YSEQ(1)=0.5*(SQRT(1.+8.*FR(1)*FR(1))-1.)*D(1)
      VSEQ(1)=QI/(B*YSEQ(1))
      DELYL=ABS(YSEQ(1)-DB(1))
      XJMP=X(1)
      DJMP=DB(1)
      UJMP=UB(1)
      JMP=1
      DO 40 I=2,NP
      YSEQ(I)=0.5*(SQRT(1.+8.*FR(I)*FR(I))-1.)*D(I)
      VSEQ(I)=QI/(B*YSEQ(I))
     DELYR=ABS(YSEQ(I)-DB(I))
      IF(DELYL-DELYR) 40,40,35
35    DELYL=DELYR
      XJMP=X(I)
      DJMP=DB(I)
      UJMP=UB(I)
      JMP=I
40    CONTINUE
      REY1=4.*R(D(1))      *U(1)/GNU
      FF1=F(D(1),U(1))
      REY2=4.*R(DB(NP))        *UB(NP)/GNU
      FF2=F(DB(NP),UB(NP))
      WRITE(6,45) REY1,FF1,REY2,FF2
45    FORMAT(5X,22HUPSTREAM REYNOLDS NO.=,E12.6,5X,16HFRICTION FACTOR
  1=,F8.7/5X,10HDOWNSTREAM,12X,E12.6,21X,F8.7//)
      WRITE(6,46) XJMP,QI
46    FORMAT(5X,20HLOCATION OF JUMP, X=,F8.2,5X,15HINI. DISCHARGE=,
  1          F8.5//)
      WRITE(6,50)
50    FORMAT(5X,44HINITIAL STEADY STATE FLOW PROFILE PARAMETERS//)
      WRITE(6,60)
60    FORMAT(5X,13HDISTANCE, FT.,10X,10HDEPTH, FT.,15X,
  1          16HVELOCITY, FT/SEC,10X,10HFROUDE NO./21X,5HSUPER,6X,
  2          3HSUB,4X,7HSEQUENT,8X,5HSUPER,5X,3HSUB,10X,5HSUPER,5X,
  3          3HSUB)
      WRITE(6,70) (X(I),D(I),DB(I),YSEQ(I),U(I),UB(I),FR(I),FRB(I),
  1                I=1,NP)
70    FORMAT(8X,F9.2,2X,F8.6,2X,F8.6,2X,F8.6,5X,F8.5,2X,F8.5,5X,F8.5,
  1          2X,F8.5)
      JMPA=JMP+1
      DO 80 I=JMPA,NP
      D(I)=DB(I)
80    U(I)=UB(I)
      RETURN
      END
```

```
-XQT
 1
 3
SERIES D8---RUNS WHICH NUMERICALLY SIMULATE A POSITIVE BORE PROPAGATION.  THESE
            RUNS CAN BE DIRECTLY COMPARED TO EXPERIMENTAL DATA TAKEN IN THE
            80 FOOT TILTING FLUME.
 $INPUT  NX=79,
         XL=79.,
         S=0.0060,
         B=3.487  ,
         GNU=.00001104,
         TL=300.,
         TMAX=320.,
         RUNNO=1.,
 $END
 $INPUT2 YSTART=0.102,
         QI=0.82761,
         YDOWN=0.215,
 $END
 $DATA
         IDATA=60,
         TDATA=5.,
         YDATA=0.222,  0.231,  0.240,  0.249,  0.257,  0.266,  0.274,
         0.283,  0.294,  0.306,  0.317,  0.329,  0.340,  0.351,  0.362,
         0.373,  0.380,  0.388,  0.395,  0.403,  0.413,  0.423,  0.433,
         0.443,  0.450,  0.458,  0.465,  0.473,  0.480,  0.488,  0.495,
         0.503,  0.510,  0.518,  0.525,  0.533,  0.540,  0.548,  0.555,
         0.563,  0.568,  0.573,  0.578,  0.583,  0.588,  0.593,  0.598,
         0.603,  0.605,  0.608,  0.610,  0.613,  0.617,  0.620,  0.623,
         0.626,  0.626,  0.627,  0.627,  0.628,
 $END
 $INPLOT
         ZEROY=0.,          DELY=0.2,       DELX=20.,
 $END
- FIN
```

Table 16. A Portion of the Printed Output for the Bore No. 1 Simulation Showing the Propagation from x=68 ft to x=63 ft

STREETER FIXED GRID, BORE PROPAGATION

DISTANCE,FT	DEPTH,FT	VELOCITY,FT/SEC	DISCHARGE,CFS	
TIME= 20.031SEC				
67.00	.0927	2.5677	.8304	68
68.00	.1634	1.3462	.7669	69
69.00	.1739	1.2446	.7548	70
70.00	.1829	1.1703	.7463	71
71.00	.1913	1.1068	.7384	72
72.00	.1993	1.0530	.7317	73
73.00	.2067	1.0105	.7285	74
74.00	.2138	.9775	.7287	75
75.00	.2202	.9453	.7257	76
76.00	.2254	.9044	.7108	77
77.00	.2305	.8651	.6953	78
78.00	.2369	.8425	.6959	79
79.00	.2490	.7416	.6439	80
TIME= 30.038SEC				
DISTANCE,FT	DEPTH,FT	VELOCITY,FT/SEC	DISCHARGE,CFS	
64.00	.0928	2.5689	.8315	65
65.00	.1600	1.4015	.7818	66
66.00	.1706	1.2947	.7702	67
67.00	.1794	1.2200	.7633	68
68.00	.1876	1.1629	.7608	69
69.00	.1958	1.1140	.7604	70
70.00	.2028	1.0554	.7463	71
71.00	.2081	.9842	.7141	72
72.00	.2153	.9469	.7108	73
73.00	.2221	.9157	.7090	74
74.00	.2286	.8889	.7085	75
75.00	.2350	.8646	.7084	76
76.00	.2413	.8421	.7085	77
77.00	.2476	.8207	.7085	78
78.00	.2538	.8003	.7083	79
79.00	.2660	.7038	.6528	80
TIME= 40.045SEC				
DISTANCE,FT	DEPTH,FT	VELOCITY,FT/SEC	DISCHARGE,CFS	
62.00	.0928	2.5691	.8316	63
63.00	.1624	1.3640	.7724	64
64.00	.1728	1.2635	.7613	65
65.00	.1818	1.1885	.7532	66
66.00	.1898	1.1292	.7474	67
67.00	.1975	1.0772	.7419	68
68.00	.2053	1.0267	.7350	69
69.00	.2132	.9769	.7264	70
70.00	.2211	.9314	.7181	71
71.00	.2286	.8937	.7124	72
72.00	.2355	.8622	.7080	73
73.00	.2414	.8301	.6988	74
74.00	.2466	.7952	.6838	75
75.00	.2521	.7668	.6742	76
76.00	.2584	.7484	.6742	77
77.00	.2646	.7309	.6743	78
78.00	.2707	.7142	.6743	79
79.00	.2830	.6226	.6144	80

BIBLIOGRAPHY

1. Baltzer, R. A. and J. Shen, "Flows of Homogeneous Density in Tidal Reaches," Water Resources Division, U. S. Geological Survey, Washington, D. C., September, 1961, 98 pages.

2. Benjamin, T. B. and M. J. Lighthill, "On Cnoidal Waves and Bores," Proceedings of the Royal Society of London, Series A, Mathematical and Physical Sciences, Volume 224, June-July, 1954, pp. 448-460.

3. Binnie, A. M., "Instability in a Slightly Inclined Water Channel," Journal of Fluid Mechanics, Volume 5, May, 1959, pp. 561-570.

4. Chow, V. T., Open-Channel Hydraulics, McGraw-Hill Book Company, Inc., New York, 1959, pp. 557-583, 395.

5. Conte, S. D., Elementary Numerical Analysis, McGraw-Hill Book Company, Inc., New York, 1965, pp. 119-122.

6. Craya, A., "The Criterion for the Possibility of Roll-Wave Formation," Gravity Waves, National Bureau of Standards, Circular 521, 1952, pp. 141-151.

7. Dressler, R. F., "Mathematical Solution of the Problem of Roll Waves in Open Channels," Communications on Pure and Applied Mathematics, Volume 2, Nos. 2-3, 1949, pp. 149-194.

8. Dronkers, J. J., Tidal Computations in Rivers and Estuaries, North-Holland Publishing Company, Amsterdam, 1964, pp. 355-371, 395-400.

9. Escoffier, F. F., "A Graphical Method for Investigating the Stability of Flow in Open Channels or in Closed Conduits Flowing Partly Full," Transactions, American Geophysical Union, Volume 30, No. 4, August, 1950, pp. 583-586.

10. Favre, H., Etude Théorique et Expérimentale des Ondes de Translation dans les Canaux Découverts, Paris: Dunod, 1935.

11. Garrison, J. M., J. P. Granju, and J. T. Price, "Unsteady Flow Simulation in Rivers and Reservoirs," Journal of the Hydraulics Division, ASCE, Volume 95, No. HY5, September, 1969, pp. 1559-1576.

12. Godunov, S. K. and V. S. Ryabenki, The Theory of Difference Schemes, Interscience Press, New York, 1964, 289 pages.

13. Henderson, F. M., Open Channel Flow, The Macmillan Co., New York, 1966, pp. 75-77.

14. Isaacson, E., J. J. Stoker, and B. A. Troesch, "Numerical Solution of Flood Prediction and River Regulation Problems. Report 2. Numerical Solution of Flood Problems in Simplified Models of the Ohio River and the Junction of the Ohio and Mississippi Rivers," New York University, Institute of Mathematical Sciences, Report No. IMM-205, 1954.

15. Isaacson, E., J. J. Stoker, and B. A. Troesch, "Numerical Solution of Flood Prediction and River Regulation Problems. Report 3. Results of the Numerical Prediction of the 1945 and 1948 Floods in the Ohio River, of the 1947 Flood through the Junction of the Ohio and Mississippi Rivers, and of the Floods of 1950 and 1948 through Kentucky Reservoir," New York University, Institute of Mathematical Sciences, Report No. IMM-NYU-235, 1956, page 70.

16. Iwagaki, Y., "Fundamental Studies on the Runoff Analysis by Characteristics," Bulletin No. 10, Kyoto University, Disaster Prevention Research Institute, December, 1955 (English), 25 pages.

17. Iwasa, Y., "The Criterion for Instability of Steady Uniform Flows in Open Channels," Memoirs of the Faculty of Engineering, Kyoto University, Volume XVI, No. 6, 1954 (English), pp. 264-275.

18. Jeffreys, H., "The Flow of Water in an Inclined Channel of Rectangular Section," Philosophical Magazine, Series 6, Volume 49, No. 223, May, 1925, pp. 793-807.

19. "The Johnstown Disaster," Engineering News, Volume 21, No. 23, June 8, 1889, pp. 517-518.

20. Keulegan, G. H. and G. W. Patterson, "A Criterion for Instability of Flow in Steep Channels," Transactions, American Geophysical Union, Volume 21, Washington, D. C., 1940, pp. 594-602.

21. Koloseus, H. J. and J. Davidian, "Free-Surface Instability Correlations," U. S. Geological Survey Water-Supply Paper 1592-C, Washington, D. C., 1966, 72 pages.

22. Lamb, H., Hydrodynamics, 6th edition, Cambridge University Press, Cambridge, England, 1932.

23. Liggett, J. A., "Unsteady Open Channel Flow with Lateral Inflow," Technical Report No. 2, Department of Civil Engineering, Stanford University, Stanford, California, July, 1959, 73 pages.

24. Liggett, J. A. and D. A. Woolhiser, "Difference Solutions of the Shallow-Water Equation," Journal of the Engineering Mechanics Division, ASCE, Volume 93, No. EM2, April, 1967, pp. 39-71; with Discussions by T. E. Harbaugh, Volume 93, No. EM5, October, 1967, pp. 186-190; R. Prasad, C. B. Vreugdenhill, and A. A. Smith, Volume 94, No. EM1, February, 1968, pp. 332-342; Closure, Volume 95, EM1, February, 1969, pp. 303-311.

25. Lin, P. N., "Numerical Analysis of Continuous Unsteady Flow in Open Channels," Transactions, American Geophysical Union, Volume 33, No. 2, April, 1952, pp. 227-234.

26. Lister, M., "The Numerical Solution of Hyperbolic Partial Differential Equations by the Method of Characteristics," in A. Ralston and H. S. Wilf, Mathematical Methods for Digital Computers, John Wiley and Sons, Inc., New York, 1960, pp. 165-179.

27. Martin, C. S. and F. G. DeFazio, "Open-Channel Surge Simulation by Digital Computer," Journal of the Hydraulics Division, ASCE, Volume 95, No. HY6, November, 1969, pp. 2049-2070.

28. Massau, J., "Memoire sur L'intégration Graphique des Équations aux Derivées Partielles," Annales des Ingénieurs Sortis de Gand, Tome XII, 1889.

29. Mayer, P. G., "Roll Waves and Slug Flows in Inclined Open Channels," Transactions, ASCE, Volume 126, Part I, 1961, pp. 505-564; with Discussion by Messrs. F. F. Escoffier; R. Hugh Taylor and J. F. Kennedy; T. Ishihara, Y. Iwagaki, and Y. Iwasa; and P. G. Mayer.

30. Miller, W. A., Jr., "Numerical Solution of the Unsteady Open-Channel Flow Equations," Ph.D. Thesis, School of Civil Engineering, Georgia Institute of Technology, Atlanta, Georgia, June, 1970.

31. Nomenclature for Hydraulics, ASCE, Manuals and Reports on Engineering Practice, No. 43, New York, 1962, 501 pages.

32. Perkins, F. E., "The Role of Damping in Numerical Stability," ASCE National Meeting on Environmental Engineering, Meeting Preprint No. 689, Chattanooga, Tennessee, May 13-17, 1968, 12 pages.

33. Richtmyer, R. D. and K. W. Morton, Difference Methods for Initial-Value Problems, Interscience Publishers, New York, 1967, 405 pages.

34. Rouse, H., Engineering Hydraulics, John Wiley & Sons, Inc., New York, 1949, pp. 745-748.

35. Schönfeld, J. C., "Theoretical Considerations on an Experimental Bore," Proceedings of the Sixth Congress, International Association for Hydraulic Research, Paper No. A15, The Hague, 1955, pp. 1-12.

36. Stoker, J. J., "Numerical Solution of Flood Prediction and River Regulation Problems. Report 1. Derivation of Basic Theory and Formulation of Numerical Methods of Attack," New York University, Institute of Mathematical Sciences, Report No. IMM-200, 1953.

37. Stoker, J. J., Water Waves, Interscience Publishers, Inc., New York, 1957, pp. 22-32, 291-326, 451-509.

38. Streeter, V. L. and E. B. Wylie, Hydraulic Transients, McGraw-Hill Book Company, Inc., New York, 1967, pp. 246-259.

39. Thomas, H. A., "The Propagation of Waves in Steep Prismatic Conduits," Proceedings of the Hydraulics Conference, Iowa City, Iowa, 1940, pp. 214-229.

40. Tracy, H. J. and C. M. Lester, "Resistance Coefficients and Velocity Distribution, Smooth Rectangular Channel," Water-Supply Paper 1592-A, U. S. Geological Survey, Washington, D. C., 1961, 18 pages.

41. Vasiliev, O. F., M. T. Gladyshev, N. A. Pritvits, and V. G. Sudobicher, "Numerical Methods for the Calculation of Shock Wave Propagation in Open Channels," Proceedings of the Eleventh Congress, International Association for Hydraulic Research, Volume III, Paper No. 3.44, Leningrad, 1965, 11 pages.

42. Vedernikov, V. V., "Characteristic Features of a Liquid Flow in an Open Channel," Acad. Sci. Comptes Rendus (Doklady), Volume 52, U.S.S.R., 1946, pp. 207-210.

VITA

Jerome Joseph Zovne was born September 4, 1942, in Sheboygan, Wisconsin, where he attended public schools until graduation from Central High School in 1960. In September, 1960, he entered the University of Wisconsin, Madison, to follow the curriculum in Civil Engineering. He was awarded the Riess-Detling Scholarship which provided financial support for four years of undergraduate study. While an undergraduate he was elected Captain of the University's gymnastic team and represented the school in the 1964 NCAA Tournament. He was also a member of Delta Tau Delta, Student Athletic Board, "W" Club, and the ASCE Student Chapter.

Upon graduation in January, 1965, he began an M.S. program in Civil Engineering at the University of Wisconsin. He was awarded a research assistantship from the Wisconsin Alumni Research Foundation in order to conduct the investigation for his M.S. thesis entitled, "Screen-Disturbed Laminar Flow in Pipes." He received his M.S. degree in June, 1966.

In September, 1966, he enrolled in the Civil Engineering Ph.D. program at the Georgia Institute of Technology with a major in Hydraulics and Fluid Mechanics and a minor in Mathematics. While pursuing the Ph.D. program, he has been active in judging Georgia Tech and local High School gymnastic meets, in teaching Sunday School, and in sponsoring Luther League. His Ph.D. program was financed primarily by a three-year NDEA Title IV Fellowship.

He is a member of Chi Epsilon, Sigma Xi, ASCE, AGU, and IAHR. He has had practical experience working for the Navy Civil Engineering Laboratory, Port Hueneme, California, in summer, 1966, and for the Naval Ship Research and Development Laboratory, Panama City, Florida, in summer, 1968.

He will be employed as a staff member of the Civil Engineering Department at Kansas State University upon completion of the Ph.D. program at Georgia Tech.

He was married to Karen Louise Larson on September 9, 1966, and they have a daughter, Kari, born May 3, 1969.